An Abstract of the Thesis of

Sanjay Dixit for the degree of Master of Science in Atmospheric Sciences presented on August 12, 1987

Title: Simulation of Tropical Pacific Circulation Anomalies with Linear Atmosphere and Ocean Models

Abstract Approved: Redacted for privacy

W. Lawrence Gates

A simple atmosphere and ocean model of relevance to El Nino and Southern Oscillation (ENSO) is discussed. Both the atmosphere and ocean models are two layer, three dimensional, linear and baroclinic, and generally follow the Oregon State University coupled general circulation model. However, the parameterization differs considerably from previous work in the treatment of the atmospheric latent heat release. This new parameterization follows the formula used in the theory of conditional instability of the second kind (CISK). In this the latent heat release is proportional to the low level convergence. Utilising the "Comprehensive Ocean Atmosphere Data Set" (COADS), which contains all oceanic and atmospheric surface variables over

the global ocean from 1946-1979, experimental model results are discussed for determination of the validity of the parameterizations. In particular, the years 1957, 1965 and 1972 in which El Nino events occurred are examined. The parameterization is deemed to be realistic, and should permit simulation of the El Nino upon coupling the two models.

Simulation of Tropical Pacific Circulation Anomalies with Linear Atmosphere and Ocean Models

by

Sanjay Dixit

A Thesis

submitted to

Oregon State University

In partial fulfillment of

the requirements for the

degree of

Master of Science

Completed August 12, 1987

Commencement June 1988

APPROVED:

Redacted for privacy

Professor of Atmospheric Sciences in charge of major

Redacted for privacy

Head of Department of Atmospheric Sciences

Redacted for privacy

Dean of Graduate School

Date thesis is presented August 12, 1987

Typed by Sanjay Dixit for Sanjay Dixit

Acknowledgments

I gratefully acknowledge the guidance provided me by Dr. W. Lawrence Gates and Dr. Young-June Han throughout the course of this work. I sincerely appreciate the patience with which they provided me with suggestions and answered my questions. I will always remember the warmth and friendship bestowed upon me by the Department of Atmospheric Sciences and the Climatic Research Institute. I kindly acknowledge the assistance provided in COADS data analysis by William McKie of the Climatic Research Institute and by my colleague Joong Bae Ahn. I sincerely acknowledge the financial support provided by National Science Foundation grant number ATM-8512525 during the course of this work. Above all, I am very grateful to my mother Smt. Indu Dixit, who provided me with moral support throughout my life and who has been a constant source of encouragement to contribute my best in everything I do.

TABLE OF CONTENTS

List of Figures

Simulation of Tropical Pacific Circulation Anomalies with Linear Atmosphere and Ocean Models

1.0 Introduction

The interannual variability of sea surface temperature (SST) in the equatorial Pacific Ocean is dominated by the El Nino phenomenon. Originally, the name was associated with a weak warm coastal current which runs southward along the Ecuador coast around the Christmas season (Wyrtki,1975). In scientific parlance, the term is now associated with extreme warming encompassing the whole equatorial Pacific every few years, resulting in catastrophic effects on the economic and ecological system of the region (Caviedes,1975). The El Nino event exhibits various amplitudes of anomalous SST and periodicity between two and ten years. A dominant period of four years is observed.

The following events describe a typical El Nino year. In December of the onset phase, warm equatorial waters move slowly southward along the coast of Peru through April of the following year. As the warm waters become stronger, coastal areas of Ecuador and Peru experience heavy rainfall, while farther inland areas experience dry conditions. Normally cool, nutrient rich upwelling areas are no longer suitable for fishing. During the peak phase starting in May, SST anomalies move off the coast and cover an extensive area of the Pacific Ocean along the equator. From May through October the broadening of the SST anomaly band is accompanied by heavy rainfall and increased incidence of tropical cyclone development in near-equatorial central Pacific islands. From November through February of the following year is the mature phase. During this time, SST anomalies are localized to the central Pacific and the coasts of Ecuador and Peru are beginning to return to normal conditions. The communication with the extratropics in the Northern Hemisphere are the strongest in this period. Near-equatorial islands experience very little precipitation anomalies, or are past the peak of precipitation anomalies. However, farther west, the Indonesian region receives somewhat less than normal rainfall and eastern Australia experiences severe drought. From March through May is the retrieval phase where the SST anomalies rapidly decrease, returning the conditions to normal throughout the Pacific Ocean.

Seasonal climate anomalies are observed in distant regions, for example over India in summer and over North America during winter in an El Nino year. Almost two-thirds of the globe is effected by El Nino directly or indirectly.

These events are the most significant pattern of interannual climate variability on the time scales of decades or less (Weare et al.,1976).

There are many atmospheric features associated with SST anomalies during the El Nino event, for example, weakening of the trades over the western ocean, and changes in cloudiness and solar insolation. As the atmospheric or the oceanic system alone does not exhibit the long periods associated with the El Nino, the emerging view is that El Nino is a highly coupled event involving interactions between the ocean and the atmosphere. There has been a lot of observational and modeling work done on this problem.

Apart from the SST and precipitation anomalies mentioned above, there are some characteristic features associated with the El Nino.

1) There is strong observational evidence of correlation among the interannual eastern Pacific SST, atmospheric pressure, surface and 200 mb winds, mean tropospheric temperature and cloudiness (Rasmusson and Carpenter,1982; Heddinghaus and Krueger,1981). These observations lend credence to the theory of coupling between the ocean and the atmosphere during El Nino.

2) The zonal scale of atmospheric variability during El Nino is of the order of the width of the Pacific Ocean. The

Southern Oscillation index is defined by the surface pressure difference between Tahiti (17.5 S,149.6 W) and Darwin (12.4 S,130 E). During El Nino the surface pressure at Darwin is high and that at Tahiti is low. This change in the zonal Walker circulation is closely related to the SST anomalies of the tropical Pacific Ocean. The dominant period for the Southern Oscillation has been found from observations to be 38 months. It is for this reason the Southern Oscillation and El Nino events are viewed as ocean-atmosphere coupled events referred to as El Nino-Southern Oscillation (ENSO). During the mature phase of El Nino, surface winds and SST anomalies exhibit a coherent spatial structure along the equator.

3) In the vertical structure, the 200 mb and near surface wind anomalies exhibit a marked out of phase relationship.

4) ENSO is very aperiodic. Rasmusson and Carpenter's (1982) composite data show a dominant period of between three and four years. The duration of each event is slightly greater than one year.

5) ENSO exhibits a remarkable tendency for phase locking to the annual cycle. During an event, in the central and western Pacific the SST and wind anomalies achieve their peak at the end of the year, decaying rapidly

thereafter. However, the 1982-83 El Nino event was different. The SST peaked first in the central ocean in December and in the eastern ocean the following June.

6) There have been numerous studies of teleconnections of the ENSO to events in the Northern Hemisphere extratropics (Horel and Wallace,1981; Trenberth,1976; Barnett,1983). The exact relationship between the extratropical forcing and ENSO is not very clear.

A number of atmosphere and ocean models have been formulated by several investigators in the past to explain the dynamics, the initiation mechanism, and the stochastic forcing of ENSO. There are basically two types of models. General circulation models (GCM), though complete in physics, are expensive to run. Moreover, it is difficult to interpret the contributions of a given process. On the other hand, simple models have parameterized physics. Such models are very cost effective and it is easy to understand the contributions of each process.

The atmosphere and ocean models discussed here are linear perturbation models. In such models only deviations from the mean fields are explicitly calculated. In the tropical atmosphere and ocean, simulating the mean field is complicated due to heating and interaction with the extratropics, which is not possible in the present simple model. Moreover, in the present study, only anomalous fields need to be simulated.

In the models, only the deterministic processes of heating, inter-layer momentum exchange and wind stress effects are examined. The intent of this study is to understand the importance of such parameterizations in simulating the salient characteristics of ENSO. The domain considered here is the tropical Pacific Ocean from 30 S to 30 N. This is because the largest tropical atmosphere-ocean interaction occurs in the Pacific Ocean.

The atmospheric and oceanic models are discussed in the next few chapters. The atmosphere model is tested by prescribing various heat sources and sinks, and comparing the simulated field with the dynamics of the tropical atmosphere. The Comprehensive Ocean Atmosphere Data Set (COADS) contains various atmospheric and oceanic surface variables, for example SST, wind vector components, and air-sea temperature difference on a 2° latitude x 2° longitude grid over the global ocean from 1946-1979. This COADS data set has many spatial and temporal data gaps especially in the southern ocean and some parts of the tropical oceans. Significantly, many interesting meteorological phenomena including ENSO have occurred during the data period. In the years 1957-58, 1965-66 and

1972-73 major El Nino events have occurred.

The atmospheric model is examined for similarity with observations in these particular years by prescribing calculated anomalous heating fields from the COADS data. The anomalous heating includes latent heat release and sensible heat flux. While the parameterization for sensible heat flux follows the one used in several studies with the Oregon State University general circulation model (OSU GCM), the latent heat release follows the process of moisture condensation through low-level convergence. Such a study provides information on the feasibility of linear models to simulate the salient features of ENSO. The ocean model is examined for the wind stress effects on the progression of the SST anomaly field.

In Chapter 2 the atmospheric model is discussed completely, together with model simulations and corresponding observed data. It will be shown that the linearized model with the new latent heat parameterization captures the salient characteristics of the atmospheric response during a typical ENSO event. It is expected that such a model, on being coupled to the ocean model, would simulate an ENSO-like disturbance. In Chapter 3 a similar treatment of the ocean model follows. It will be shown that the linearized ocean model captures the elements of the anomalous wind-driven currents during ENSO. Lastly, in Chapter 4 some conclusions and opinions on the direction of future work are offered.

2.0 Atmospheric Modeling of ENSO

2.1 Introduction

The atmospheric response to a changing SST field during ENSO can be understood in terms of a heating anomaly. The processes involved in realising the anomalous heating of the tropical atmosphere is complicated with both positive and negative feedback mechanisms. The ocean communicates with the atmosphere through the flux of sensible heat and the flux of water vapor. These fluxes depend upon the SST, wind speed, near surface air temperature and near surface specific humidity. Further, in the case of water vapor, the latent heat is not realized until condensation occurs. The regions of condensation depend very closely on the regions of low-level convergence. Cloudiness is associated with convergence in the atmosphere, and in turn effects the incoming short-wave solar radiation and the outgoing long-wave radiation from the surface.

Obviously, the problem is not at all simple. However, simple linearized atmospheric models with parameterizations of heating directly in terms of SST fields give results which are comparable with observations and GCM models. Many of the early simple atmosphere models specified only the wind anomalies. Hughes (1979,1984) in his coupled atmosphere-ocean model has an atmospheric model with externally specified wind stress which responds to the depth of the oceanic pycnocline. His model is inadequate because it does not have any means to realize latent heat. In the tropical atmosphere latent heating is the single important feature for producing the anomalous winds. This was shown by Gill (1980) and Webster (1972).

Lau (1982) and Philander (1984) included a single baroclinic mode atmospheric model forced by a heating function. The heating function was taken to be directly proportional to the pycnocline depth anomaly of the ocean. This greatly simplified the coupling between the atmosphere and ocean. Observations indicate that heating is correlated to pycnocline depth anomalies only in the far eastern Pacific Ocean. McCreary's (1983) atmosphere model had two patches of wind stress anomalies corresponding to the typical ENSO wind anomaly field with weaker trades in the western ocean. McCreary and Anderson (1984) had an externally specified wind stress anomaly for the atmospheric model. However, it contained two equilibrium states with a random wind "trigger" mechanism to switch from one state to the other.

Anderson and McCreary (1983) introduced a dynamical atmosphere forced by heating. The single baroclinic mode model forcing depended solely on the SST field. Yamagata (1985) developed a dynamical atmospheric model with latent heat release parameterized as directly proportional to the thermocline depth. Hirst (1985) had a similar atmospheric model,but differing in parameterizing the latent heat release as proportional to SST. Zebiak (1986) introduced a feedback mechanism for the effects of low-level moisture convergence. However, the latent heat release parameterization was given by the linearized form of Clausius-Clapeyron equation. His results shows that such a feedback mechanism greatly improves the model results.

As seen from the above models, the success of a model depends upon the parameterization for the latent heat. As discussed before, the latent heat is not realized unless condensation occurs. Moisture could be advected from one region to an area of active convergence where precipitation occurs. One can include this non-local dependence in two ways. Introducing the moisture equation into the model would complicate the dynamics, although one advantage would be to make the model physics explicit. A second method which is very simple in computation would be to parameterize latent heating in terms of low-level divergence. In regions of active convergence there is rising motion as implied from the mass conservation equation. As the air particle rises, condensation occurs due to cooling. This process of interaction between convection and low-level convergence sometimes leads to unstable growth of the large scale system, and is referred to as conditional instability of the second kind (CISK). In this chapter, an atmospheric model with such a parameterization is discussed. This chapter presents model simulations along with observations to facilitate comparisons for the ENSO years of 1957, 1965 and 1973.

2.2 Atmosphere Model

The starting point for this model was the coupled ocean-atmosphere Oregon State University general circulation model (OSU GCM). Gates, Han and Schlesinger

(1985) discuss a sixteen year simulation of the coupled model. A major drawback of the OSU GCM is in the simulation of SST. The coupled model simulates the January El Nino-like collapse of the trades over the western Pacific ocean and the appearance of warm waters across the equatorial Pacific reasonably well. However, this occurs every year and does not simulate the aperiodicity of ENSO. The present model was developed in order to understand the deficiencies of the OSU GCM and to make recommendations for future improvements in the OSU GCM. Hence, this model generally follows the OSU GCM but with simplifications appropriate for such a linear model.

Observational evidence that the vertical structure of the atmospheric heating has a single maximum around 500 mb was given by Yanai et al. (1973). The simplest atmospheric model to resolve the vertical structure is a two layer model. The time scales associated with barotropic processes over the Pacific atmosphere through gravity waves is of the order of half a day. As discussed earlier, ENSO is a slowly varying phenomenon of duration of a year or more. Hence, only slowly varying baroclinic modes need be examined for the simulation of ENSO. Including barotropic processes would necessiate smaller time steps in the numerical procedure due to the stability criterion. This would increase the computational effort tremendously.

Figure 1 shows the vertical structure of the two layer model. Each layer is 500 mb thick with horizontal velocity components carried at the middle of each layer.

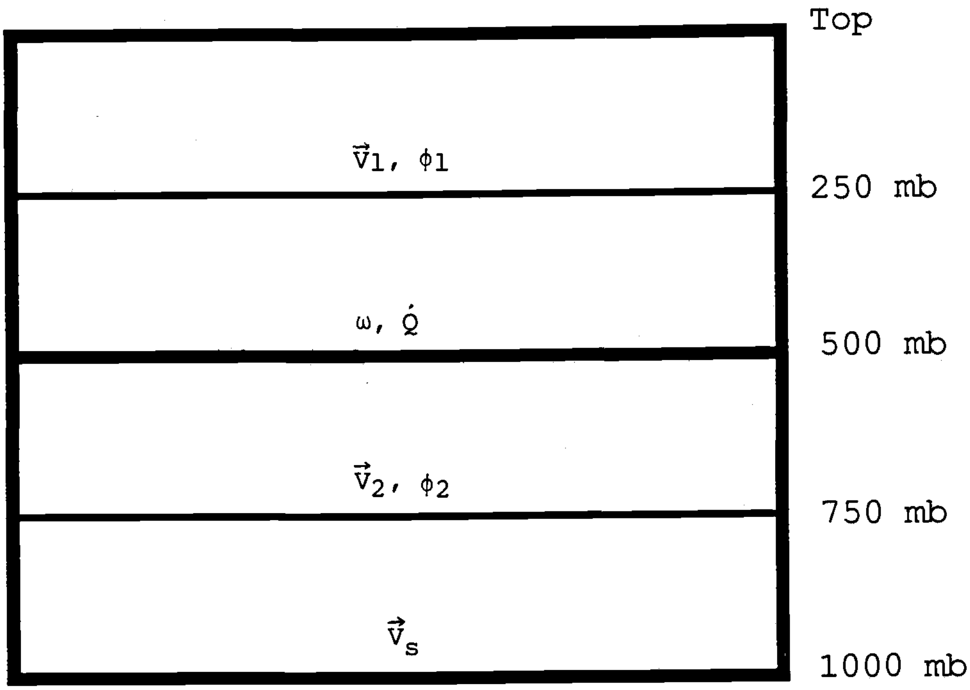

Fig.1. Vertical structure of the atmosphere model. Each layer is 500 mb thick with ω = dp/dt assumed zero at the top and bottom of the atmosphere. The vertical velocity and heating are calculated at the interface layer.

The heating and the vertical velocity are realized at the interface level. The linearized momentum equations for each layer with interlayer momentum exchange and surface frictional dissipation are as given below.

$$\frac{\partial \vec{V}_1}{\partial t} + f\hat{k}x\vec{V}_1 + \nabla\phi_1 = -k_1(\vec{V}_1-\vec{V}_2) \tag{1}$$

$$\frac{\partial \vec{V}_2}{\partial t} + f\hat{k}x\vec{V}_2 + \nabla\phi_2 = k_1(\vec{V}_1 - \vec{V}_2) - k_2\vec{V}_s \tag{2}$$

Here $\vec{V}_1$ and $\vec{V}_2$ are the horizontal velocity vectors, ϕ_1 and ϕ_2 are the geopotential heights of each layer, k_1 and k_2 are the frictional coefficients and $\vec{V}_s$ is the surface velocity.

The linearized thermodynamic equation relating the geopotential height difference between the two layers and the heating can be written as

$$\frac{\partial}{\partial t}(\phi_2-\phi_1) + \omega\, S\, \Delta p = -\alpha_0 \frac{\Delta p}{T_0} \frac{\dot{Q}}{C_p} \tag{3}$$

In deriving the above equation, the static stability S is assumed to be constant. Also, ω is assumed to be zero at the surface and at the top of the atmosphere. Assuming zero vertical velocity at the surface is a consequence of neglecting boundary layer forcing through Ekman pumping. The zero vertical velocity at the top of the atmosphere is a consequence of the free surface approximation. This results in suppressing the vertical propagation of energy. Here α_0, T_0 and C_p are the thermal expansion coefficient, the mean tropospheric temperature, and the specific heat at constant pressure of the atmosphere, respectively. The values of S, α_0, C_p and T_0 in the model are 3.2 x 10^{-7} $m^3s^4kg^{-2}$, 0.0003 K^{-1}, 1004 J kg^{-1} K^{-1} and 250 K, respectively. The heating rate $\dot{Q}$ is specified by calculating the anomalous heating from the COADS data set.

Summing equations (1) and (2) yields the first barotropic mode equation, while the difference of the two equations describes the first baroclinic mode behavior. As mentioned earlier, barotropic processes are neglected for the simulation of ENSO. Introducing $\vec{V}_d = \vec{V}_2 - \vec{V}_1$, the shear velocity of the two layers, and $\phi_d = \phi_2 - \phi_1$, the geopotential height difference, the first baroclinic mode equations are given as

$$\frac{\partial \vec{V}_d}{\partial t} + f\hat{k}x\vec{V}_d + \nabla\phi_d = -2k_1\vec{V}_d - k_2\vec{V}_s \qquad (4)$$

$$\frac{\partial \phi_d}{\partial t} + \frac{(\Delta p)^2 S}{2}\nabla.\vec{V}_d = -\frac{\alpha_0}{T_0}\frac{\Delta p}{C_p}\dot{Q} \qquad (5)$$

In going from equation (3) to (5) use is made of the continuity equation to substitute for the vertical velocity. The relevance of the above model for large-scale processes has been tested before by several authors (Zebiak,1982; Matsuno, 1966; Hirst,1985).

One potential problem with this type of linearized model is that perturbations are calculated from a zero basic state. This results in neglecting inertial effects. Hoskins and Karoly (1981), using a five layer baroclinic model, showed that for subtropical thermal forcing, the model response was insensitive to the specified zonal mean flow. Other investigators (Keshavmurthy,1983; Shukla and Wallace,1984) have verified the above result using general circulation models. However, this is not valid away from the equator where advection effects become important.

Observations in the tropics indicate that low level wind anomalies and upper atmosphere wind anomalies are remarkably out of phase as shown in Fig.2. Thus, assuming that the mean velocity field in the model is zero and linearly extrapolating the 500 mb velocity, $\vec{V}_s$ can be taken as directly proportional to $\vec{V}_d$.

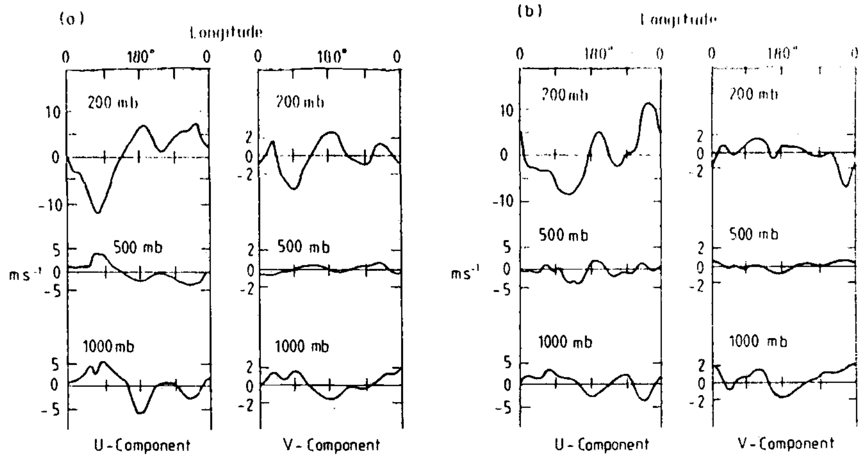

Fig.2. Observed longitudinal wind anomaly structure for (a) June, July and August mean and (b) December, January and February mean. The 1000 mb and 200 mb winds are out of phase with the 500 mb wind that is nearly zero. From Webster (1983).

The Comprehensive Ocean Atmosphere Data Set (COADS) contains monthly mean and interannual monthly mean values of several oceanic and atmospheric surface variables from the years 1946-1979. Anonymous (1984) describes in detail the compositing methods of various data sets and some statistical analysis. The data set covers the global ocean on a 2° latitude x 2° longitude grid. However, the data are sparse over the tropical oceans. The method of smoothing this data set and its use in evaluating the anomalous heating rate $\dot{Q}$ will be discussed later in this chapter.

2.3 Numerical Procedure

Equations (4) and (5) are solved numerically for various specified values of $\dot{Q}$. One of the simplest and explicit numerical procedures is the finite difference method. Stability of the numerical procedure depends upon the time step, horizontal grid spacing and the relative distribution of variables in the grid box. The Courant-Friedrichs-Lewy (CFL) condition for an elliptic partial differential equation with characteristic wave speed c states that for the numerical procedure to be stable, $c\,\Delta t/\Delta x \leq 1$ must be satisfied . Here Δt and Δx are the time step and horizontal grid space, respectively.

Studies by Winninghoff (1968), Arakawa and Lamb (1977) and Schoenstadt (1978) have shown that simulation of geostrophic adjustment processes is highly dependent upon the choice of grid scheme and the ratio of the horizontal grid size to the Rossby radius of deformation. The choice of grid scheme means the distribution of velocity and pressure variables in a grid array. The Rossby radius of deformation is a ratio of the speed of gravity waves in the atmosphere to the Earth's rotation rate and is calculated to be of order 1000 km. Hence, the Arakawa B or C grid is suitable for atmospheric models with grid spacing less than the radius of deformation. In this study the Arakawa B scheme is adopted in which the zonal and meridional velocities are evaluated at half grid points while the geopotential height is evaluated at the full grid points as shown in Fig.3.

To speed up the time integration a leap-frog time scheme is adopted. The first time step is evaluated using the Euler forward scheme as the leap-frog scheme requires a two time history. One of the disadvantages of using a leap-frog scheme throughout is the time-splitting which is inherent in this method. An Euler-backward scheme (also method called the Matsuno scheme in meteorology) is adopted every 10 time steps to suppress this computational mode.

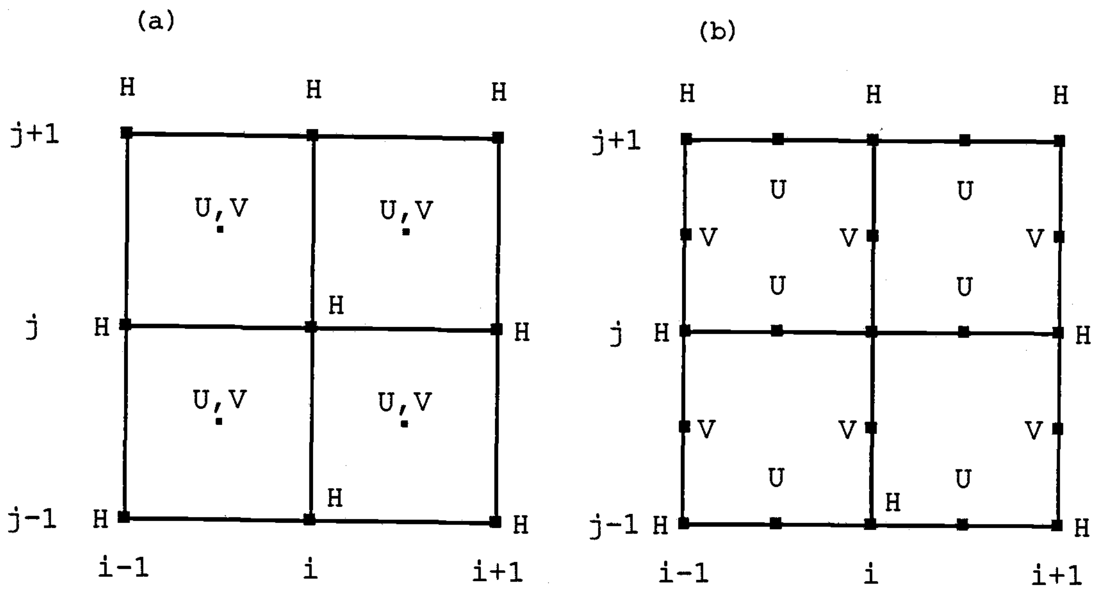

Fig.3. Stable grid schemes for atmospheric models. (a) Arakawa B-grid and (b) Arakawa C-grid. These two grid schemes are stable for grid spacing less than the Rossby radius of deformation. U,V are the horizontal velocity components and H is the pressure variable. The longitudinal and latitudinal grid point is represented by i and j, respectively.

As mentioned earlier, the domain for the model is the tropical Pacific ocean. The domain extends from 30 S to 30

N and 120 E to 120 W. This is because the largest seasonal anomalies due to atmosphere-ocean interaction are confined to the Pacific ocean. Cyclic boundary conditions are used on the eastern and western walls, while the no normal flow condition is used on the northern and southern walls.

Finite difference analogs of equations (4) and (5) are given as follows.

$$U^{n+1}_{i+\frac{1}{2},\, j+\frac{1}{2}} = U^{n-1}_{i+\frac{1}{2},\, j+\frac{1}{2}} + 2\Delta t [f_{j+\frac{1}{2}} V^{n}_{i+\frac{1}{2},\, j+\frac{1}{2}} - \frac{\phi^{n}_{i+\frac{1}{2},\, j+\frac{1}{2}} - \phi^{n}_{i-\frac{1}{2},\, j+\frac{1}{2}}}{\Delta x}$$

$$2k_1 U^{n-1}_{i+\frac{1}{2},\, j+\frac{1}{2}} - k_2 U^{n-1}_{i+\frac{1}{2},\, j+\frac{1}{2}}] \qquad (6)$$

$$V^{n+1}_{i+\frac{1}{2},\, j+\frac{1}{2}} = V^{n-1}_{i+\frac{1}{2},\, j+\frac{1}{2}} - 2\Delta t [f_{j+\frac{1}{2}} U^{n}_{i+\frac{1}{2},\, j+\frac{1}{2}} - \frac{\phi^{n}_{i+\frac{1}{2},\, j+\frac{1}{2}} - \phi^{n}_{i+\frac{1}{2},\, j-\frac{1}{2}}}{\Delta y}$$

$$+ 2k_1 V^{n-1}_{i+\frac{1}{2},\, j+\frac{1}{2}} + k_2 V^{n-1}_{i+\frac{1}{2},\, j+\frac{1}{2}}] \qquad (7)$$

$$\phi^{n+1}_{i,j} = \phi^{n-1}_{i,j} - 2\Delta t\{ \frac{(\Delta p)^2 S}{2} (\frac{U^n_{i+\frac{1}{2},j} - U^n_{i-\frac{1}{2},j}}{\Delta x} + \frac{V^n_{i,j+\frac{1}{2}} - V^n_{i,j-\frac{1}{2}}}{\Delta y})$$

$$+ \frac{\alpha_0}{T_0} \frac{\Delta p}{C_p} \dot{Q}_{i,j}\} \tag{8}$$

$$U^{n+1}_{*i+\frac{1}{2},j+\frac{1}{2}} = U^n_{i+\frac{1}{2},j+\frac{1}{2}} + \Delta t[f_{j+\frac{1}{2}} V^n_{i+\frac{1}{2},j+\frac{1}{2}} - \frac{\phi^n_{i+\frac{1}{2},j+\frac{1}{2}} - \phi^n_{i-\frac{1}{2},j+\frac{1}{2}}}{\Delta x}$$

$$- 2k_1 U^n_{i+\frac{1}{2},j+\frac{1}{2}} - k_2 U^n_{i+\frac{1}{2},j+\frac{1}{2}}] \tag{9}$$

$$V^{n+1}_{*i+\frac{1}{2},j+\frac{1}{2}} = V^n_{i+\frac{1}{2},j+\frac{1}{2}} - \Delta t[f_{j+\frac{1}{2}} U^n_{i+\frac{1}{2},j+\frac{1}{2}} + \frac{\phi^n_{i+\frac{1}{2},j+\frac{1}{2}} - \phi^n_{i+\frac{1}{2},j-\frac{1}{2}}}{\Delta y}$$

$$+ 2k_1 V^n_{i+\frac{1}{2},j+\frac{1}{2}} + k_2 V^n_{i+\frac{1}{2},j+\frac{1}{2}}] \tag{10}$$

$$U^{n+1}_{i+\frac{1}{2},\, j+\frac{1}{2}} = U^{n}_{i+\frac{1}{2},\, j+\frac{1}{2}} + \Delta t\Big[f_{j+\frac{1}{2}} V^{n+1}_{*i+\frac{1}{2},\, j+\frac{1}{2}} - \frac{\phi^{n}_{i+\frac{1}{2},\, j+\frac{1}{2}} - \phi^{n}_{i-\frac{1}{2},\, j+\frac{1}{2}}}{\Delta x}$$

$$- 2k_1 U^{n+1}_{*i+\frac{1}{2},\, j+\frac{1}{2}} - k_2 U^{n+1}_{*i+\frac{1}{2},\, j+\frac{1}{2}}\Big] \tag{11}$$

$$V^{n+1}_{i+\frac{1}{2},\, j+\frac{1}{2}} = V^{n}_{i+\frac{1}{2},\, j+\frac{1}{2}} - \Delta t\Big[f_{j+\frac{1}{2}} U^{n+1}_{*i+\frac{1}{2},\, j+\frac{1}{2}} + \frac{\phi^{n}_{i+\frac{1}{2},\, j+\frac{1}{2}} - \phi^{n}_{i+\frac{1}{2},\, j-\frac{1}{2}}}{\Delta y}$$

$$+ 2k_1 V^{n+1}_{*i+\frac{1}{2},\, j+\frac{1}{2}} + k_2 V^{n+1}_{*i+\frac{1}{2},\, j+\frac{1}{2}}\Big] \tag{12}$$

Here the superscript represents the time step while the subscripts refer to the grid points. Please note from Fig.2 that for the B-grid scheme, the velocity grid points are different from the geopotential height grid points. Equations (6), (7) and (8) represent the leap-frog scheme while equations (9), (10), (11) and (12) represent the Euler-backward scheme. The starred equations represent the predictor step in the Euler-backward scheme. The initial conditions used are zero velocity anomalies and a uniform height field of 9.8×10^5 geopotential meters. The grid resolution is 4° longitude by 1° latitude giving Δx= 450 km and Δy= 112 km on the spherical Earth. After experimenting with various k_1 and k_2 and timesteps Δt, values of $k_1 = 3.0 \times 10^{-5}\ s^{-1}$, $k_2 = 2.5 \times 10^{-4}\ s^{-1}$ and Δt= 30 min., respectively, were found to be stable. In the next section, the model simulations are compared with observations and with other results for reasonableness.

2.4 Model Simulations

1) Symmetrical heat source

The Tropics are one of the regions of greatest anomalous heating rates on the globe. Most of this heating is realized in the atmosphere in the form of latent heat release. The narrow ascending branch of the Hadley cell occurs in the form of the intertropical convergence zone (ITCZ) with cores of large cumulonimbus clouds. To examine the anomalous velocity field, the atmosphere model was run by specifying a narrow region of heat source placed symmetrically on the equator and at 180 E. The maximum heating was 1200 W m^{-2}, decreasing to zero linearly within

3 grid boxes in both directions from the center.

Figure 4a shows the steady state model lower-layer velocity field. The upper-layer velocity in such linearized two-layer models will be exactly opposite to the lower-layer flow field; hence, only the lower-layer fields will be presented for all simulations. The heating in the tropical troposphere raises the geopotential height difference in the column. Geostrophic adjustment is then realized through convergence in the lower layer and divergence in the upper layer. The characteristic waves associated with this adjustment process are the eastward propagating Kelvin waves and the westward propagating Rossby waves. In equatorial areas the wave speed for the Rossby wave is almost two-thirds that of the Kelvin wave speed. Thus, information passes eastward faster than it propagates to the west. This can be checked in the model, for example by considering a time series of the zonal velocity at two symmetrical points far away from the heating region on either side. Such an analysis has confirmed the model's ability to simulate the waves correctly.

One of the faults of linear models is symmetrical

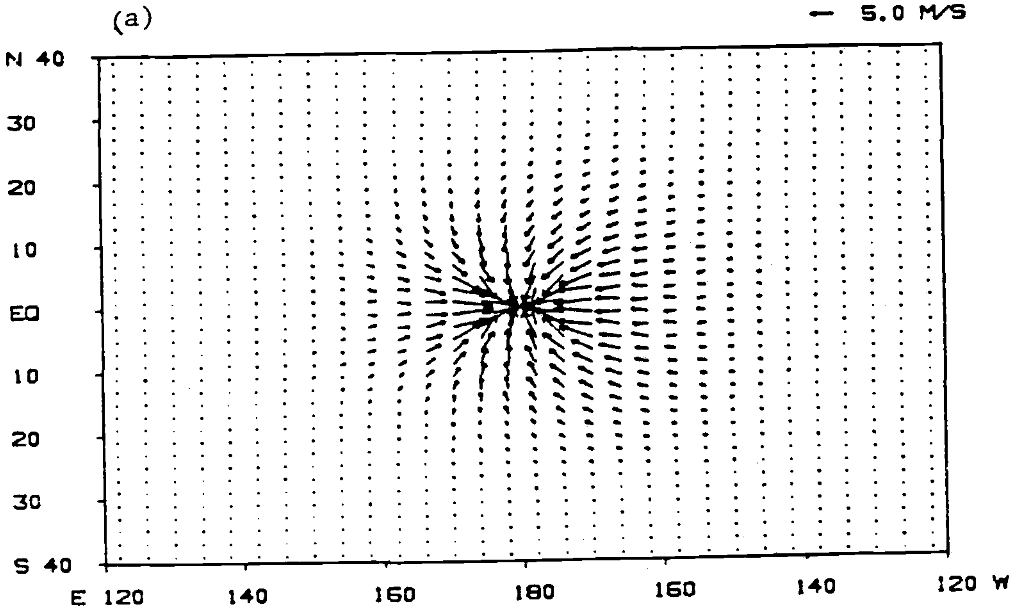

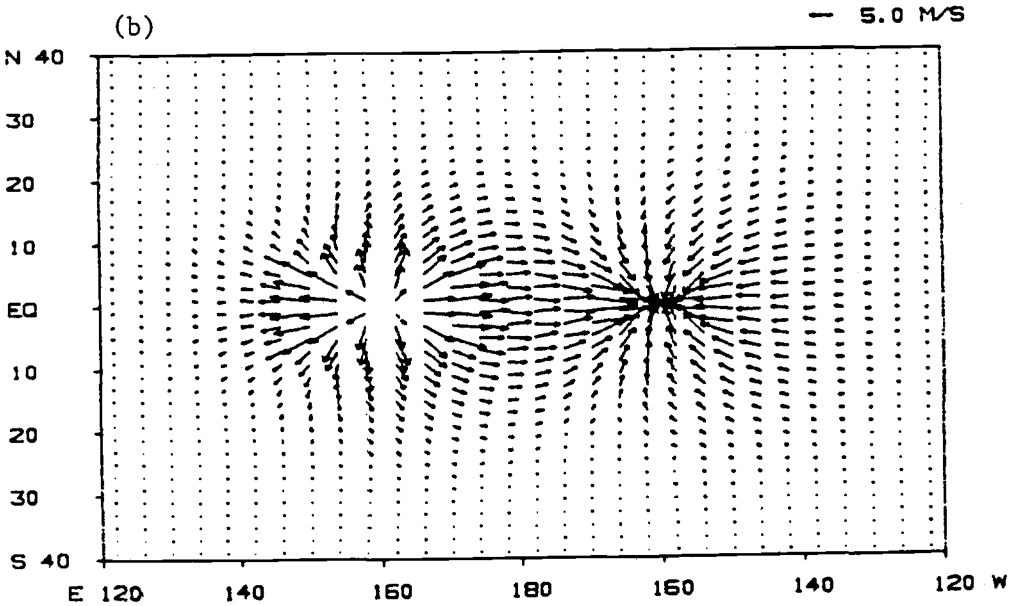

Fig.4. Model simulations for prescribed (a) heat source located on equator and 180 E; (b) heat source-sink dipole located 22 deg. on either side of 180 E and the equator.

(c)

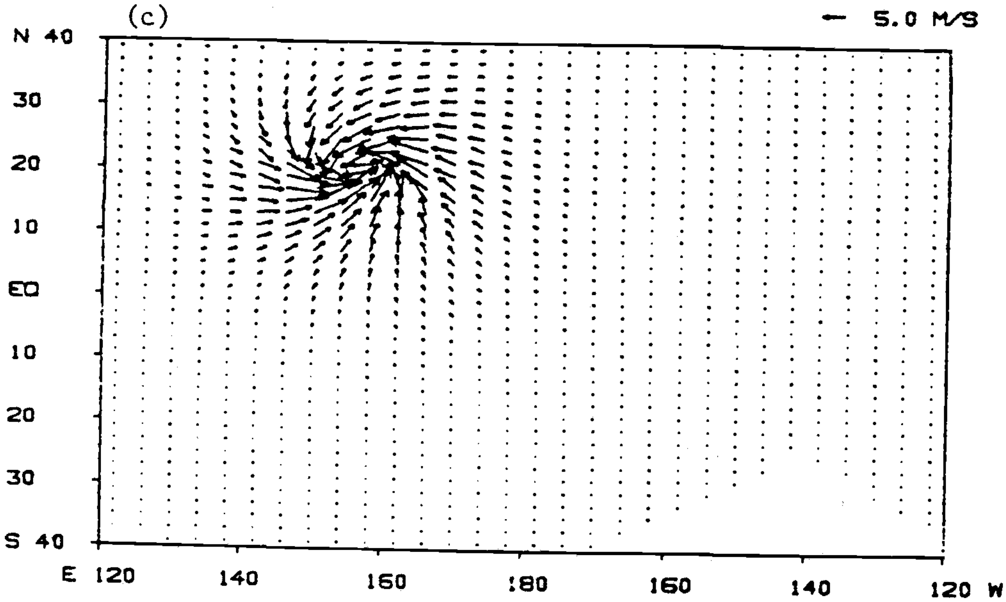

Fig.4. (cont'd). (c) heat source located at 22 N and 154 E.

response relative to a forcing. Though the model correctly simulates the adjustment process, the intensities of the field are not correct. Observations indicate that easterlies east of the forcing are weaker than those the model simulates. This has also been noticed by other investigators. Zebiak (1982) suggests a convergence feedback mechanism to simulate the actual easterlies more adequately.

2) Heat dipole

One of the characteristics of ENSO is anomalous precipitation in the central and eastern Pacific and low precipitation over the western ocean. This suggests the presence of a heat dipole with a heat source over the eastern ocean and a heat sink over the western ocean. In the case of Fig.4b such a dipole was prescribed by placing it symmetrically on the equator and 20° on either side of 180 E. The maximum heating was the same as that used in Fig.4a. As expected, the geopotential height increases in the region of the heat source and decreases in the region of heat sink. The corresponding anomalous pressure field is high around the heat sink and low around the heat source.

This results in a west-east current between the sink and source. Matsuno (1966) analysed a similar equatorial model with a mass source-sink. Comparison of Fig.4b to his results indicates that a heat sink is analogous to a mass source, and a heat source is analogous to a mass sink.

One of the consequences of this result to ENSO is the possibility of a positive feedback mechanism. A small strength dipole during the initial stages of ENSO could grow rapidly through advection of moisture from the western ocean and convergence in the eastern ocean, leading to large scale instability. While the model suggests an infinitely growing instability, in the real atmosphere negative feedback mechanisms reduce the instability rapidly after about a year.

3) Asymmetrical heat source

Until now the model response to symmetrical forcing has been examined. In the real atmosphere the forcing is not always symmetrical. For completeness the asymmetrical model response to asymmetrical forcing will now be examined. Observations, especially satellite photographs, indicate that the ITCZ is located north of the equator.

Moreover, the position of the ITCZ exhibits a seasonal cycle. In the winter the approximate location of ITCZ is 12 N while in the summer it is at 8 N. The model response to such an asymmetrical forcing is given in Fig.4c. A similar heat source is used as in experiment 1, but now centered at 22 N and 154 E. The effect of Coriolis force is dominant for this type of asymmetric forcing. The turning of the flow to the right as it crosses the equator from the south is due to the change in the sign of the Coriolis parameter. The anticyclonic circulation around the heat source in the Northern Hemisphere corresponds well to the theory. To adjust to the increase of geopotential height due to the heating, the flow is convergent in the lower layer. Once the fluid is in motion, it turns to the right in the Northern Hemisphere under the influence of Coriolis acceleration, giving an anticyclonic circulation.

4) Latent heat forcing

Having determined the model behavior to simple forcings to be consistent with theory, it would be instructive and revealing to test the model parameterizations. Latent heating is the single most important forcing for large scale motions in the tropics. Latent heat release is closely associated with low-level moisture convergence, and due to non-linearity it is difficult to parameterize. Therefore, the success of the model depends to a large extent on the success of correct parametrization. The parameterization used here follows the one used in the CISK theory which relates the heating to low-level convergence. The latent heating rate is given as

$$\dot{Q}_L = -\eta \, C_p \frac{\partial \theta}{\partial p} \, \omega \qquad (13)$$

where

η = 1.1, a constant of proportionality

C_p = 1004 J kg^{-1} K^{-1}, the specific heat of air

$\partial\theta/\partial p$ = $3x10^{-4}$ K m^2 N^{-1}, a constant related to the mean stability of the atmosphere

ω is the pressure vertical velocity given by low-level convergence as $\omega = \Delta p \, \nabla . \vec{V}_S$ (14)

Equation (13) is used only when ω is negative, corresponding to low-level convergence. If ω is positive then $\dot{Q}_L$ is zero.

The above parameterization of latent heating is believed to be representative of the true atmospheric processes. It will be shown that this type of parameterization captures the essentials of heating in the tropics during ENSO. One of the drawbacks of this parameterization is that the effects in the model are localized. In other words, if there is low-level convergence then the latent heat is realized in the model instantly. In the real atmosphere feedback mechanisms prevent condensation for weak convergence. One of the consequences of neglecting these feedback mechanisms is symmetry of model behavior. Zebiak (1986) has shown that including such a mechanism improves the model response. The purpose of the present study was to test the new parameterization and its characteristics. Therefore, no feedback mechanisms were included. Neglect of this time lag is not critical in regions of deep convection.

As mentioned earlier, the COADS data set contains the monthly mean as well as the long-term monthly mean surface wind vector data for 1946-1979 over the global ocean. A subset of January and July interannual monthly mean data, applicable to the present model domain, was used to evaluate the latent heat release in this run. The data gaps in the southern ocean were filled by the zonal mean value at that latitude. Next, to smooth the data a nine point filter as in the OSU GCM was used. After calculating the latent heat release for January and July from equation (13), the model was run for these prescribed forcings. Fig.5(a,b,c,d) shows the surface wind vector from the COADS data, the latent heating rate as calculated by equation (13), the lower-layer model wind, and the lower-layer model divergence field, respectively, for the month of January. Figure 6 gives the same data for July.

In Figs.5a and 6a the strong trades and the corresponding convergence region known as the ITCZ is clearly marked. The southerly shift of the ITCZ from winter to summer is noticeable. Figures 5b and 6b indicate the strong latent heating in the regions of the ITCZ and the South Pacific Convergence Zone (SPCZ). The seasonal shift in the mean position of the ITCZ is also visible in the latent heating. The order of magnitude of the heating is 10 K per day, similar to observations in the tropics. This suggests that the parameterization for the latent heating is realistic, and is able to capture the salient characteristics of tropical atmospheric heating.

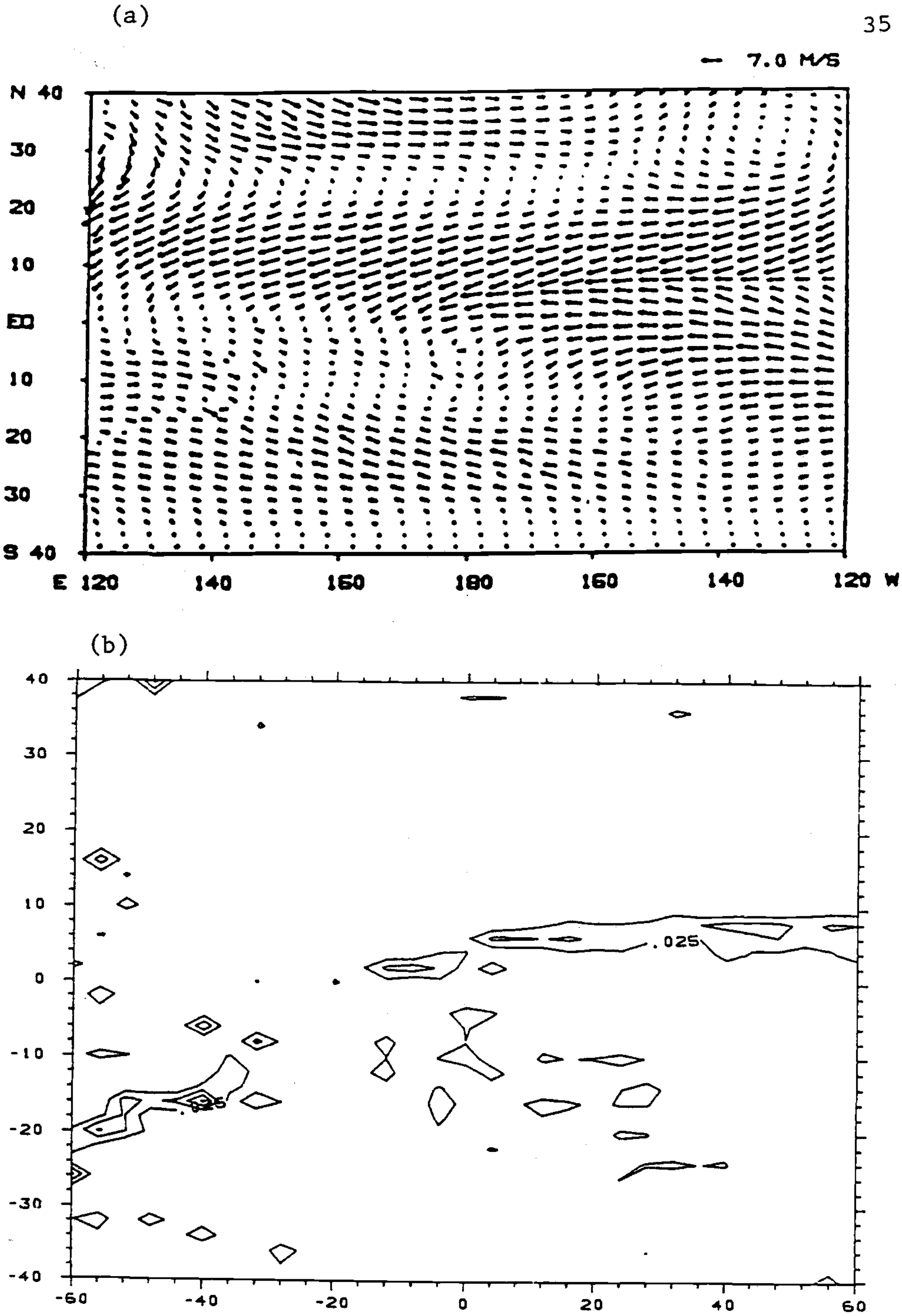

Fig.5. The latent heating parameterization for January: (a) observed interannual monthly mean wind vector from COADS data; (b) latent heat calculated by equation (13). Contour interval is 0.02 J/kg s.

(c)

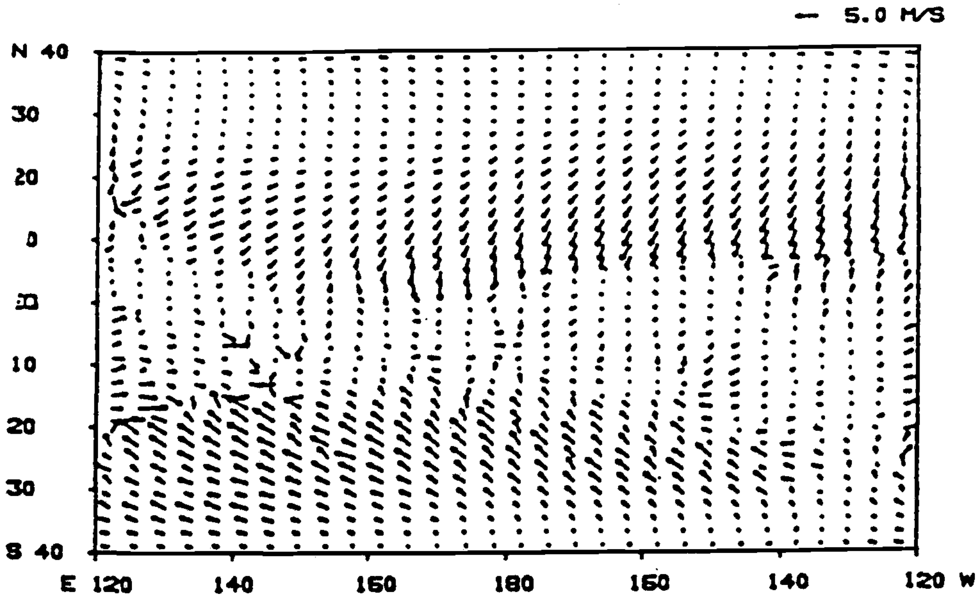

(d)

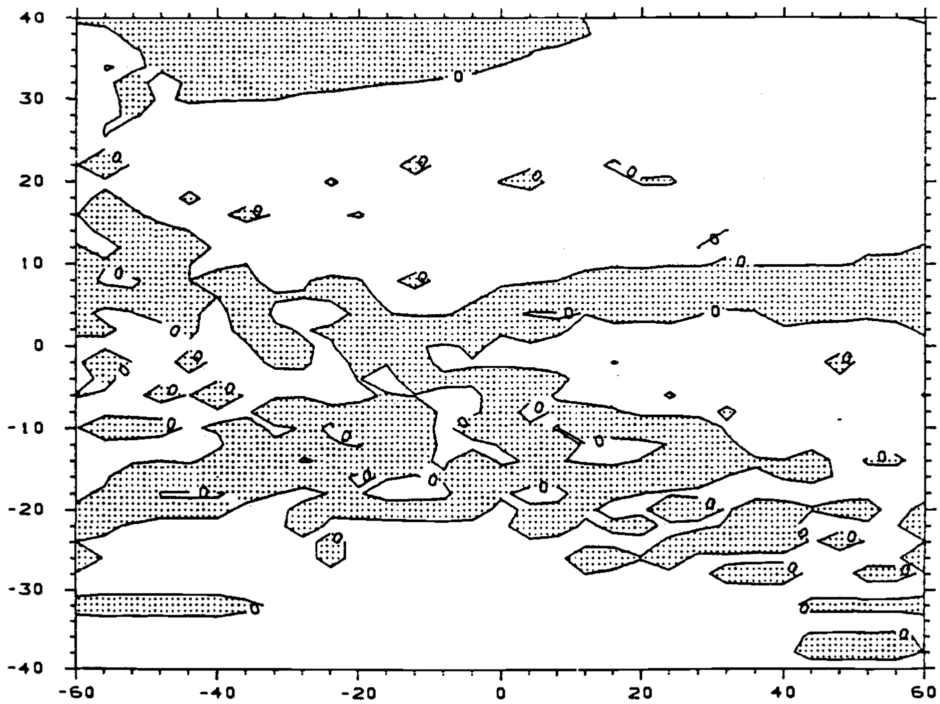

Fig.5. (Cont'd).(c) simulated wind field for heating given in(b);(d) simulated divergence field.Only zero divergence is contoured. Regions of convergence are stippled.

(a)

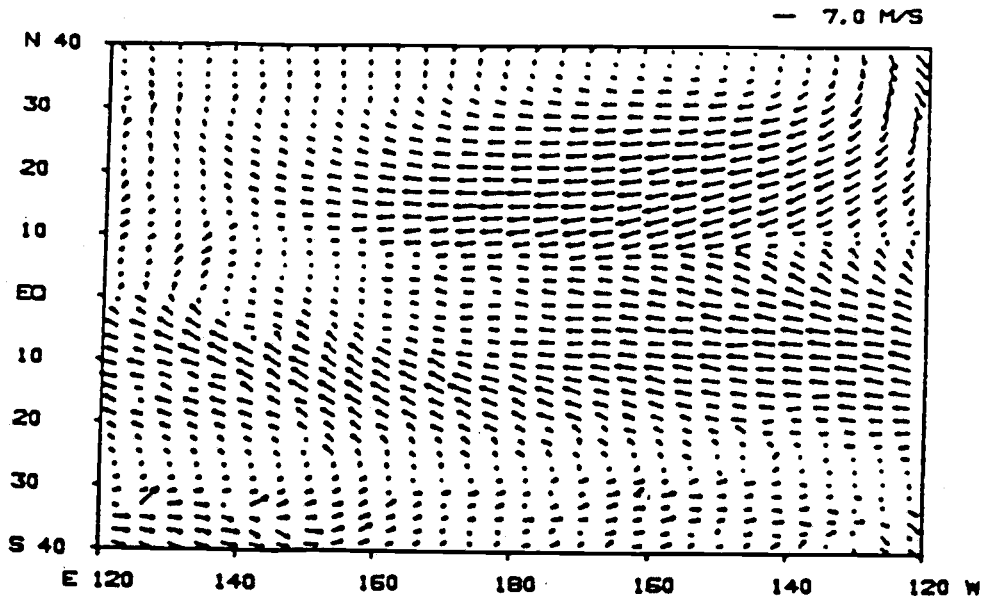

(b)

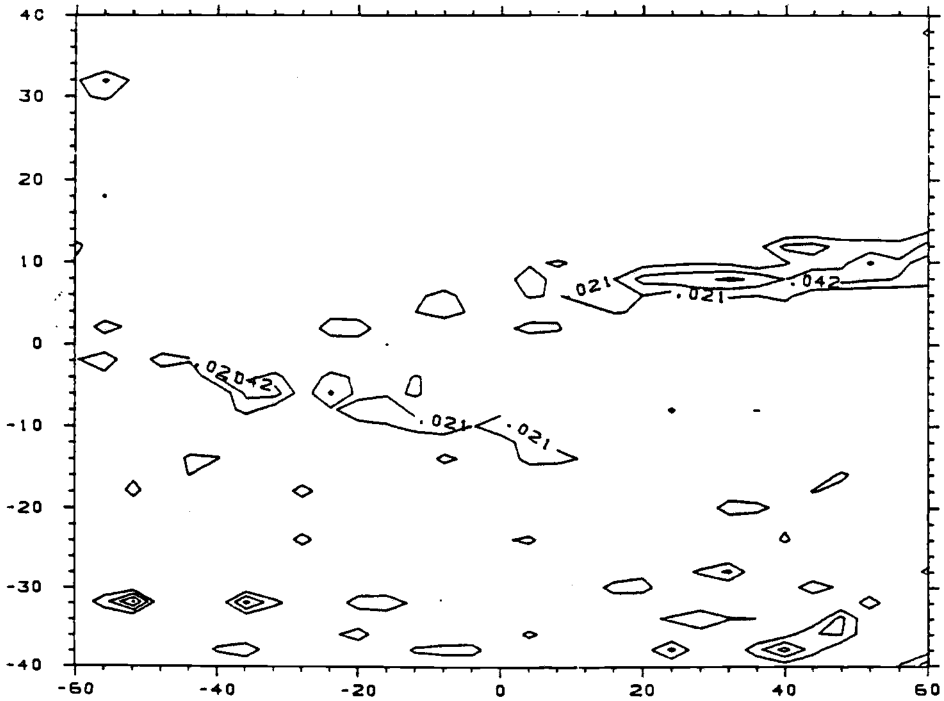

Fig.6. Same as in Fig.5 except for July.

(c)

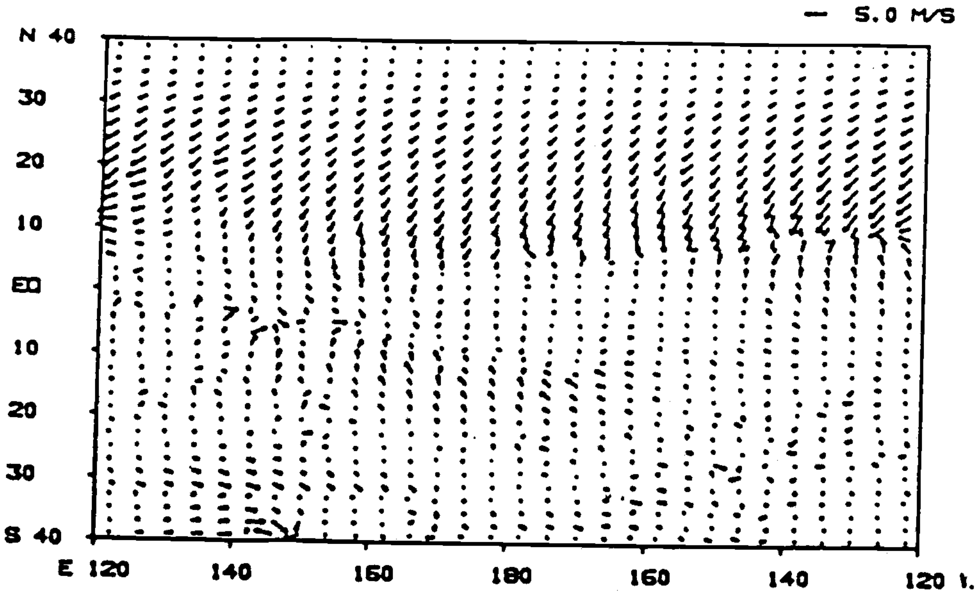

(d)

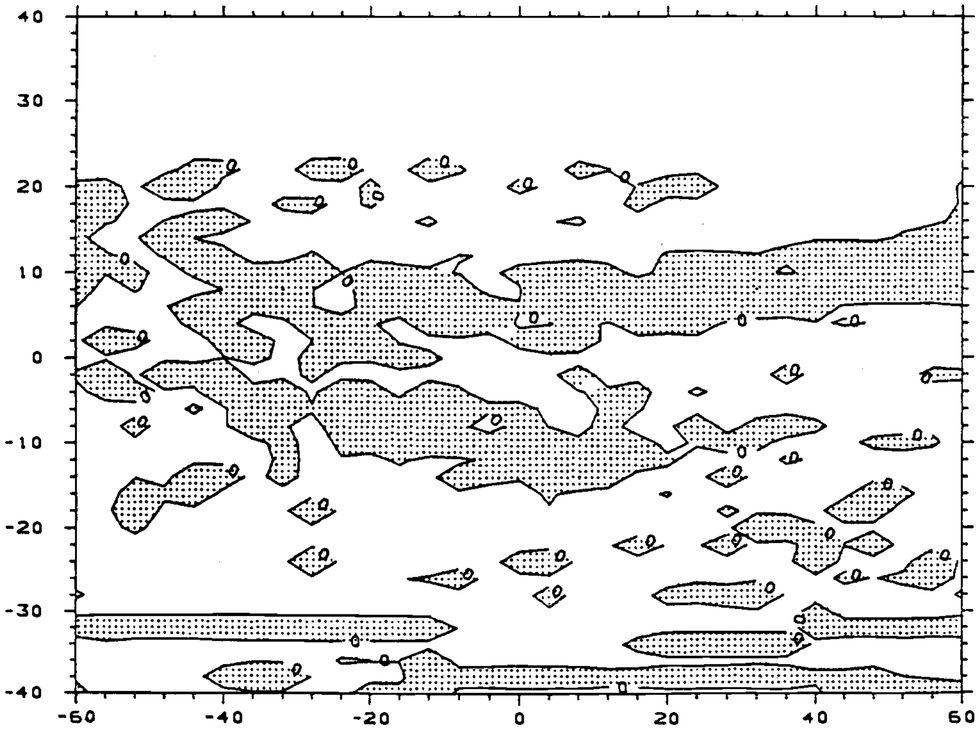

Fig.6 cont'd.

The model flow field is given in Figs.5c and 6c. These figures cannot be compared directly with those in Figs.5a and 6a; since mentioned earlier, the model is a linear perturbation model and hence cannot simulate the mean field correctly. However, there are certain similarities of the simulated field with the observed field. The general agreement of the model's position of the ITCZ and the SPCZ with that observed is specially notable. This suggests that the model's lower-layer flow field is related to the surface field in the sense of capturing the regions of strong convergence. This is clearly visible when comparing the fields in Figs.5d and 6d with those of Figs.5b and 6b, respectively. The lower-layer model divergence is very similar to the latent heating.

This run shows that the parameterization is able to capture the characteristics of latent heating, and that the model response is as expected when we recall that inear models are only perturbation models and therefore cannot simulate the mean field.

5) Anomalous forcing

From the previous run it was found that the model cannot simulate the mean field. But can it simulate the observed perturbation field? The atmospheric model presented here is expected to simulate the response of the tropical atmosphere during ENSO. Since the solar radiation cannot be parameterized in terms of the model variables, it is neglected. The sensible heat flux is ,however, included in addition to the latent heating. Significantly, during the period of the COADS data particularly strong ENSO events occurred in the years 1957, 1965 and 1972. These ENSO events exhibited many common features of the warm event and some distinct individual characteristics. Figure 7 shows the time series of the SST at Puerto Chicama (7° S) along with the annual cycle for these ENSO years. This figure, taken from Wyrtki (1975), shows that all these events appear to be closely related to the annual cycle. The 1957 event exhibited three different peaks in SST of almost the same magnitude. It was the longest lasting warm event and took close to two years to return to normal. In 1965 there was only a single peak in SST anomaly and thereafter the SST never went above the annual cycle. The

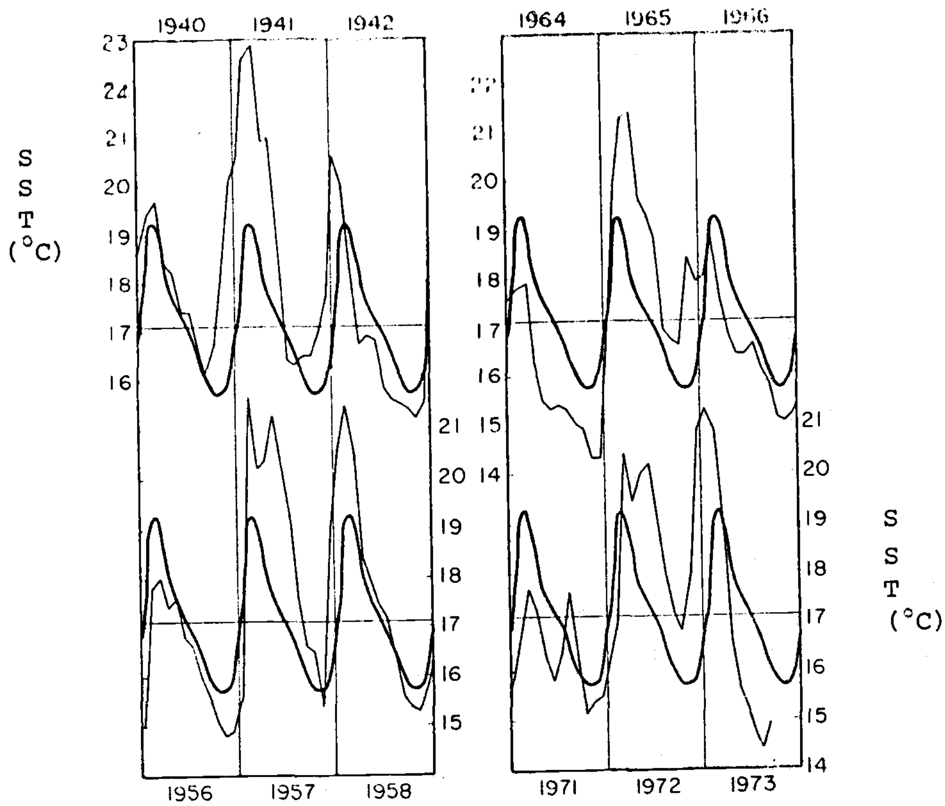

Fig.7. SST time distribution at Puerto Chicama (7 S) along the coast of South America for four El Nino events (thin line) along with the annual cycle (thick line). The 1957, 1965 and 1972 events are examined in this study. COADS data does not cover the 1941 event. From Wyrtki (1975).

1972 event exhibited three peaks in SST anomaly as in 1957, but the magnitude of the third peak in early January 1973 was at least 2 C higher than the other two peaks, and the SST anomaly decreased rapidly thereafter. Ramage (1975) and Wyrtki (1975) discuss the characteristics and analysis of these warm events.

Utilizing the COADS data, the perturbation forcing field is calculated. The simplest dynamically consistent method of getting the perturbation field is to subtract out the long term mean field from the monthly field. This is to be done with utmost caution because the small scale structure present in the data might get amplified in this process, making it difficult to identify large scale structure in the perturbation field. Therefore, each component of the forcing was smoothed using a nine point filter after filling the data gaps by the zonal mean value at that latitude. The anomalous heating was calculated by adding the sensible heat flux to the atmospheric latent heat release. The sensible heat flux was calculated using the bulk aerodynamic formula given by

$$Q_S = \rho_a C_H \, C_p \, |\vec{V}_s| (T_s - T_a) \qquad (15)$$

where

$\rho_a = 1.225$ kg m^{-3} is the density of air

$C_H = 0.0015$ is the bulk mixing coefficient

$T_s - T_a$ is the sea-air temperature difference

$|\vec{V}_s|$ is the magnitude of surface wind.

This is the same bulk formula used in the OSU GCM and by several other workers (e.g., Leetmaa,1983).

The latent heat release is as given in equation (13). The above heat fluxes are converted to heating rates by multiplying by $g/2\Delta p$. The total heating rate for the atmosphere is given by

$$\dot{Q} = \dot{Q}_L + \dot{Q}_S \qquad (16)$$

Finally, the anomalous heating rate is given by subtracting the total heating rate of the interannual monthly mean from the monthly mean data.

The model was run by forcing it with the anomalous heating as calculated above for the ENSO years of 1957, 1965 and 1972. For each of these years, the model was tested for four periods during the event. January of 1957, 1965 and 1972 correspond to the onset phase of El Nino during which the SST anomalies are limited to the eastern ocean. July of the same years correspond to the peak phase during which the SST anomalies along the coast of Peru reach their maximum and SST anomalies start to appear in the central ocean. The January simulations of the following year are for the mature phase of the warm event. By this time the SST anomalies are widespread in the western and central Pacific ocean. The July of the same year corresponds to the retrieval phase when the anomalies are rapidly decreasing and returning the conditions to normal. Each phase is discussed below by comparing it with observations from the COADS data and by analysing the successes and limitations of the model.

i) Onset Phase

Figures 8 a and b show the observed anomalous wind field and model simulated wind field, respectively, for January of 1957. Figures 8 c,d and e give the observed SST anomaly, calculated heating field and the simulated divergence. Figure 9 follows the same sequence for January 1965 and Fig.10 is for January 1972. A narrow band of weak westerlies along the equator over the eastern ocean is observed in all the ENSO years. However, a wide band of

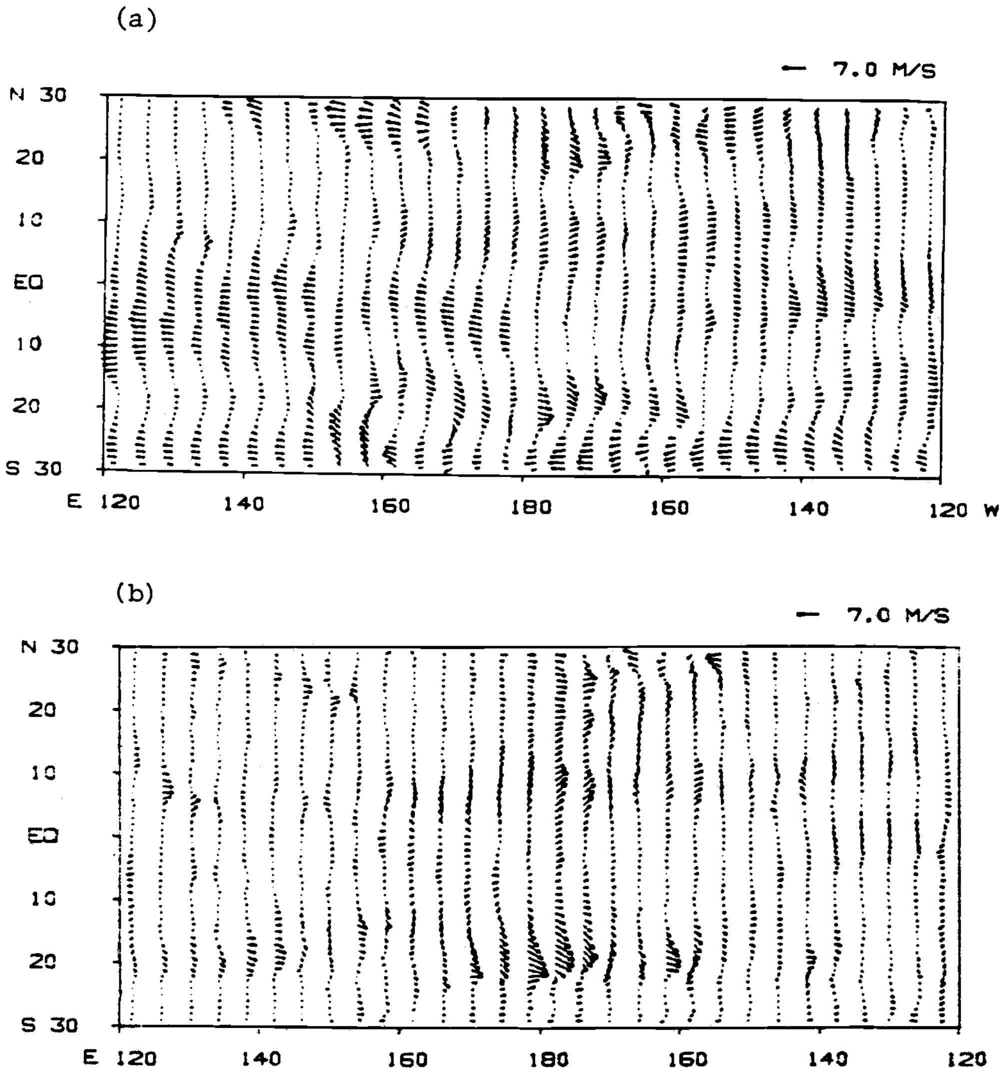

Fig.8. The onset phase: (a) observed wind anomalies for January 1957 from COADS data. (b) model lower layer simulation for the same period.

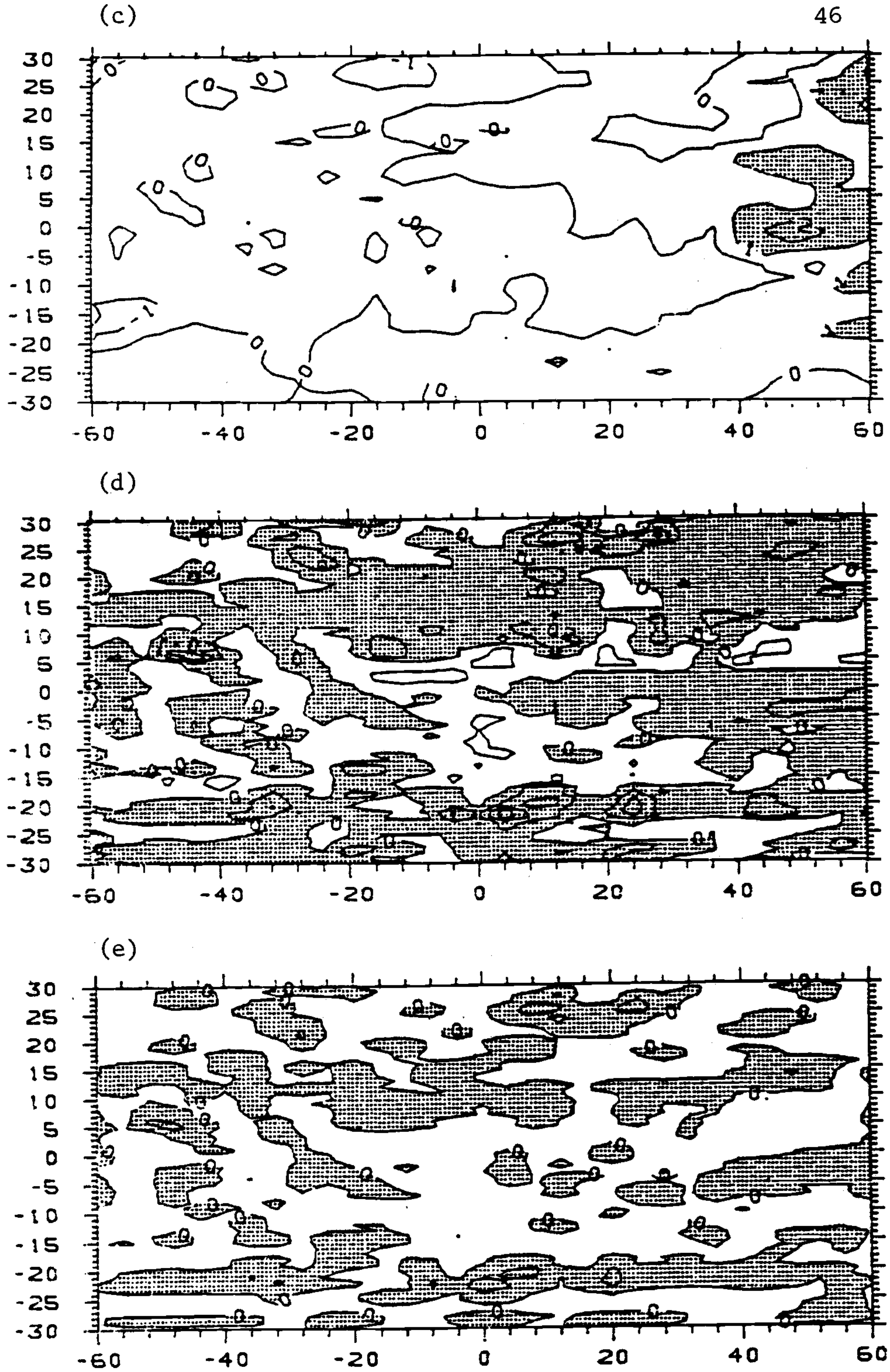

Fig.8 (cont'd.) (c) observed SST anomaly. Contour interval is 1^0C. Anomaly greater than 1^0 is stippled. (d) calculated heating rate anomaly. Contour interval is 0.02 J/kg s, Region of positive anomaly is stippled.
(e) model divergence field. Contour interval is 1.0E-5 s^{-1}. Region of convergence is stippled.

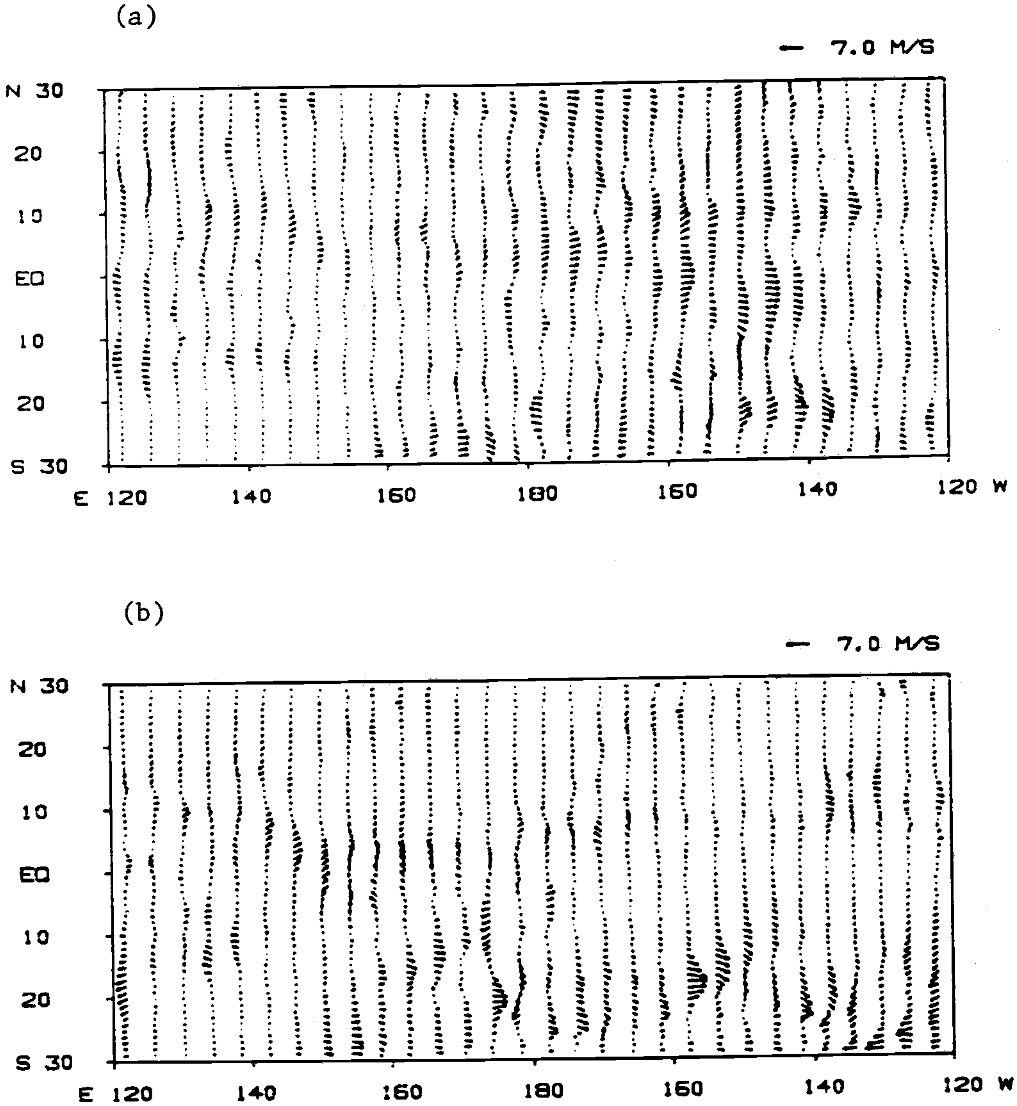

Fig.9. Same as in Fig.8 except for January 1965.

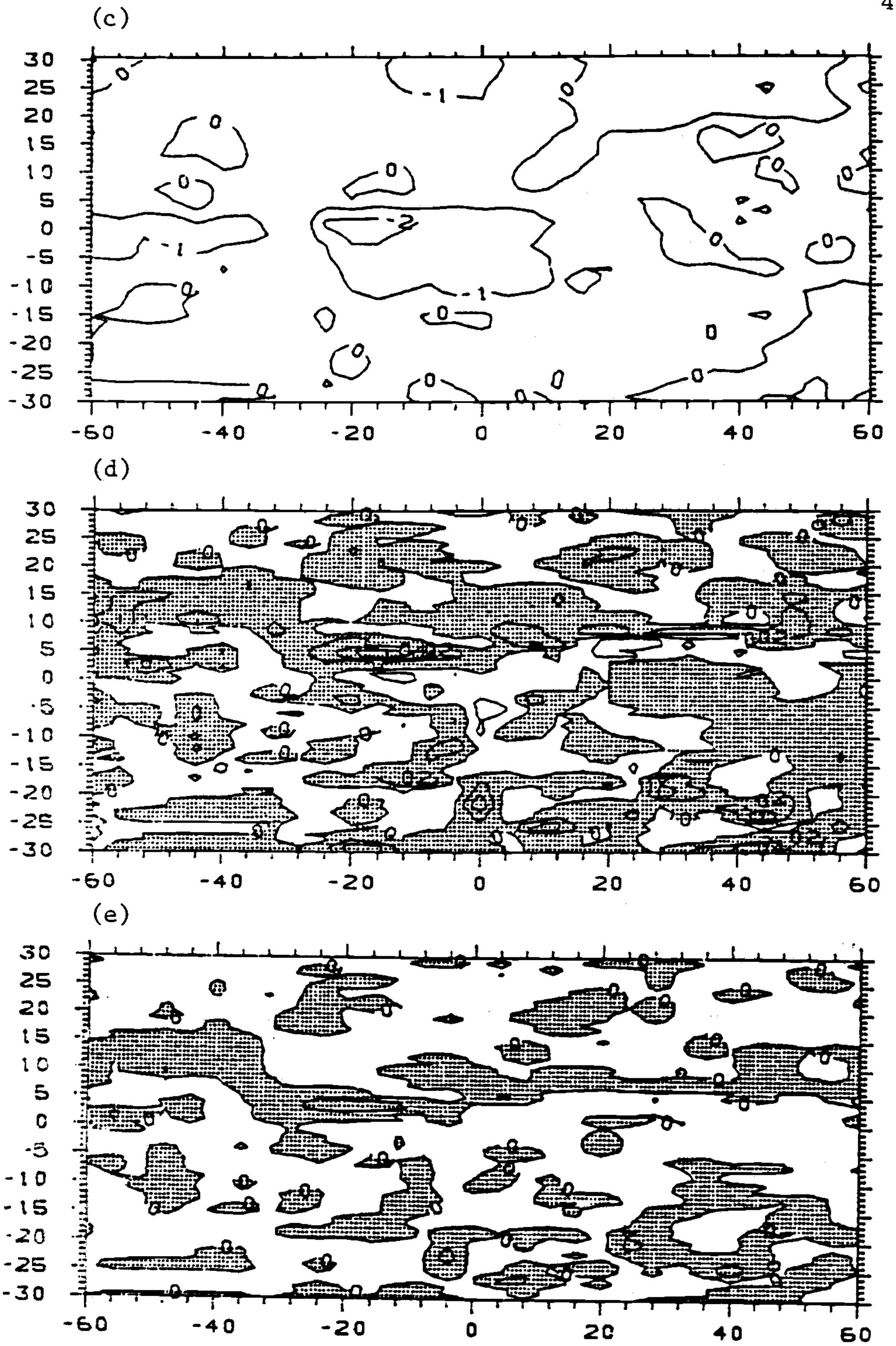

Fig.9 (cont'd.) Same as in Fig.8 except for January 1965.

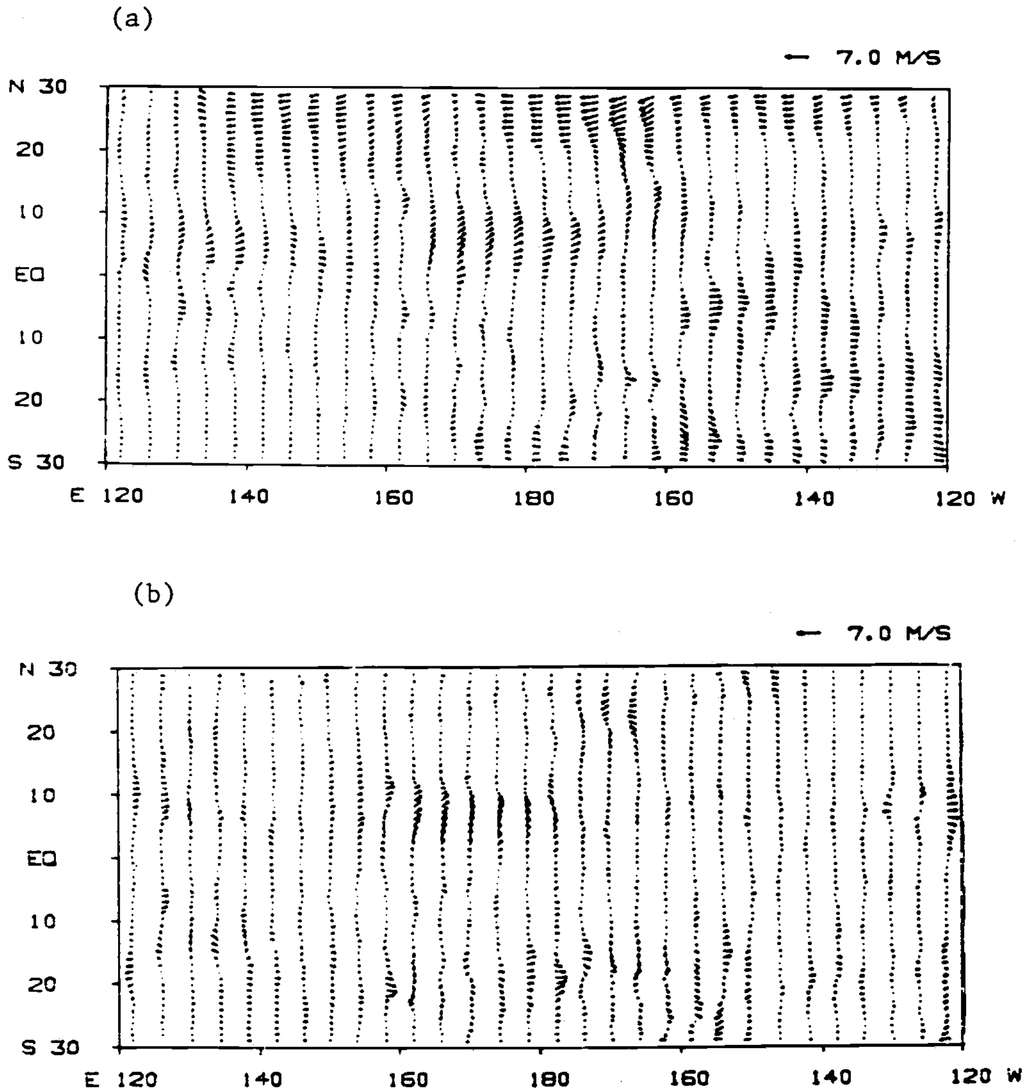

Fig.10. Same as in Fig.8 except for January 1972.

(c)

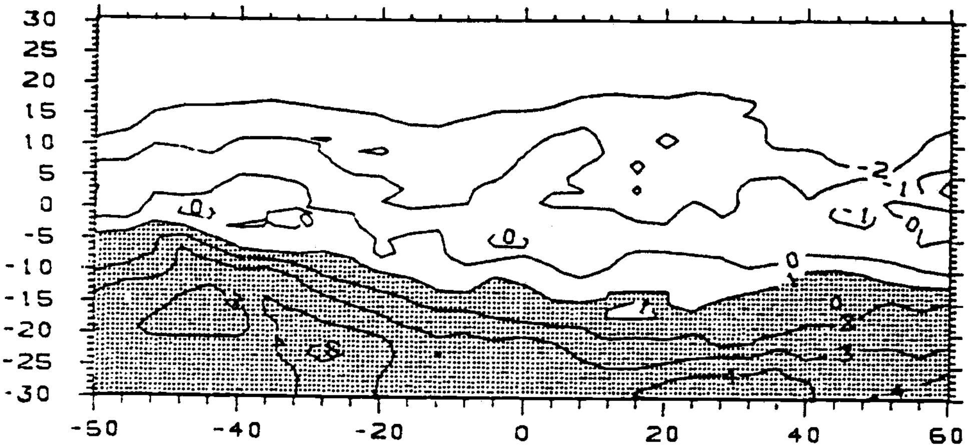

(d)

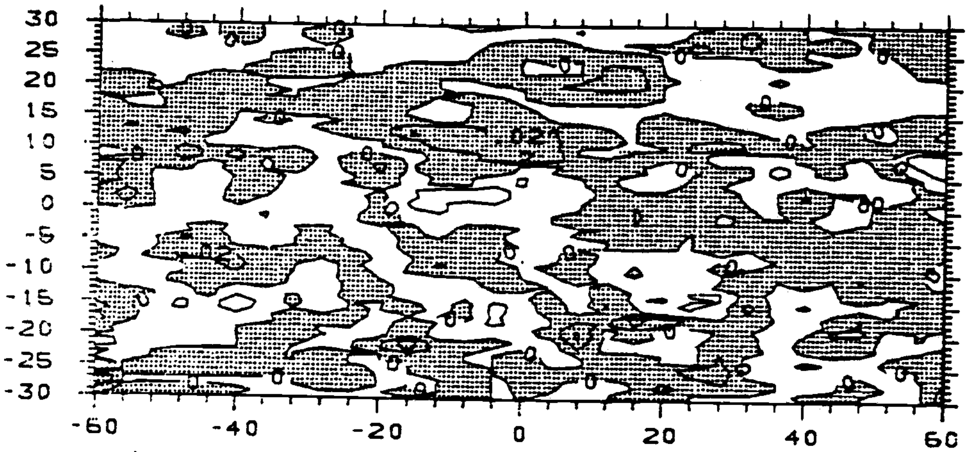

(e)

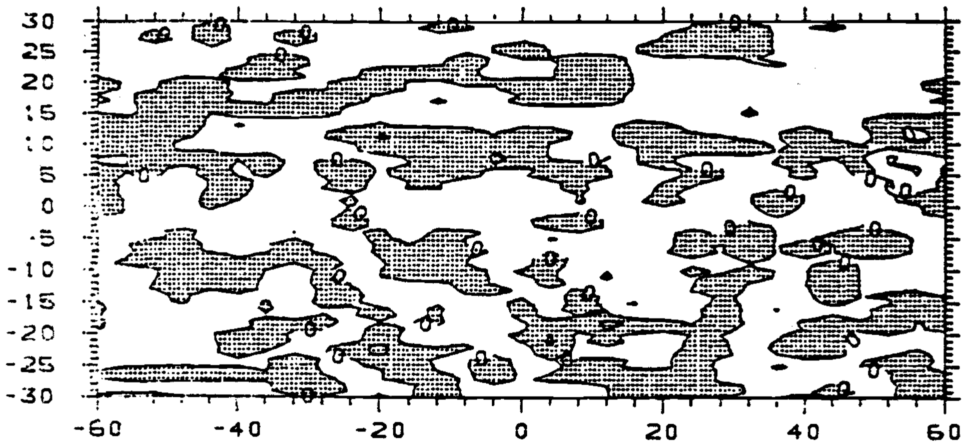

Fig.10. Same as in Fig.8 except for January 1972.

strong easterlies over the western and the central Pacific is seen only in the 1957 event. This is related to the stronger SST anomalies at this time in the 1957 event. The simulated wind field compares well with the observed anomalies in all the years. The magnitude of the simulated wind is less than the observed in all the years. For the 1957 event, the model fails to simulate the strong westerlies over the western ocean, while in the 1965 and 1972 simulations the easterlies over the eastern ocean are very weak. The model is able to capture the regions of convergence and the direction of the wind specially well in the central Pacific.

The model simulations are not good beyond 20° on either side of equator. This is to be expected as the present linear model is an equatorial model which cannot simulate extratropical winds. In higher latitudes non-linear advection terms are important but are absent in this model.

As seen from the SST anomaly field, only the 1957 event exhibits strong anomalies at this time in the eastern ocean along the coast of Peru. As mentioned earlier the onset phase is characterized by small SST anomalies in the eastern ocean. A strong heating anomaly along the equator is seen at 160 E corresponding to the strong convergence there. The simulated model divergence follows very closely to the heating field. This is seen in all the phases of these three El Nino events. This suggests that the model is able to simulate the regions of convergence correctly even if the simulated velocity field is not correct. One of the reasons for the velocity simulations to be wrong is the symmetrical response of linear models relative to a forcing.

ii) Peak Phase

Figures 11, 12 and 13 give the same fields except for July of 1957, 1965 and 1972, respectively. The region of stronger westerlies has increased in all the years with a narrow region of easterlies just north of the westerlies in the eastern ocean. Over the northwestern ocean stronger easterlies appear in 1957 and 1965, while stronger westerlies merging with the westerlies in the east are observed in 1972. The simulated wind field is again weaker than the observed anomalies. The model simulations are not good in the eastern region but compare well with the observations in the west and central Pacific.

(a)

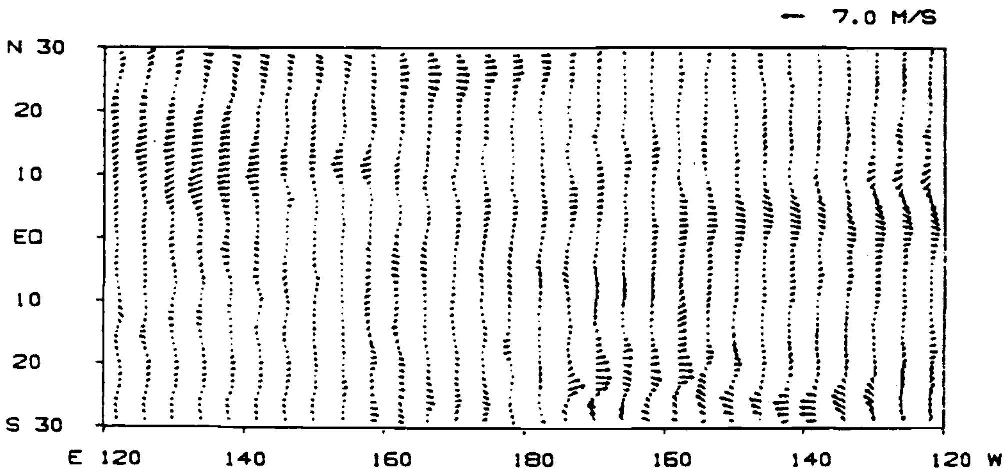

(b)

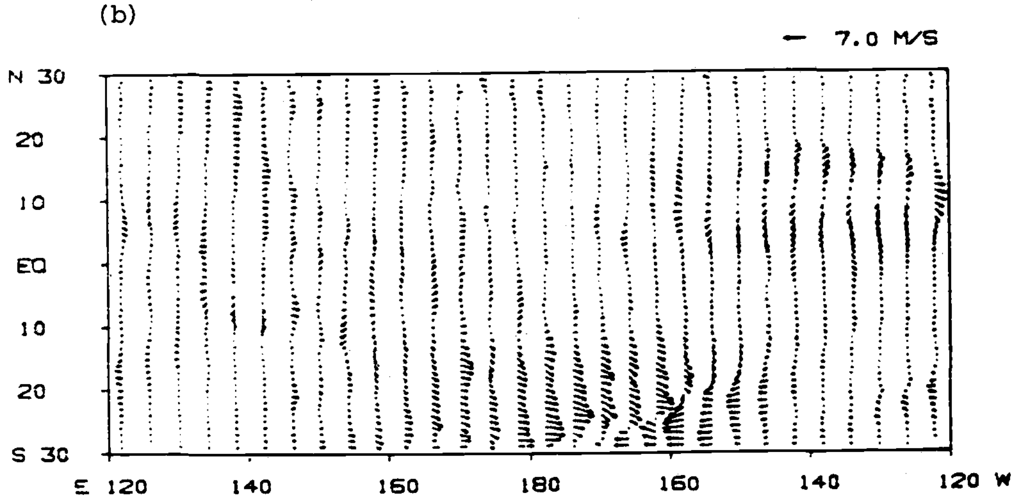

Fig.11. The peak phase: (a) observed wind anomalies for July 1957 from the COADS data. (b) model lower layer simulation for the same period.

(c)

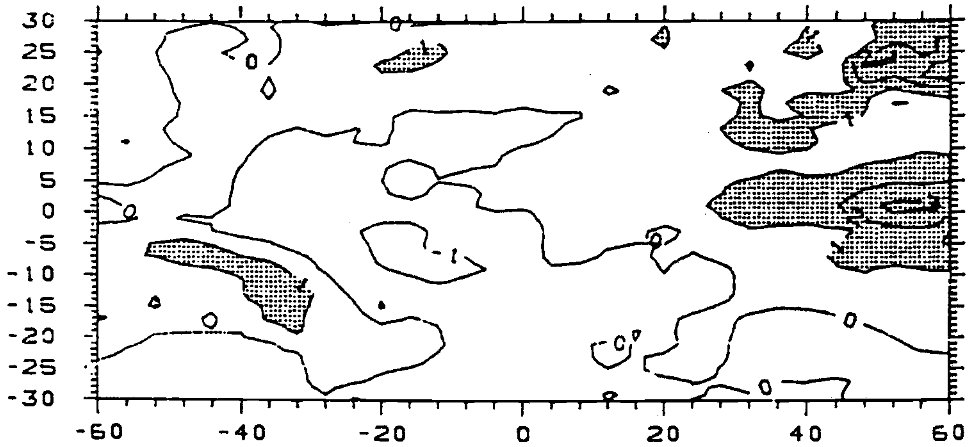

(d)

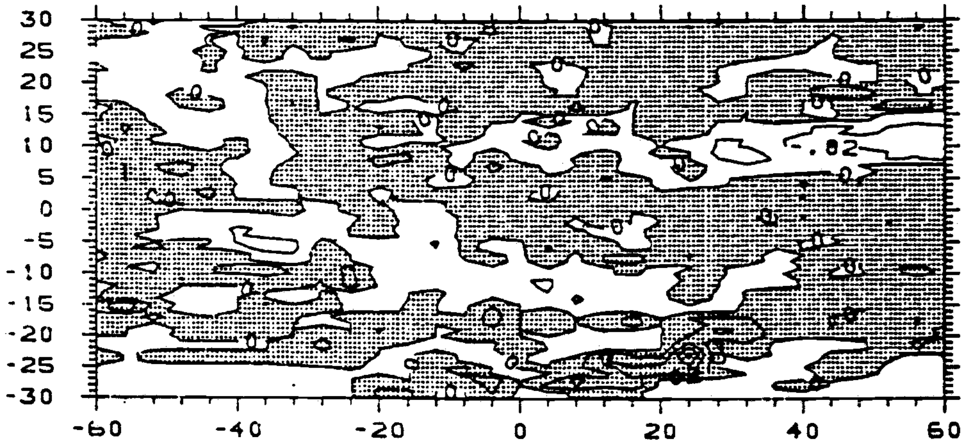

(e)

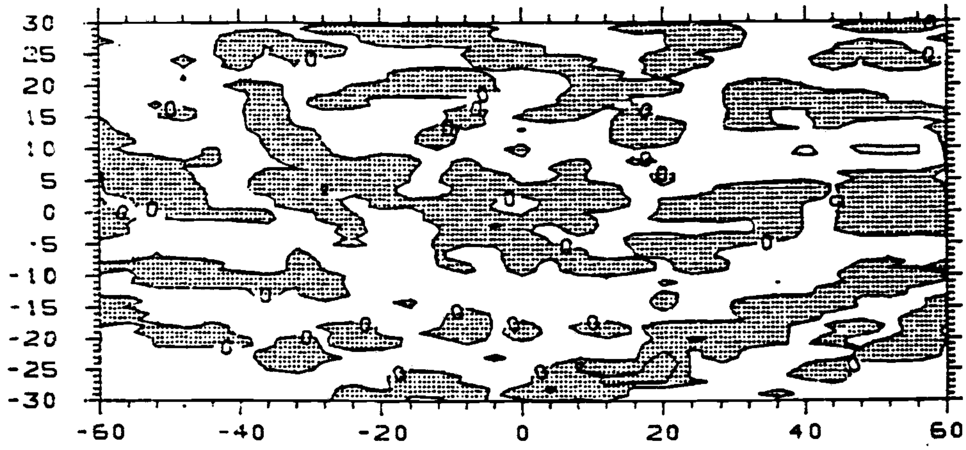

Fig.11 cont'd. (c) observed SST anomaly. Contour interval is 1^0C. Anomalies greater than 1^0 is stippled. (d) calculated heating rate anomaly. Contour interval is 0.02 J/kg s. Region of positive heating anomaly is stippled(e) model divergence field. Contour interval is 1.5E-5 s^{-1}. Region of convergence is stippled.

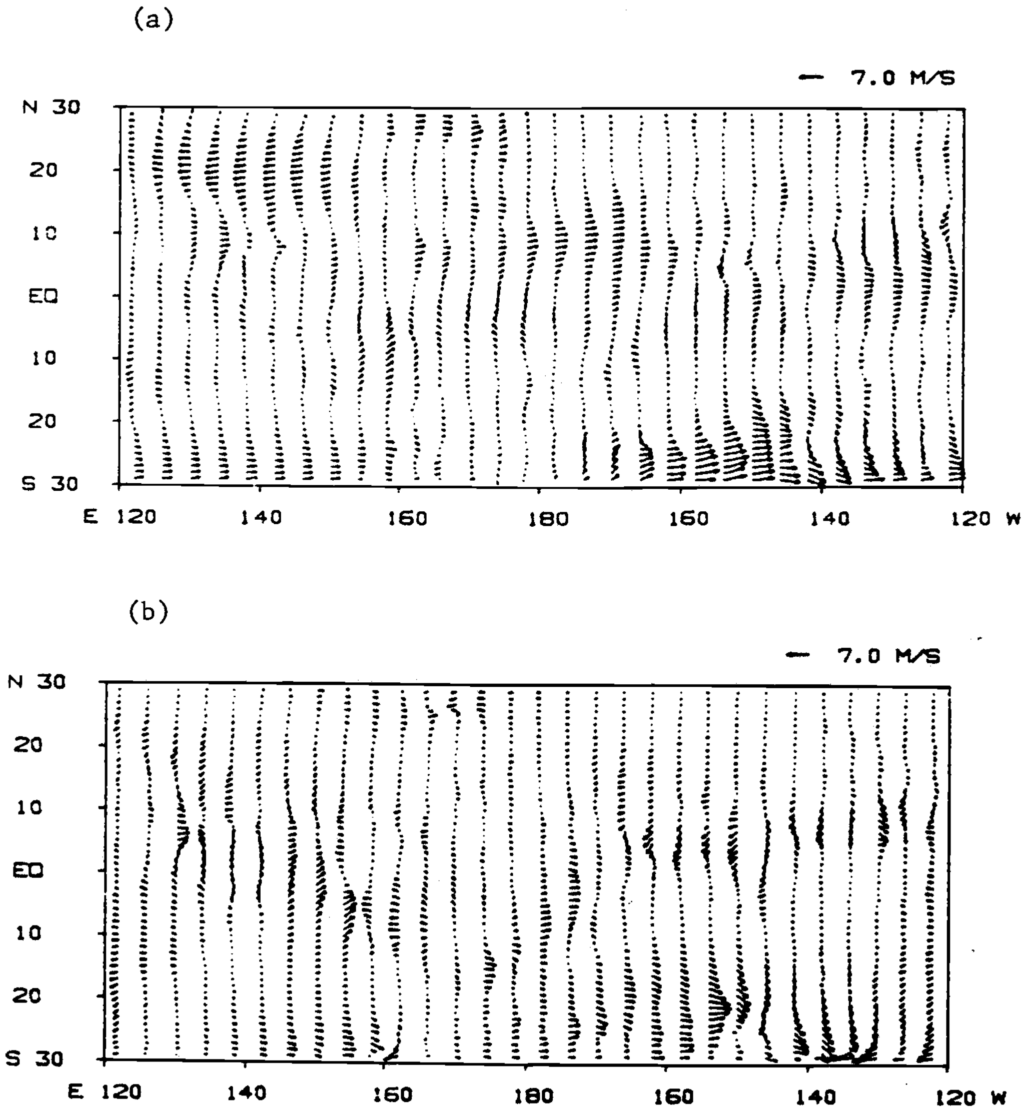

Fig.12. Same as in Fig.11 except for July 1965.

(c)

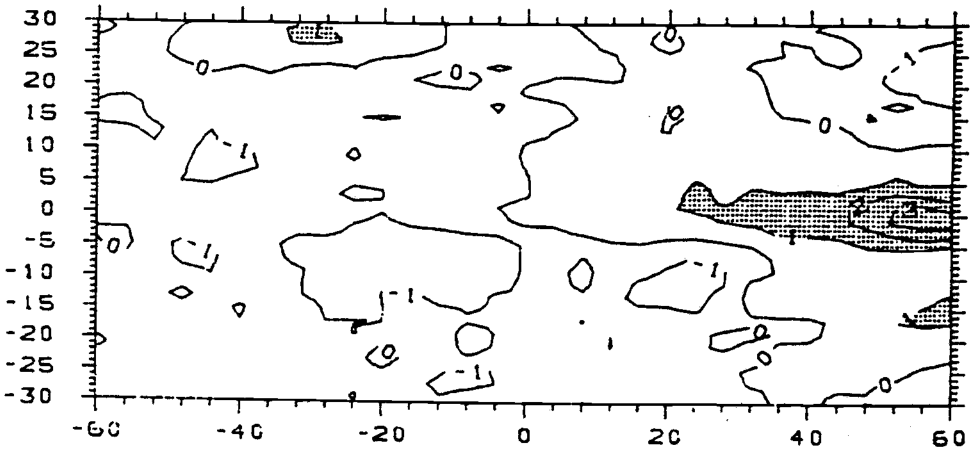

(d)

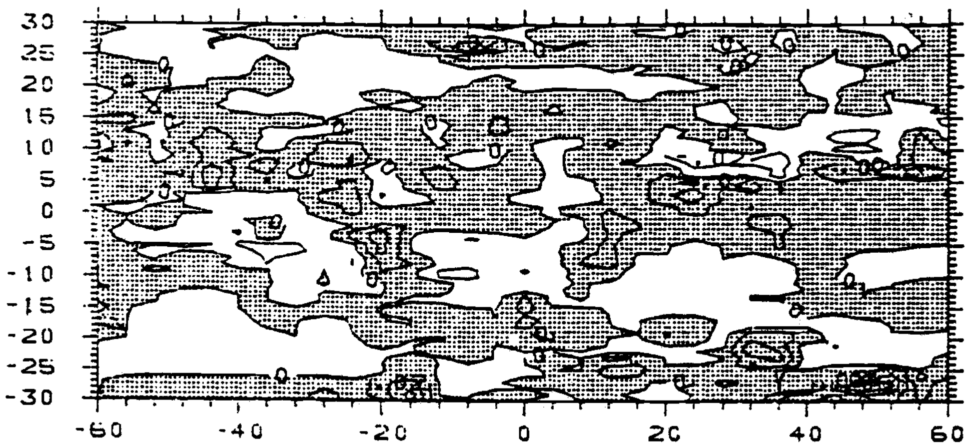

(e)

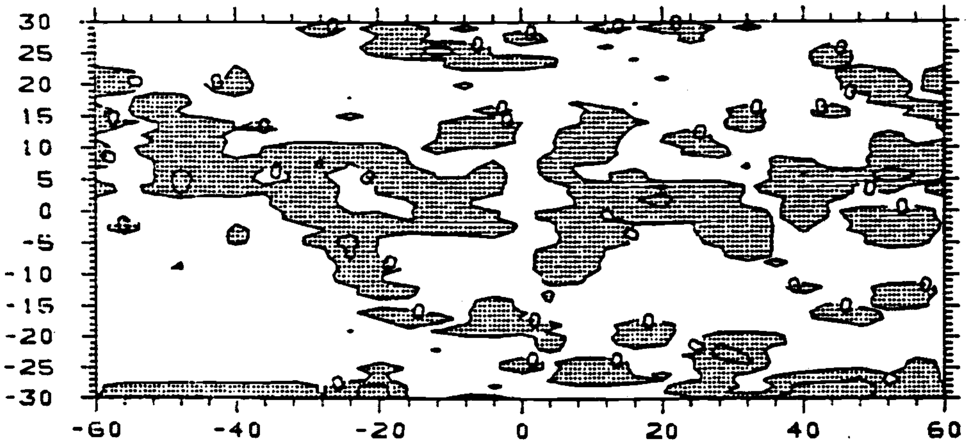

Fig.12 (cont'd) Same as in Fig.11 except for July 1965.

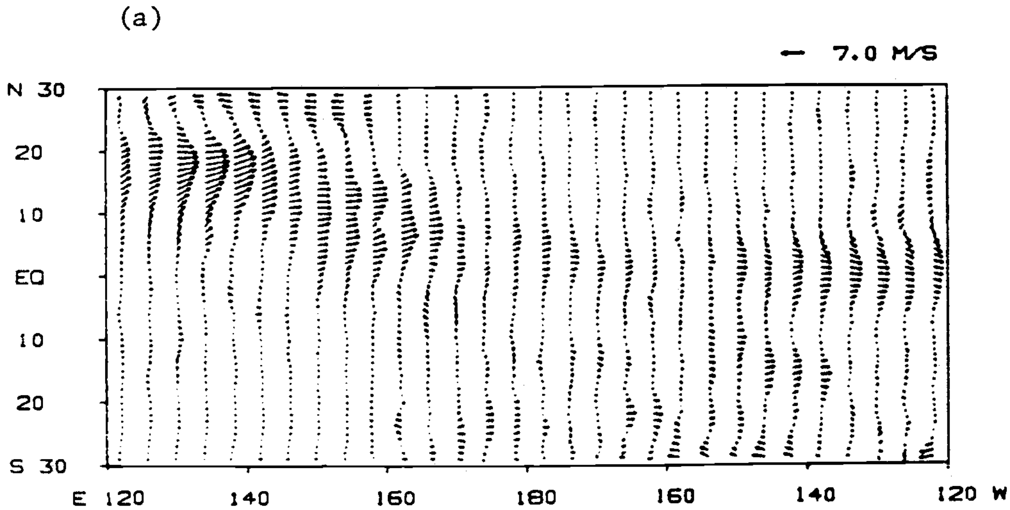

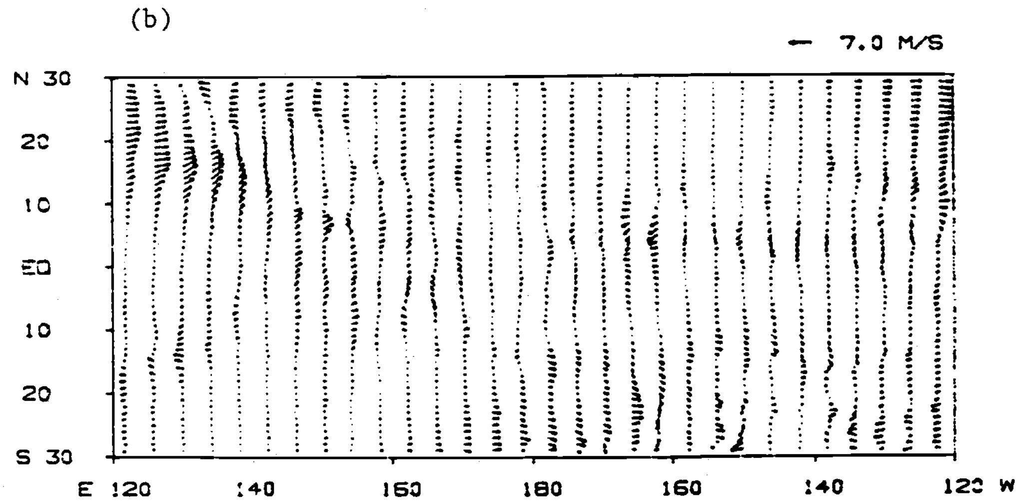

Fig.13. Same as in Fig.11 except for July 1972.

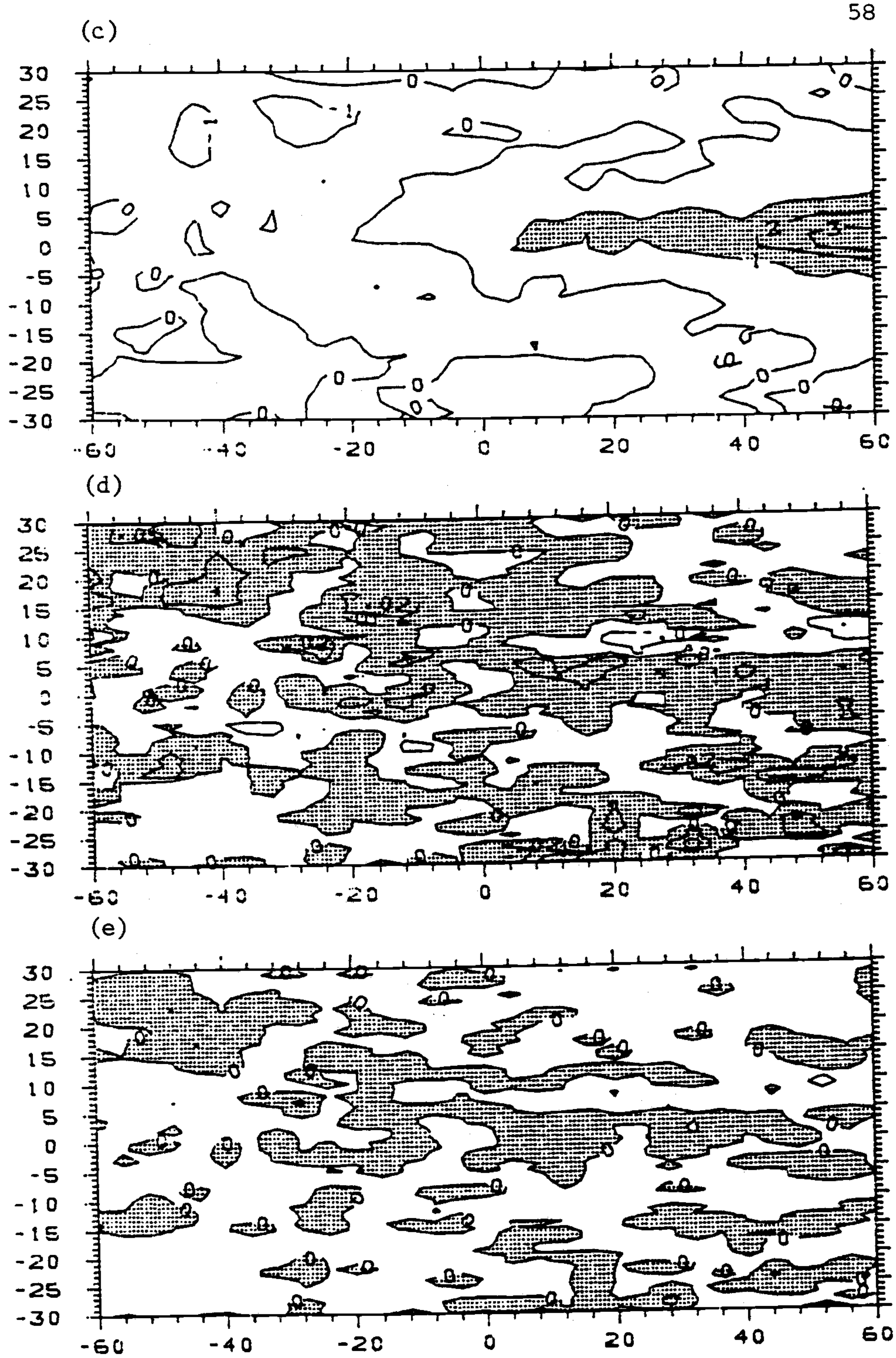

Fig.13 (cont'd) Same as in Fig.11 except for July 1972.

The SST field indicates the characteristics of the peak phase. The maximum SST anomaly appears off the coast of South America after achieving its strongest magnitude on the coast of Peru. It exhibits the slow spreading of the warm waters in both the east-west and north-south directions. The 1972 event exhibits the greatest east-west extent of SST anomaly. The magnitude of the anomaly appears to be similar in all the three years. However, negative anomalies are still visible in the western ocean, though the region of such anomalies is fast shrinking. The heating rate anomaly does not have strong heating regions in the equatorial band. This is due to the disintegration of the ITCZ and SPCZ at this time. The simulated divergence field is similar to the heating field as before. This reinforces the earlier suggestion that heating is closely related to the low-level divergence.

iii) Mature Phase

Figures 14, 15 and 16 exhibit observations from the COADS data and the model simulations for January of 1958, 1966 and 1973, respectively, corresponding to the mature phase of the El Nino events. A westerly anomaly is

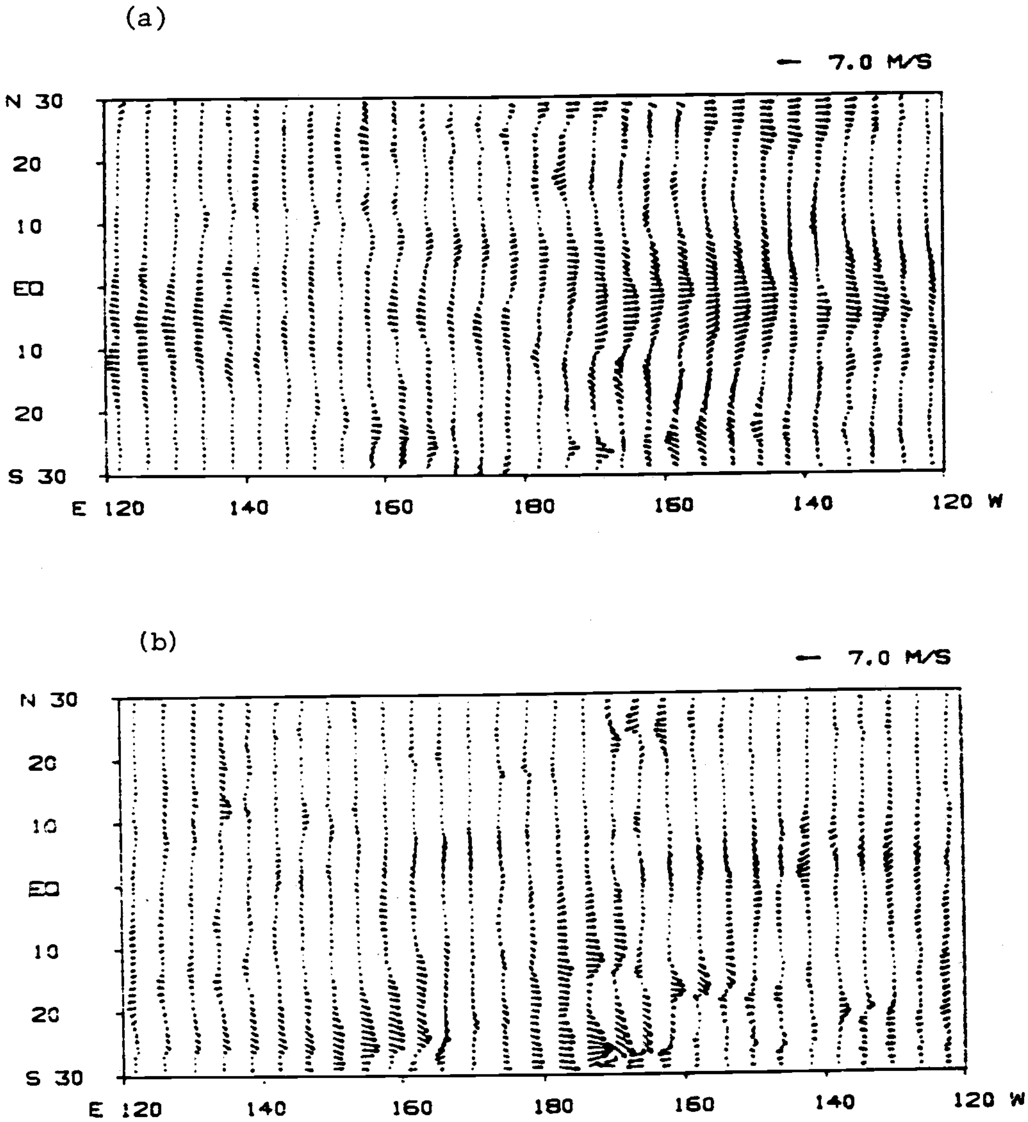

Fig.14. The mature phase: (a) observed wind anomalies for January 1958 from the COADS data. (b) model lower layer simulation for the same period.

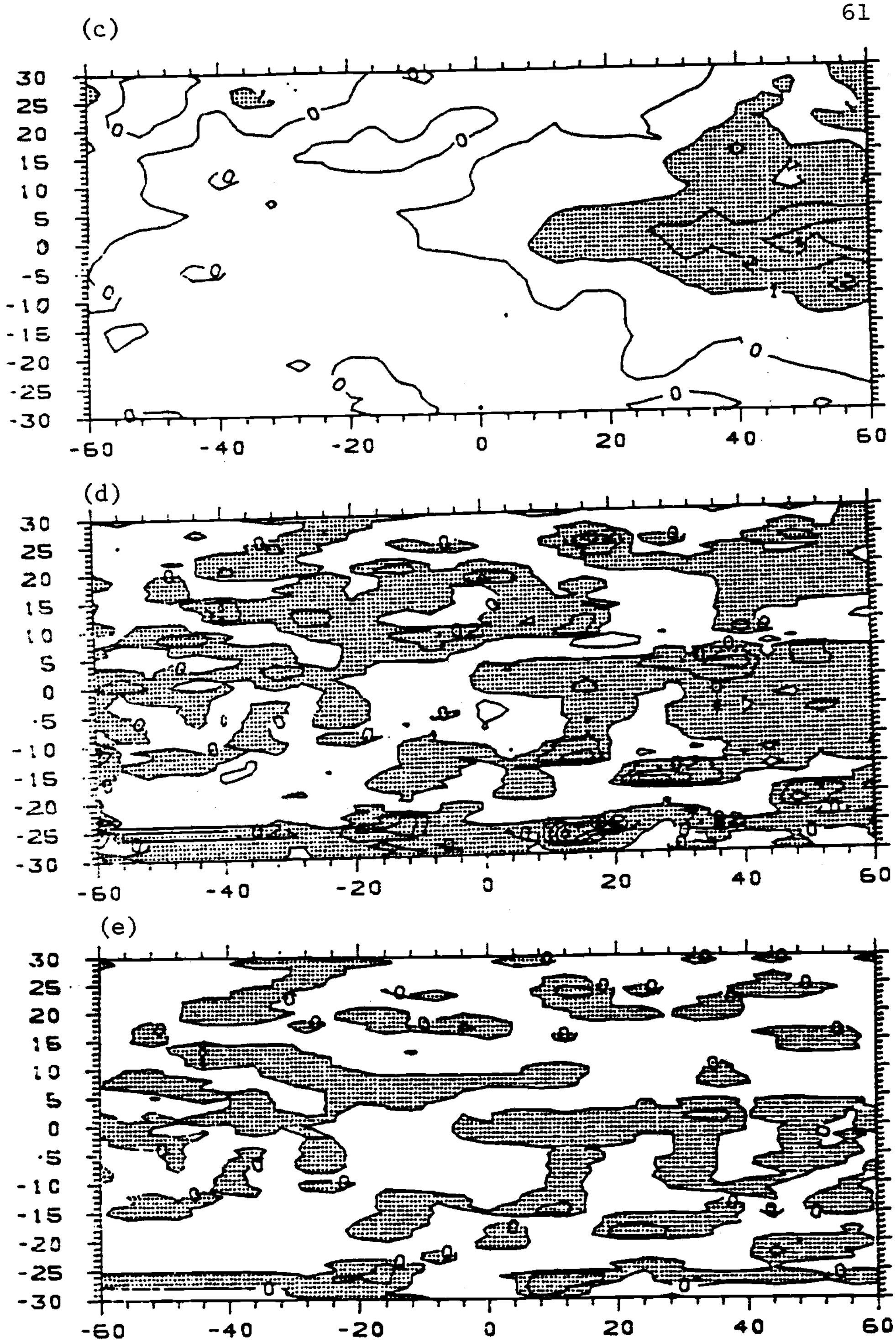

Fig.14 (cont'd.) (c) observed SST anomaly. Contour interval is 1^0C. Anomaly greater than 1^0 is stippled. (d) calculated heating rate anomaly. Contour interval is 0.02 J/kg s. Region of positive anomaly is stippled. (e) model divergence field. Contour interval is 1.5E-5 s^{-1}. Region of convergence is stippled.

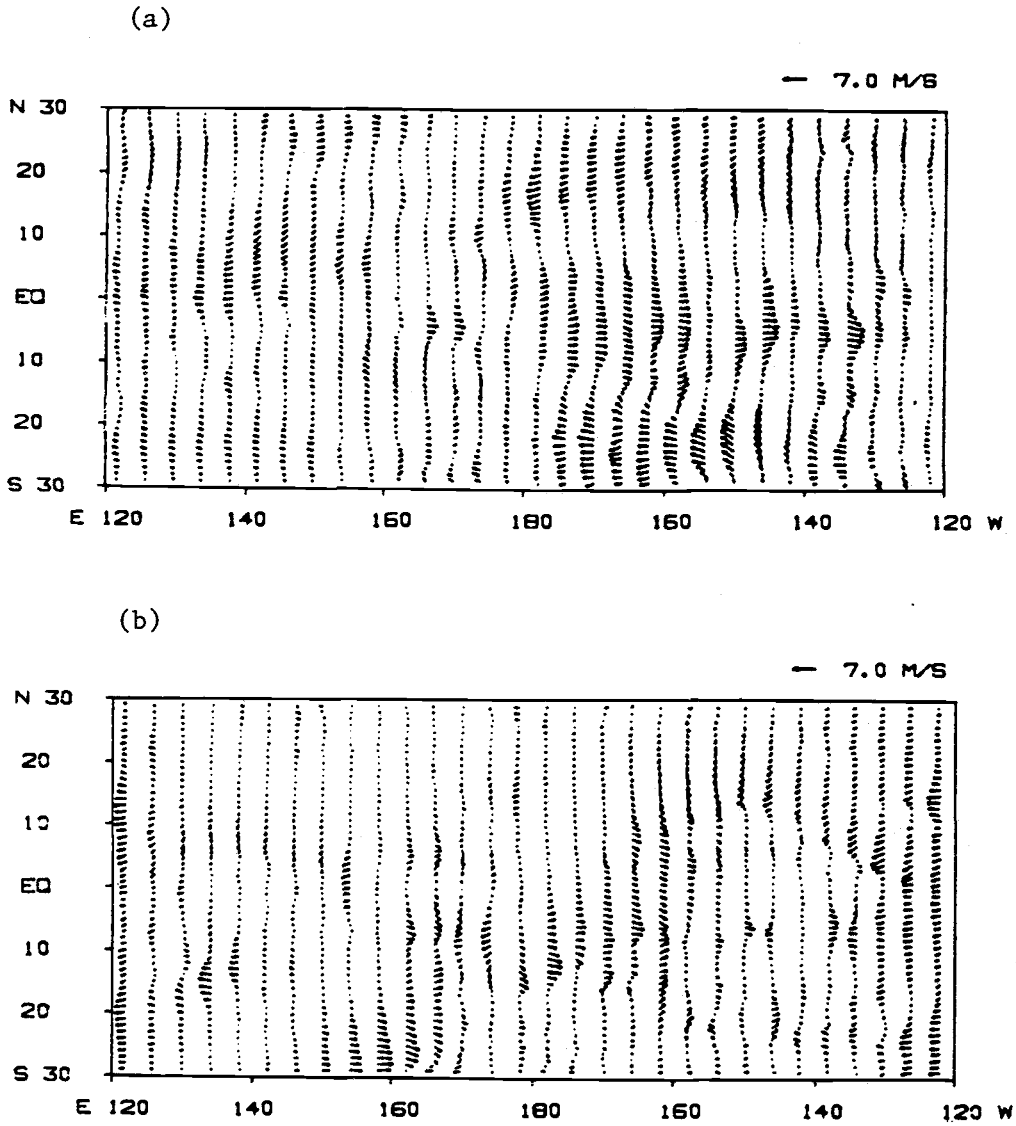

Fig.15. Same as in Fig.14 except for January 1966.

(c)

(d)

(e)

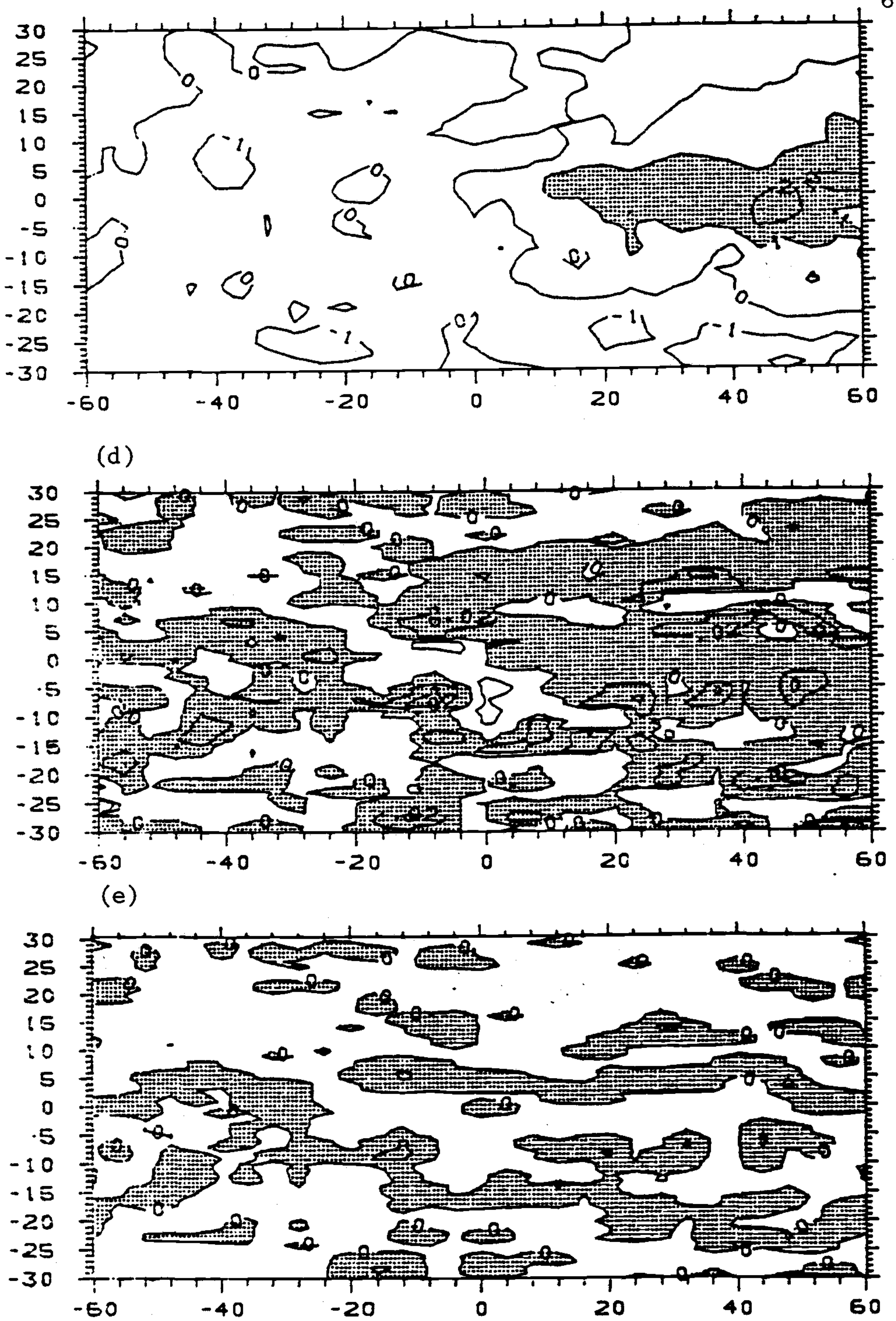

Fig.15 (cont'd.) Same as in Fig.14 except for January 1966.

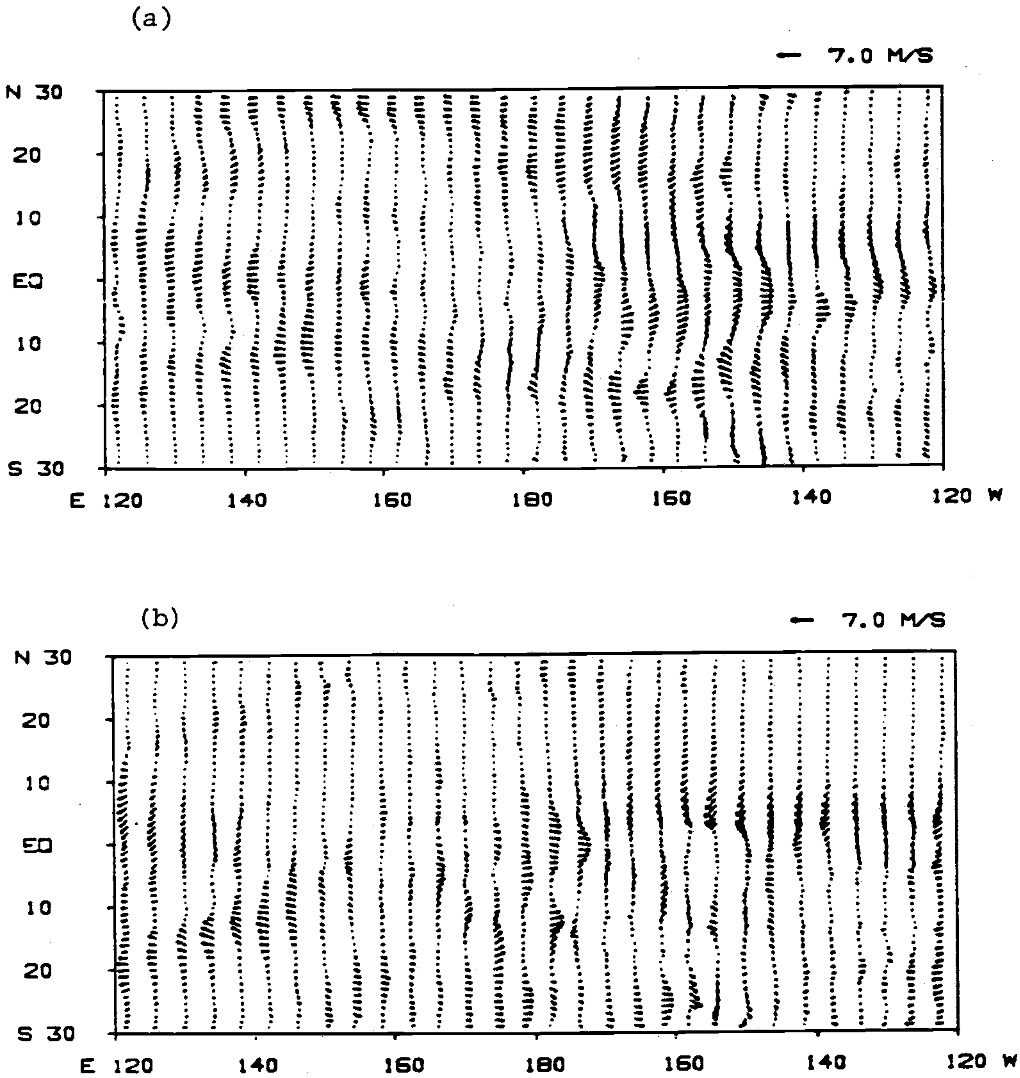

Fig.16. Same as in Fig.14 except for January 1973.

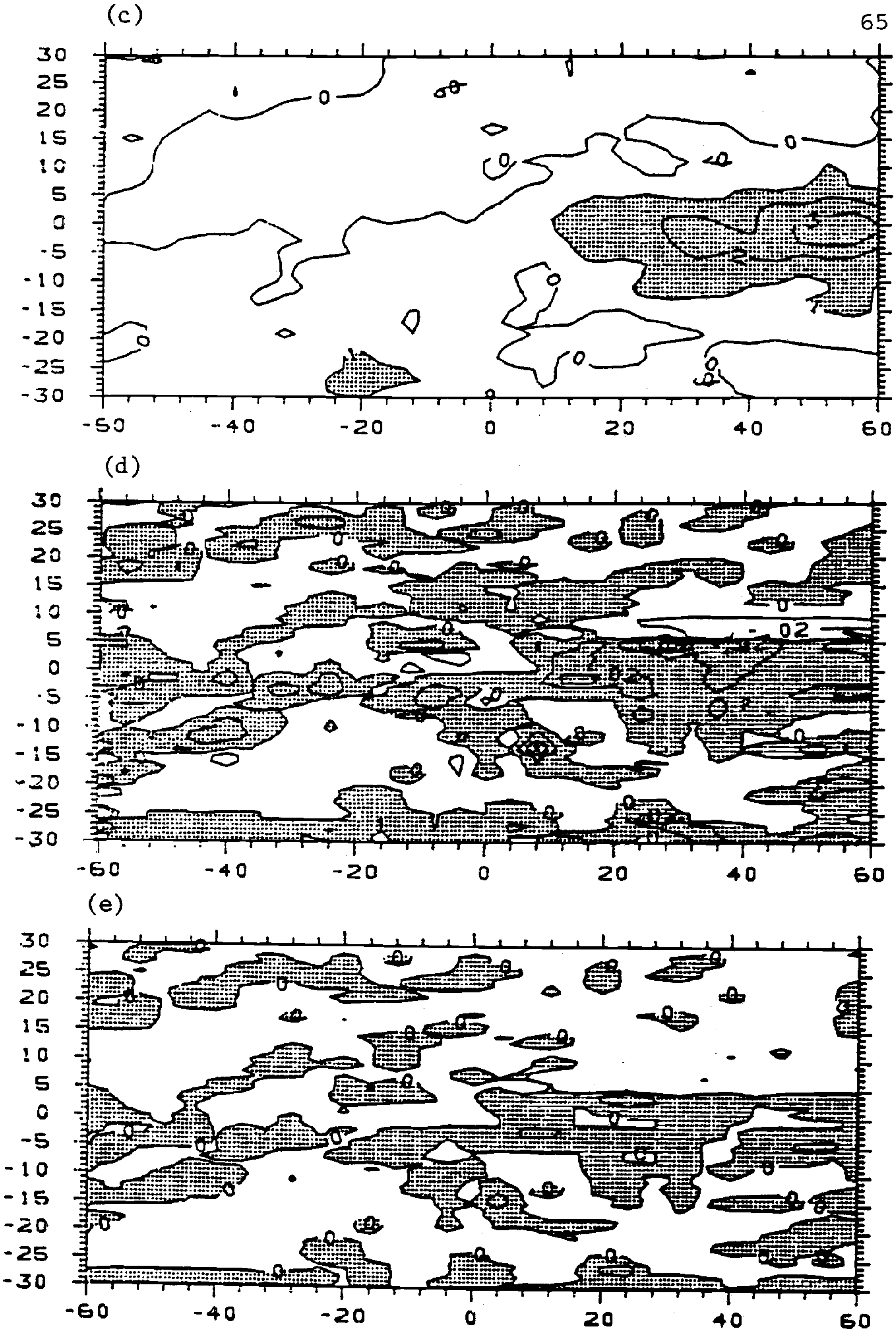

Fig.16(cont'd.)Same as in Fig.14 except for January 1973.

strongest throughout the eastern and central ocean. A weaker easterly anomaly from the equator to about 15 S with a narrow east-west extent is observed in the western ocean. The region of anomalous convergence is widespread and strongest at this time in all the El Nino years. The model simulated velocity field are weaker than observations but the general agreement with the observations is the best in the equatorial band. As mentioned earlier in higher latitudes non-linear terms are critical and hence such a linear model cannot simulate the velocity field well.

Since the region of greatest activity in the El Nino event is limited to the equatorial band, the model domain could be limited to about 15° on either side of the equato in the coupled model to save computational time. The model simulations exhibit the symmetrical behavior of the linear models to a forcing in this case also. In the real atmosphere, easterlies east of the heating are weak while the model simulates strong easterlies. This is very closely related to the paramterization of latent heating. One of the reasons for this response is due to neglecting negative feedback mechanisms in the realization of latent heat. In the present model the latent heat release is proportional to low-level convergence. In nature however, latent heating depends upon the total divergence with the mean flow convergence included. If the anomalous divergence is stronger than the mean field convergence so that the total field is divergent, then latent heat is not realized. Simmilarly, if the anomalous convergence is stronger than the mean field divergence making the total field convergent then latent heating is realized but only proportional to the differential convergence.

Zebiak (1986) included such a feedback mechanism in his atmospheric model and compared the results to a model without the convergence feedback mechanism. He showed that the model results were vastly improved with such feedback included. The present study corroborates the work of Zebiak in that linear models exhibit symmetrical response. Therefore, a feedback mechanism is suggested to be included in the paramterization for the improvement of the model.

The COADS data exhibit the characteristic SST anomaly field for the mature phase of El Nino. This phase is characterized by positive anomaly throughout the Pacific Ocean with the greatest north-south extent. This is the single largest observed interannual feature. As seen from

Fig.7, the SST anomaly in 1966 was the least and hence the extent of warm water is small in 1966. The heating field closely follows the anomalous convergence. Strong heating is seen throughout the equatorial band extending to a great extent to the north and south of the equator. The model simulated divergence is similar to the heating field as before.

iv) Retrieval Phase:

Figures 17, 18 and 19 show the observed and the simulated field for July of 1958, 1966 and 1973, respectively. After the SST peaks in the central Pacific, it decreases rapidly thereafter returning the conditions to normal. Observations show the weakening of the westerly anomaly in the eastern ocean. In July of 1966, easterlies have already appeared in the eastern ocean. In July 1973, the easterlies just north of the equator are stronger than in the other two years. The magnitude and extent of the SST anomalies are fast declining at this point. In 1966 and 1973, negative SST anomalies have already appeared in the western and central ocean. The small region of positive SST anomaly is scattered and does not exhibit coherent

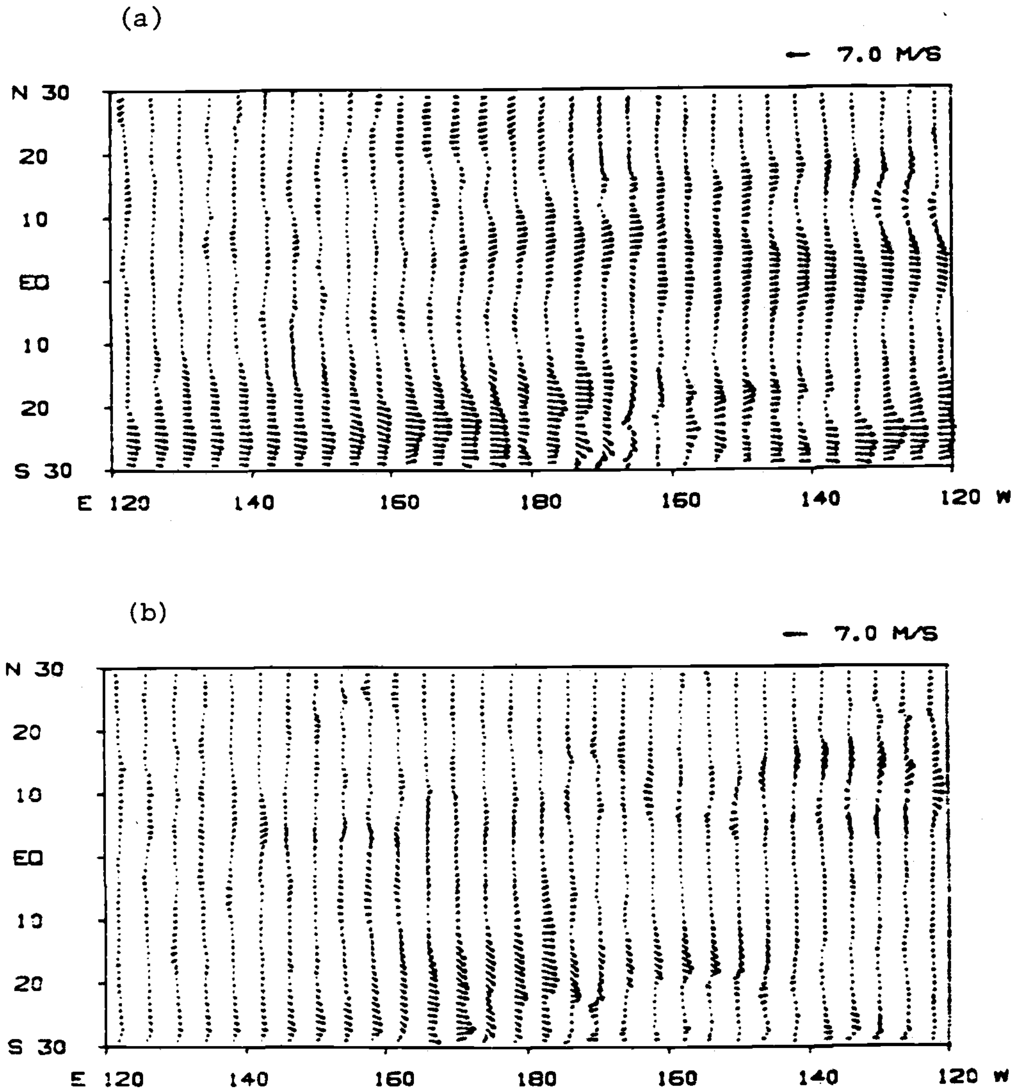

Fig.17. The retrieval phase: (a) observed wind anomalies for July 1958 from the COADS data. (b) model simulation for the same period.

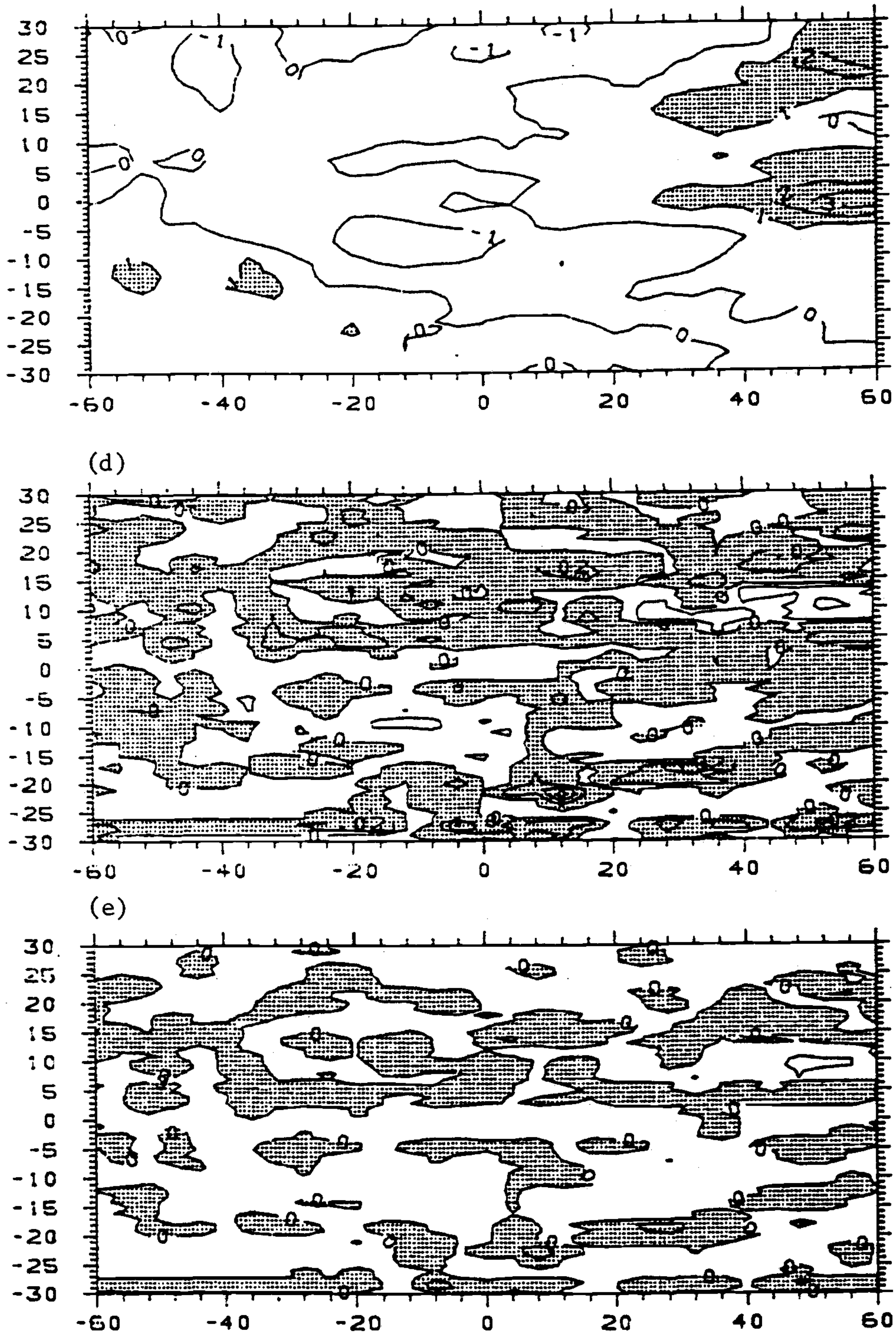

Fig.17(cont'd.) (c) observed SST anomaly. Contour interval is 1^0C. Anomaly greater than 1^0 is stippled. (d) calculated heating rate anomaly. Contour interval is 0.02 J/kg s. Region of positive anomaly is stippled. (e) model divergence field. Contour interval is 1.5E-5 s^{-1}. Region of convergence is stippled.

(a)

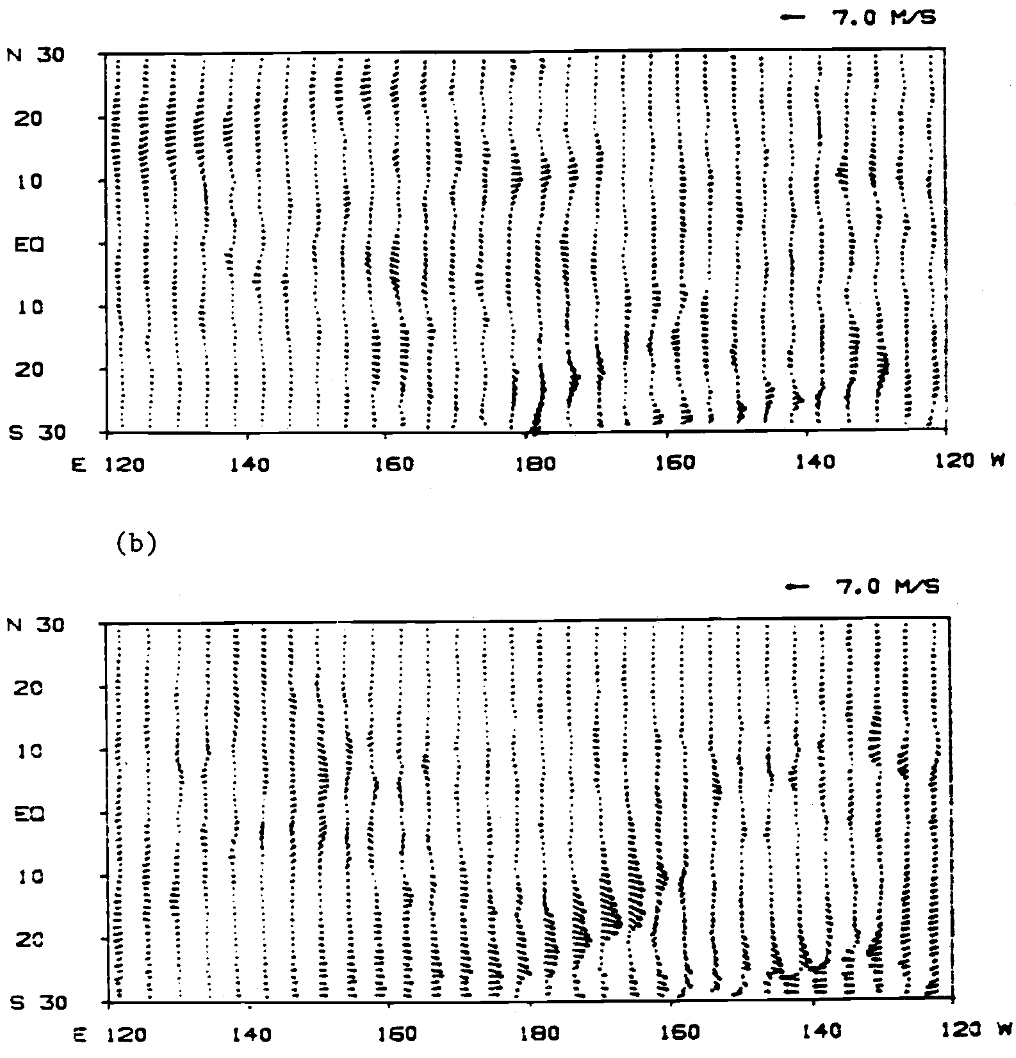

(b)

Fig.18. Same as in Fig.17 except for July 1966.

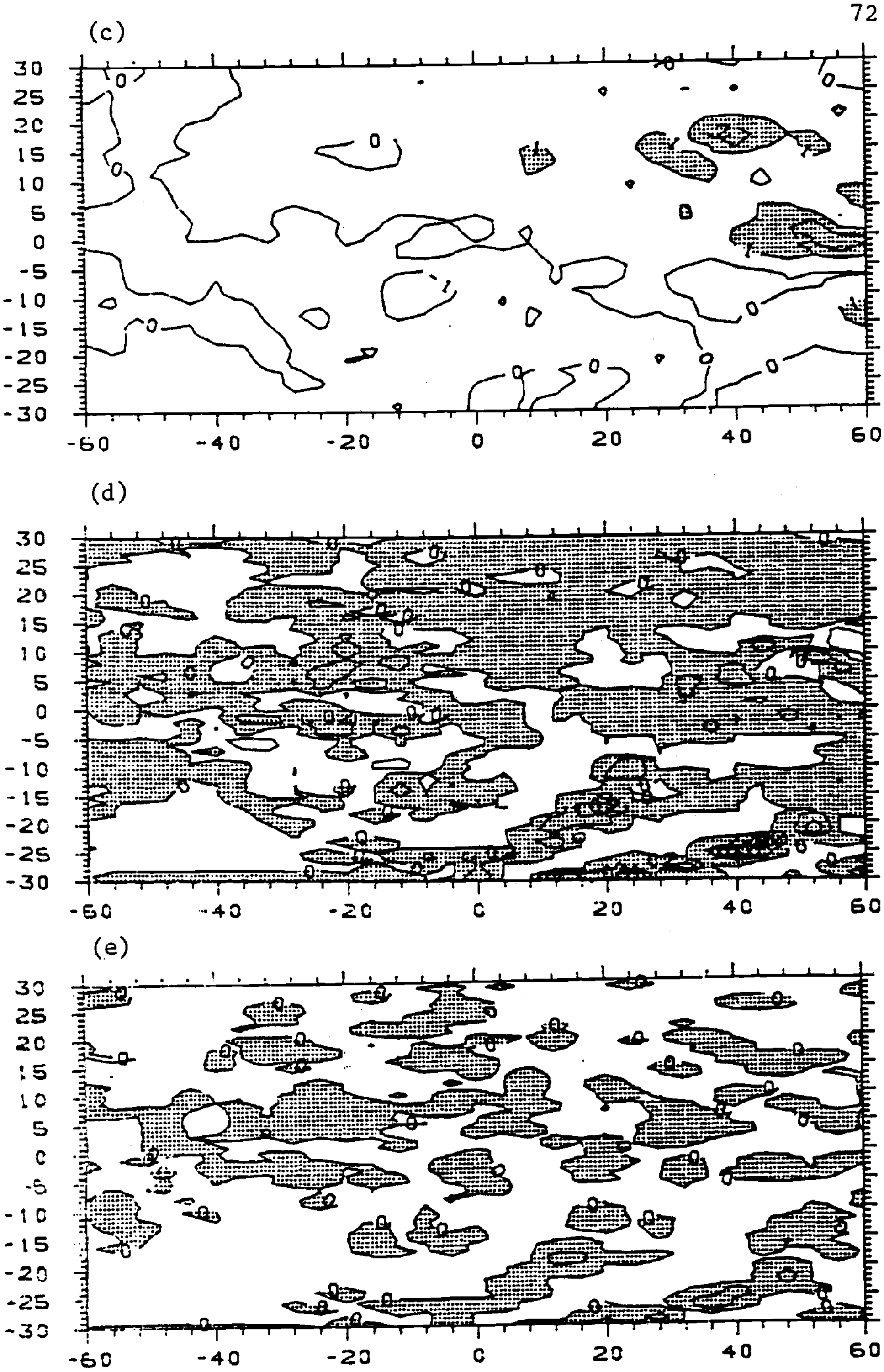

Fig.18 cont'd. Same as in Fig.17 except for July 1966.

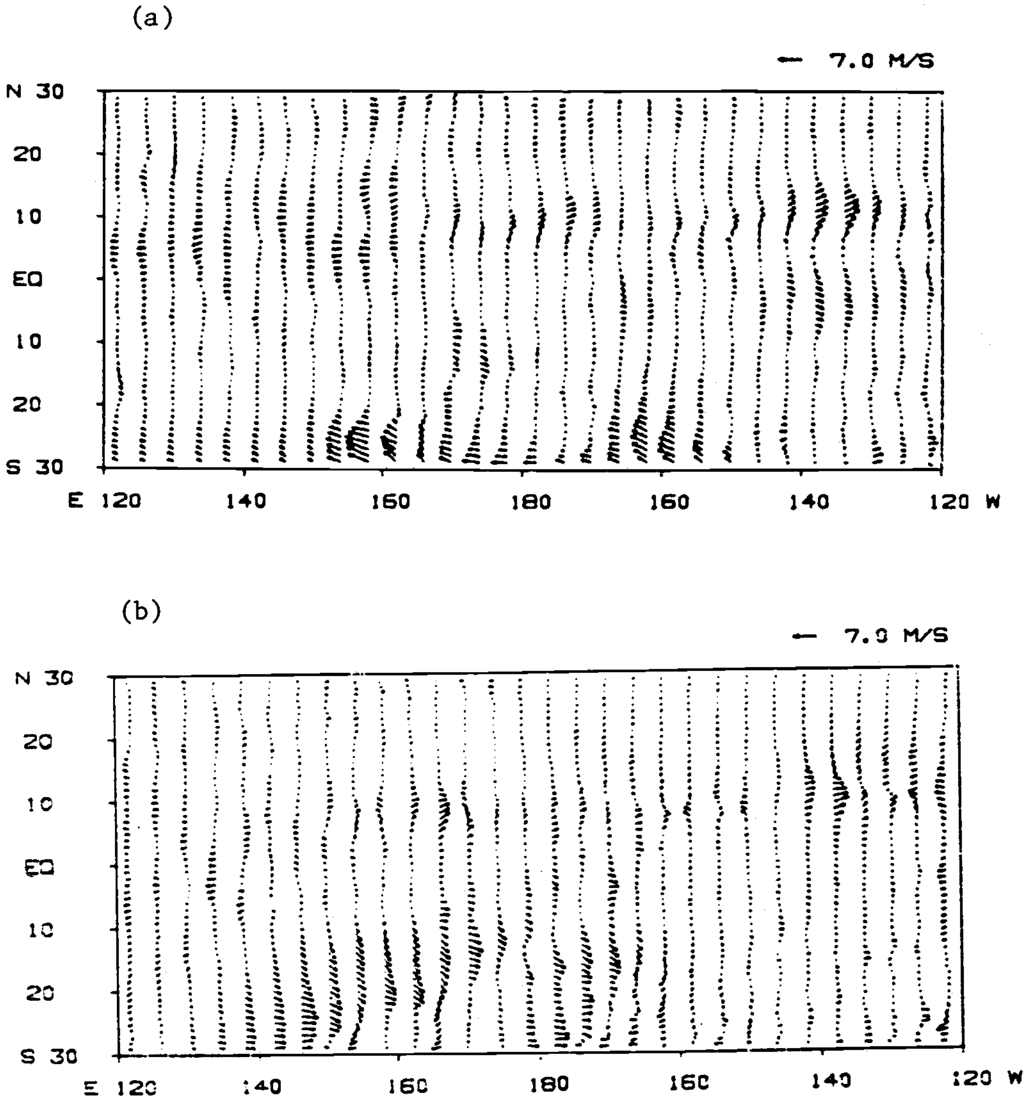

Fig. 19. Same as in Fig. 17 except for July 1973.

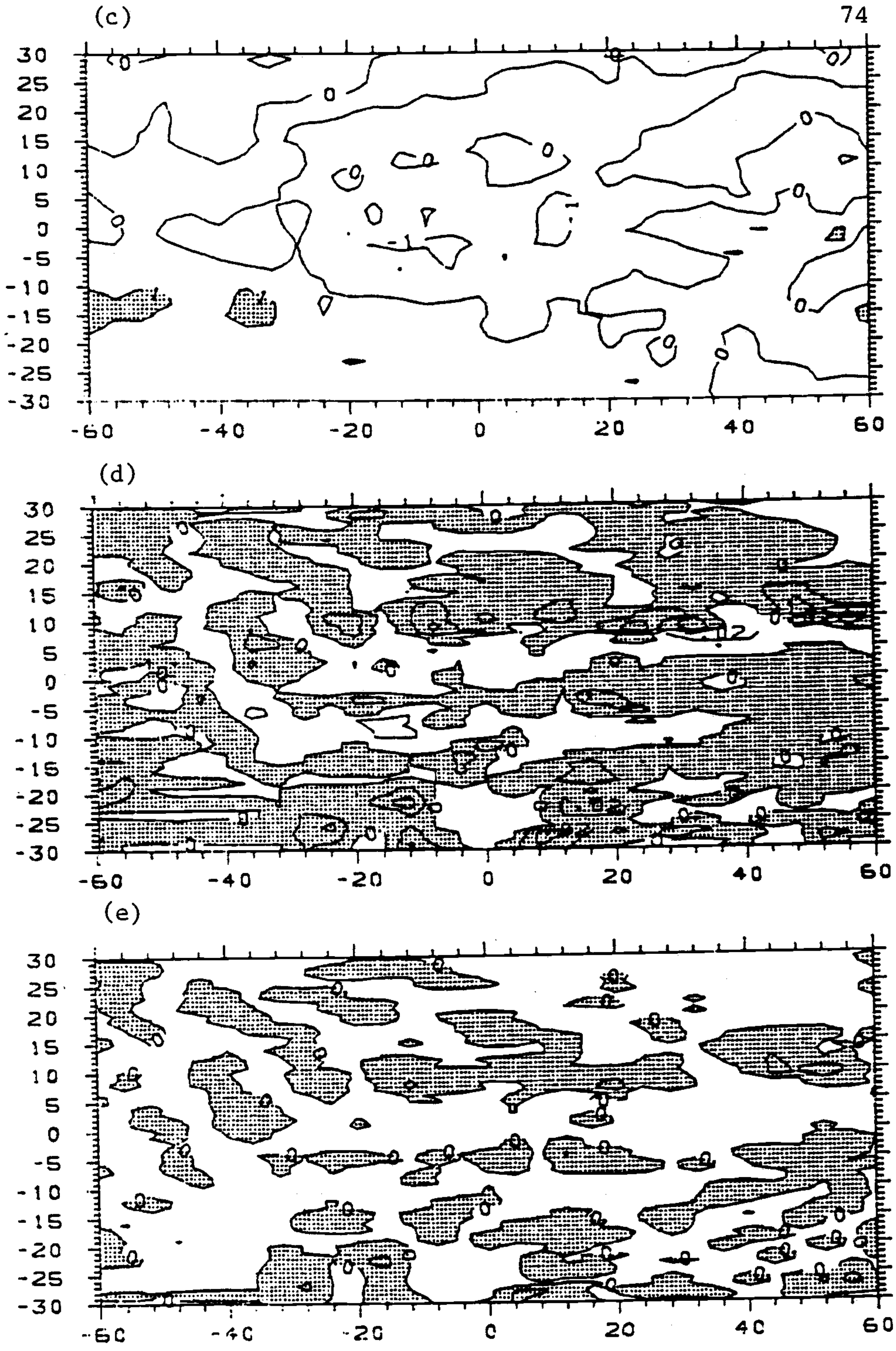

Fig.19 cont'd. Same as in Fig.17 except for July 1973.

structure at this time. However, in 1958 the SST anomaly field is still stronger in the western and central Pacific. This ENSO was particularly long-lasting as noticed from Fig.7; it took almost two years to return the conditions to normal. The simulated velocity is weaker than observed but generally agrees well with the observations in the equatorial region. In the higher latitudes the advection terms become critical in simulating the velocities, terms which were neglected in the present model. The simulated divergence is closely related to the heating field as before, indicating that the model captures the regions of convergence quite well.

6) Sensitivity to model domain

One of the concerns of the effect of the cyclic boundary condition in the model is the presence of strong heating near the eastern boundary. One way to examine the model sensitivity in this case is to extend the model domain in the east-west direction. The coast of Peru and Ecuador is located at around 80 W, and since in the mature phase the SST anomaly moves off the coast, it is extended to 90 W. The Pacific Ocean is bounded on the east by the North and South American land masses. In order to maintain a rectangular ocean, the north-south extent was reduced to 15° on either side of the equator for the extended model domain. Also, as seen earlier the model simulations are better in the tropics. This will reduce the computational time tremendously.

Such an experiment was conducted for the mature phase of all three El Nino years of 1957, 1965, and 1972. However, the atmospheric latent heat release is computed from the total divergence field by including the mean field effects. It was seen in Fig.5c that the strong easterlies east of the heating were present because of the neglect of the mean field effects. Therefore, in this run the mean field divergence and the anomalous divergence field were added together to get the total surface layer divergence field. Only if the total field was convergent, giving a rising motion to the air particle, would the atmospheric latent heat be released following equation (13).

This parameterization does include the effect of the feedback mentioned earlier. If the anomalous convergence is so strongly convergent that the total field is convergent even if the mean field is divergent, then atmospheric latent heat is realized in proportion to the difference of the two fields. Also, if the anomalous field is convergent but the total field is divergent, then there is no heating. Moreover, the latent heating is enhanced when the anomalous as well as the mean field is convergent.

Again, only the mature phase is considered. Figures 20 a,b,c,d,e give the anomalous wind field from the COADS data, the model simulated lower-layer velocity field, the observed SST anomaly field, the calculated heating field, and the model divergence field, respectively, for January 1958. Figures 21 and 22 are similar for January 1966 and 1973, respectively. As is seen from the anomalous wind field, east of 110 W the wind is very weak with westerlies present over the central and western ocean. Only in 1973 are small easterlies present over the eastern ocean. As mentioned earlier the strongest SST anomaly is located off the coast of South America. Due to the parameterization of heating, the strong effect of the ITCZ and the SPCZ is clearly seen in the heating field in all the years. Comparison of this heating with the previous parameterization shows that the heating is drastically

(a)

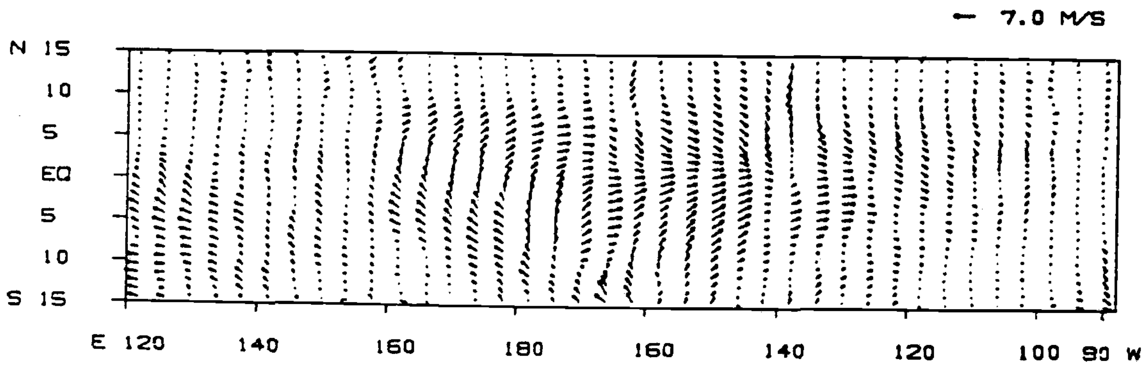

(b)

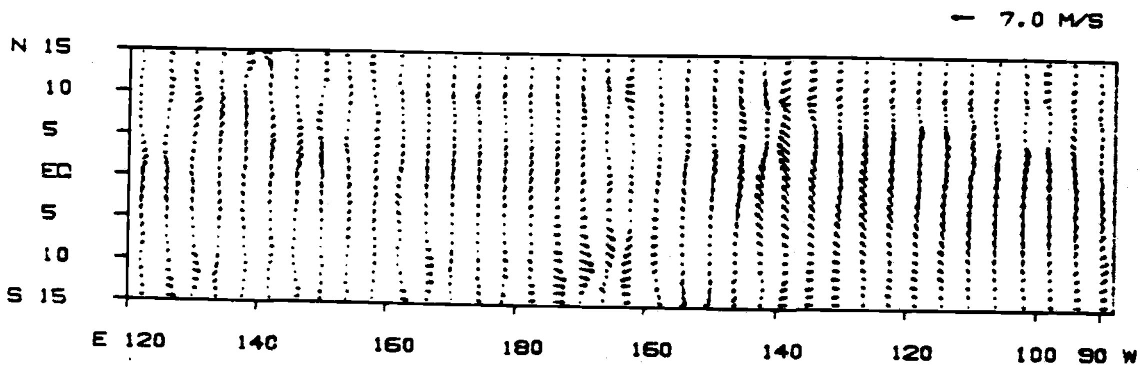

Fig.20. Expanded east-west domain for January 1958. (a) observed wind anomaly (b) model simulated lower layer velocity.

(c)

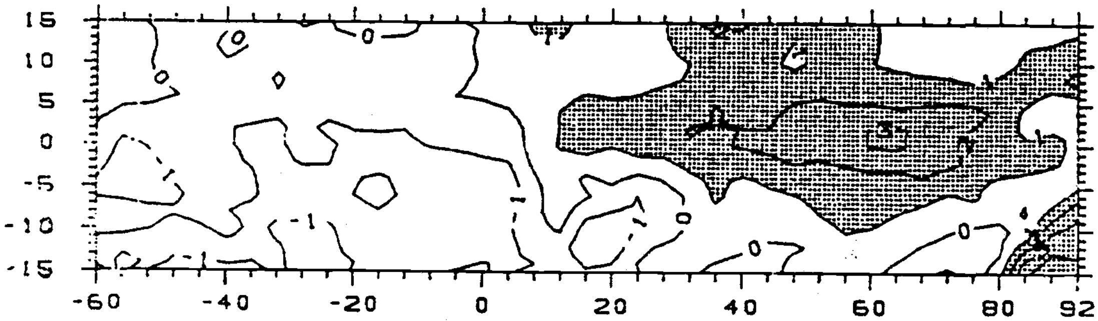

(d)

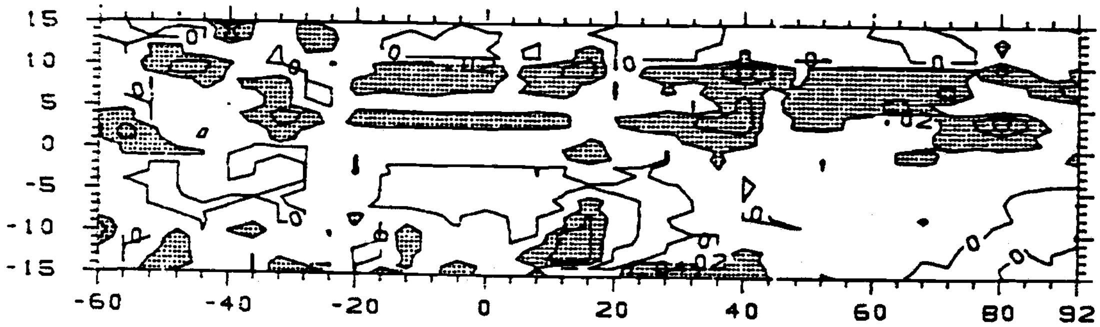

(e)

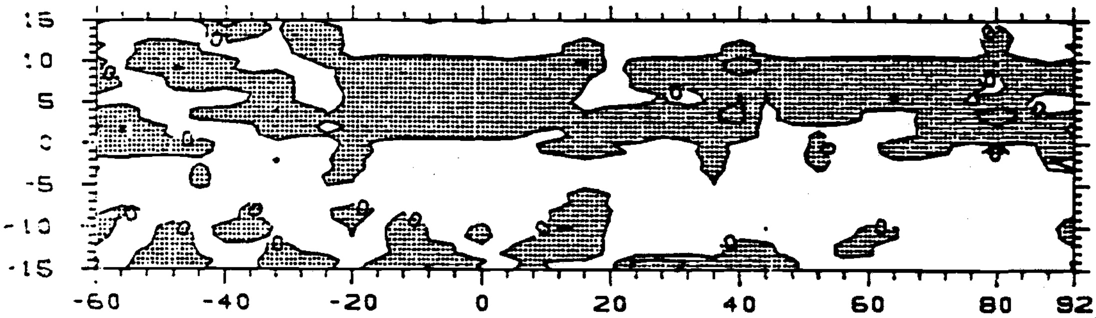

Fig.20(cont'd.) (c) observed SST anomaly. Contour interval is 1^0C. Region of positive anomaly greater than 1^0 is stippled (d) heating rate calculated from the model paramterizations. Contour interval is 0.02 J/kg s. Region of positive heating is stippled (e) model divergence. Contour interval is 1.5E-5 s^{-1}. Region of convergence is stippled.

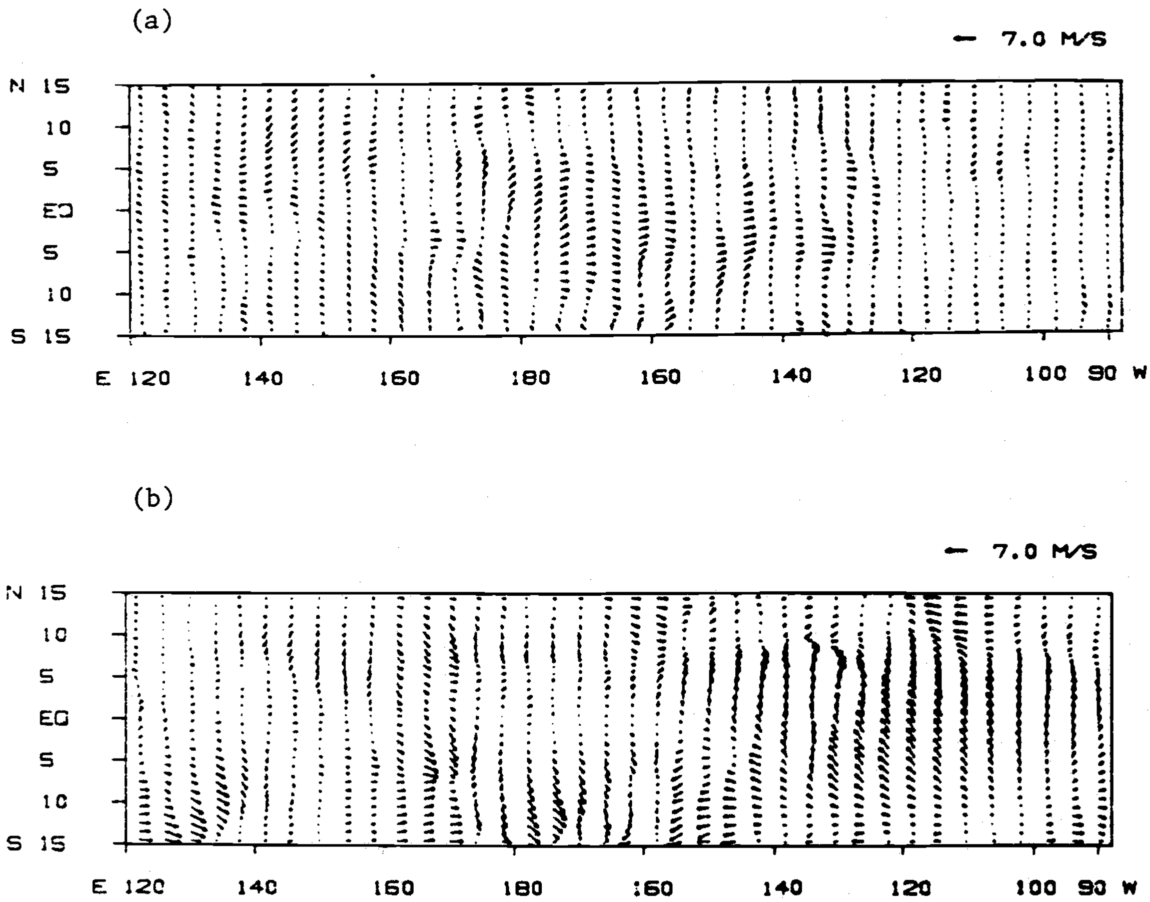

Fig.21. Same as in Fig.20 except for January 1966.

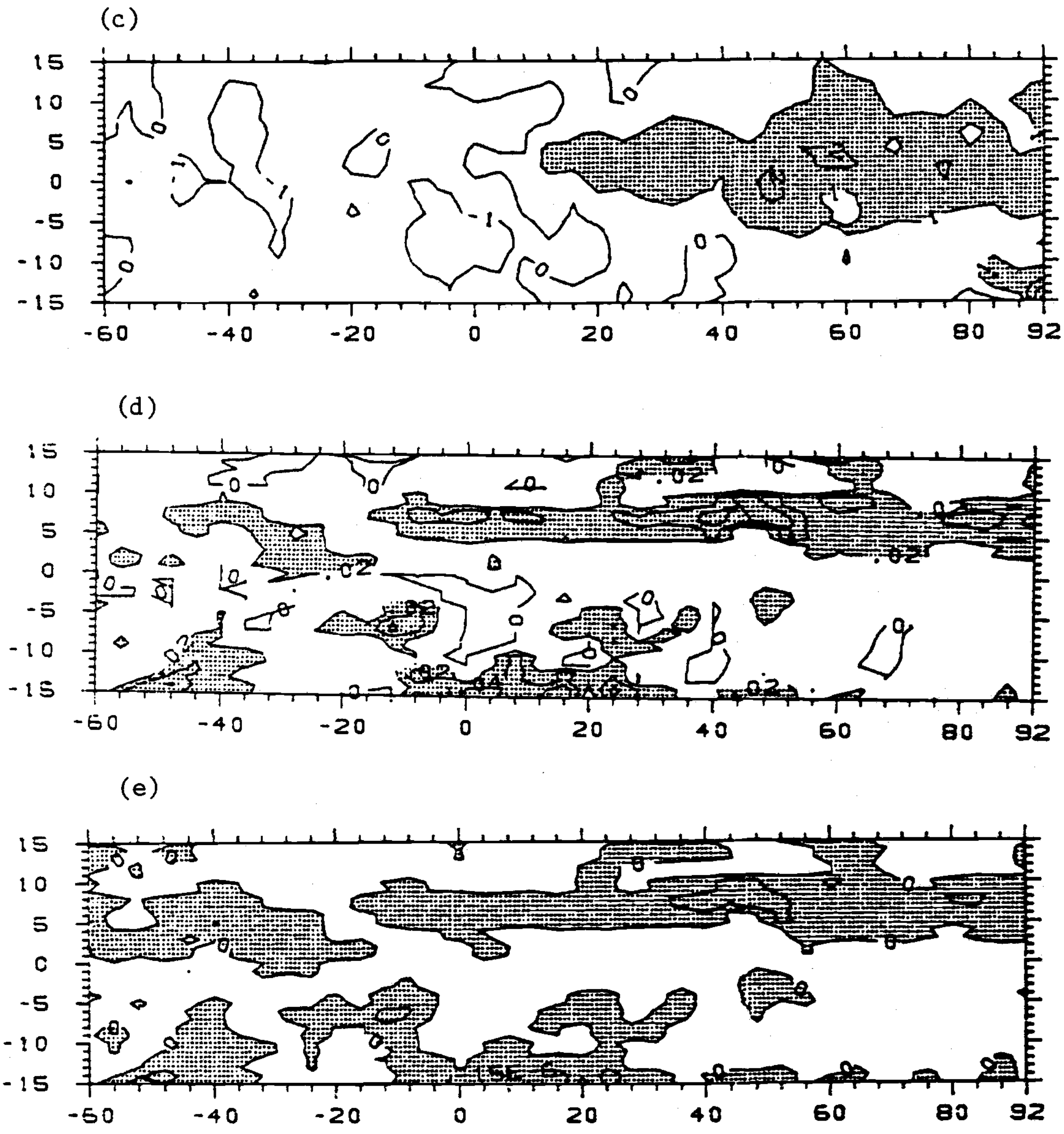

Fig.21.(cont'd).Same as in Fig.20 except for January 1966.

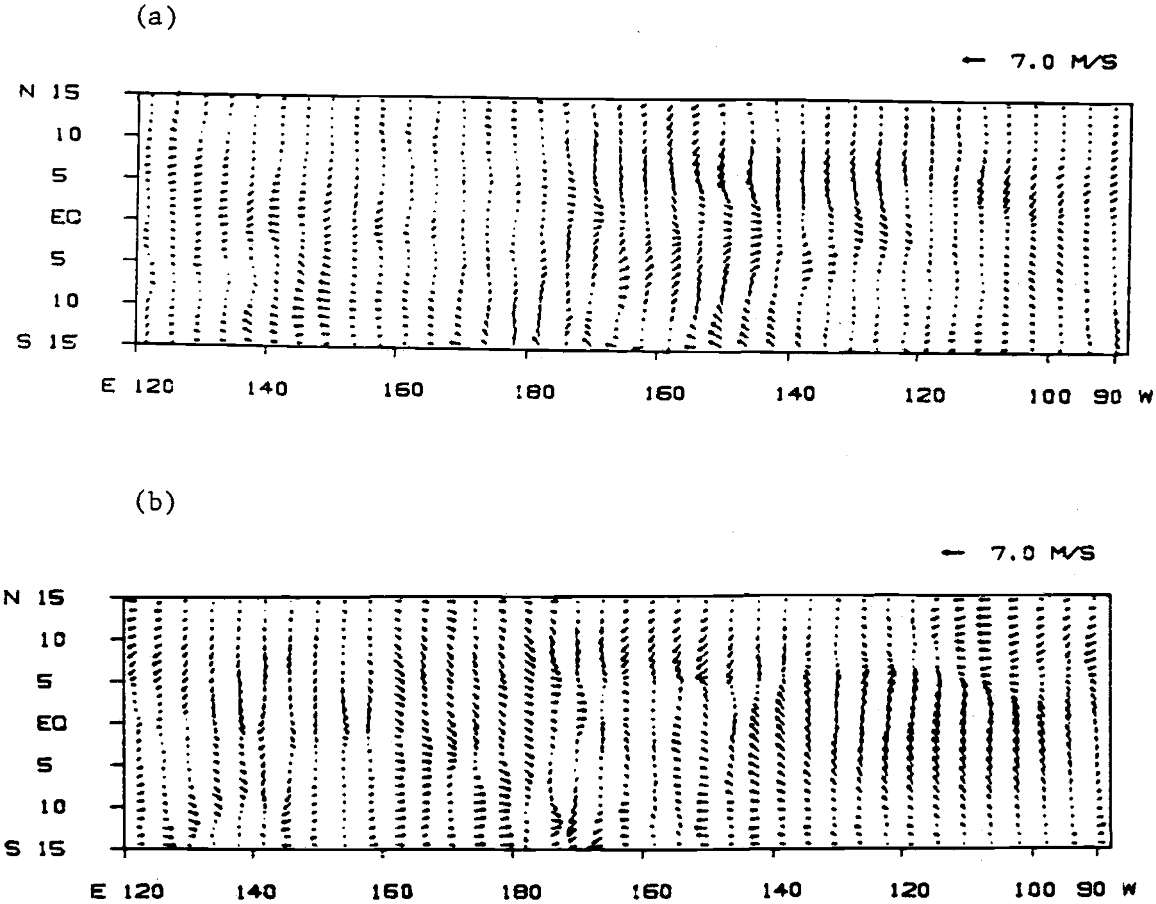

Fig.22. Same as in Fig.20 except for January 1973.

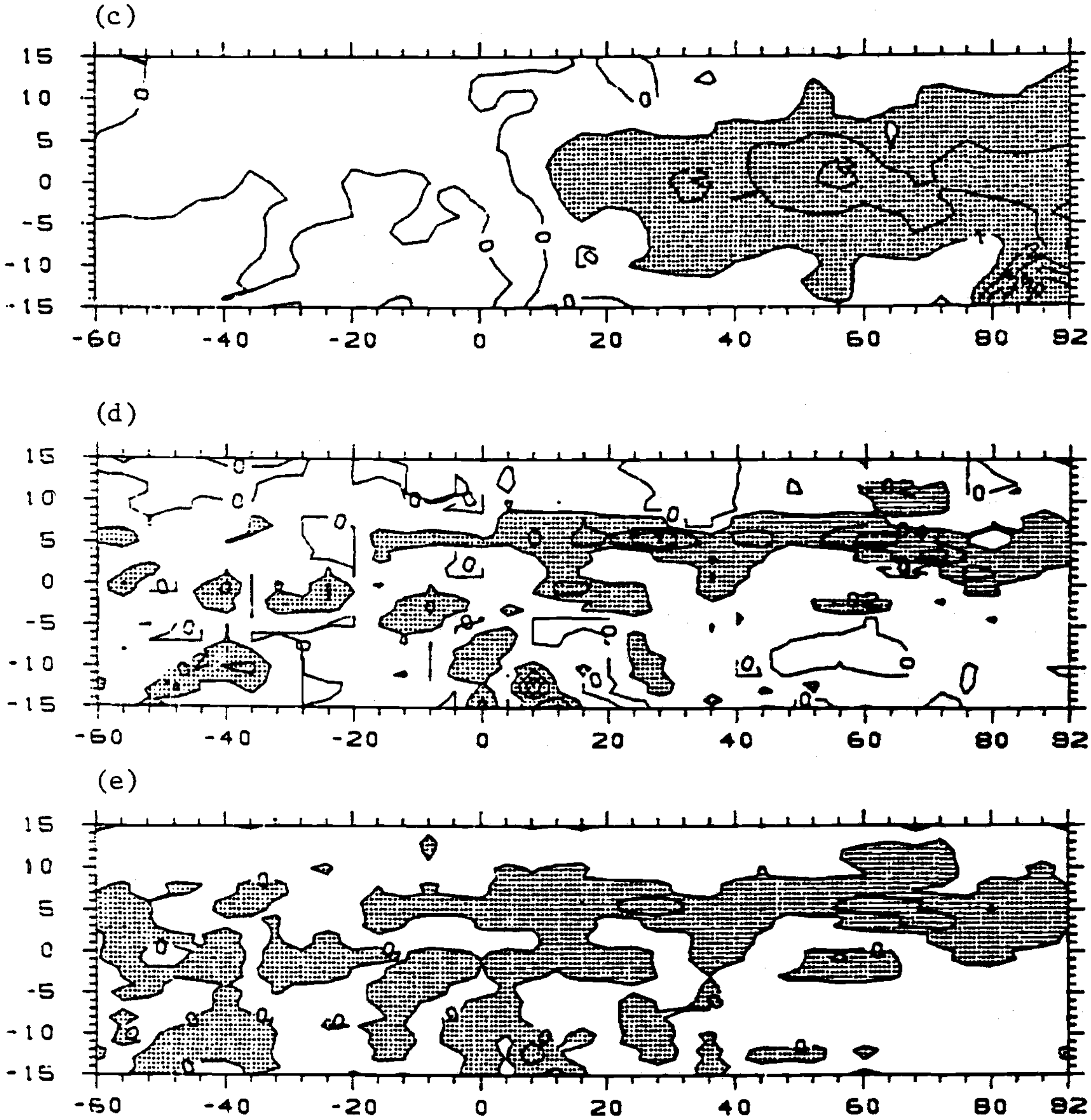

Fig.22(cont'd.)Same as in Fig.20 except for January 1973.

different. This is clearly due to the inclusion of the mean field effects.

2.5 Conclusions

The linear atmospheric model presented here with the latent heat parameterized following the CISK process is able to capture the salient characteristics of ENSO. The geostrophic adjustment of the tropical atmosphere to a small forcing was exhibited very well by the model. The model response to a dipole heat source-sink exhibited characteristics similar to Matsuno's (1966) work with a mass sink-source. Latent heat release was parameterized as proportional to low-level convergence. This parameterization was tested by utilizing the interannual monthly mean data from the COADS set. The parameterization was determined to be accurately calculating the latent heating of the tropical atmosphere, and identified the mean position of the ITCZ and the SPCZ correctly. The seasonal variation in the position of ITCZ was also correctly identified. However, the linear model when forced by the mean field forcing failed to simulate the mean field accurately.

Model results forced with anomalous forcing were compared with the observations in the COADS data for the El Nino years of 1957, 1965 and 1972. Analysis was done for the onset phase, the peak phase, the mature phase and the retrieval phase for each of these El Nino years. The model results generally agreed with the observed anomaly field in the western and central equatorial atmosphere for all the simulations. Over the eastern ocean, however, the model simulations at times were incorrect. This discrepancy is due to the symmetric response of the linear model to the forcing in the eastern ocean. The magnitude of the simulated velocity field was generally weaker than that observed. The simulations were poor in the higher latitudes due to the neglect of non-linear advection effects in the model. In higher latitudes advection plays an important role.

The defects in the model were determined to be a consequence of neglecting feedback mechanisms in the calculation of the latent heat release. Inclusion of such feedback mechanisms is deemed to be necessary in linear models to correctly simulate the true atmospheric field.

The weaker velocity simulation is probably due to the neglect of solar radiation. By neglecting the solar heat flux the magnitude of the forcing is less, which in turn simulates a weaker response. The velocity components can be made stronger by using weaker friction coefficients. However, the present numerical scheme leads to instability for lower friction coefficients; use of alternate numerical procedures is recommended to fine tune the atmospheric model.

3.0 Ocean Modeling of ENSO

3.1 Introduction

The results of Chapter 2 and those of several other investigators indicate that much of the atmospheric variability during ENSO can be related, directly or indirectly, to changes in sea surface temperature. Only recently is work being done to understand the processes necessary to bring about SST anomalies. Much work, however, has been done in understanding the dynamical changes related to the observed anomalies in surface currents, sea-level, thermocline displacements and sea surface temperature. These results suggest a strong correlation of the observed oceanic changes during ENSO to equatorial wind stress anomalies.

Wyrtki (1975) first suggested that fluctuations in the strength of the southeast trades along the equator in the central Pacific was responsible for El Nino events. It was initially assumed El Nino resulted from cessation of coastal upwelling due to the weakening of the near coastal winds in the far eastern Pacific. As a consequence of this anomalous downwelling, dramatic changes in SST occurs in the eastern Pacific ocean. However, Wrytki demonstrated that no such changes occur in the near-coastal winds. On the contrary, he showed that the central Pacific equatorial winds were stronger than normal for a year or more prior to the warm event, resulting in an accumulation of mass in the western ocean. During the warm event when there is relaxation of the winds, mass flows eastward in the form of an equatorial Kelvin wave, displacing the thermocline in the eastern ocean. SST anomalies appear as the thermocline is depressed in the eastern ocean, suggesting the idea that the SST warms not as a result of reduction in upwelling but because of the large inflow of warm waters from the west, displacing the normally cool subsurface waters in the east.

McCreary (1976) and Hurlburt et al. (1976) demonstrated Wyrtki's theory with a simple two layer ocean model forced by an idealized wind stress. They showed that large coastal thermocline depth anomalies similar to those observed during ENSO could be generated by wind stress anomalies. They identified this response with eastward propagating, equatorially trapped Kelvin waves and westward propagating Rossby waves. Busalacchi and O'Brien (1981) and Cane (1984) show that wind stress anomalies poleward of 5° contribute very little to the signal in the equatorial wave guide region. Because of the success of these simple models, the relevance of linear equatorial waves to El Nino is undisputed.

However, very little work has been done to simulate the SST anomalies. McCreary and Anderson (1984) in their coupled model parameterized SST as proportional to the depth anomaly. Anderson and McCreary (1985) introduced active thermodynamics by including an equation for the temperature of the upper layer in the ocean model. Zebiak (1982) introduced an advection temperature equation with simple surface layer dynamics to simulate the SST field. His simulations are very similar to the observed SST anomaly field during ENSO and represent the most successful oceanic models so far.

In the oceanic model presented here, the SST field is not simulated. Rather, the effects of wind stress and heating on the anomalous surface currents are explored. Analogous to the atmospheric model, model simulations are compared with the observations for the 1957, 1965 and 1972 El Nino events. It will be shown that the linear oceanic model reproduces the salient equatorial wave characteristics of ENSO and is expected to simulate an El Nino-like phenomenon upon coupling with the atmospheric model.

3.2 The ocean model

Observations indicate that the relevant ocean dynamics are largely captured by simple linear theory. The present model follows a similar idea. There is no temperature equation and hence the thermodynamics are neglected. Instead, the simulated heat content anomaly in the column is forced by heating. The aim of the present study is to see if the linear model captures the salient features of ENSO for large surface stress anomalies. However, an explicit temperature equation or parameterization would have to be included before coupling the model with the atmosphere model discussed in Chapter 2.

The dynamical model used here is similar to that in the coupled Oregon State University general circulation model, with simplifications necessary for linearization. The present model is a two layer, shallow water, equatorial f-plane model. To speed up the computations- only baroclinic large scale, low frequency variability which is characteristic of ENSO is studied. Therefore, the barotropic mode is neglected.

Busalacchi and O'Brien (1980,1981) showed the relevance of linear dynamics to the seasonal and interannual variability of the tropical Pacific with a similar model.

In the first study, they forced the model with a prescribed mean wind stress modulated with annual and semi-annual harmonics as derived by Myers (1979), and obtained thermocline depth variability similar to the observations. In the later study, the model was forced by the ten-year observed winds from 1961-1970 encompassing two ENSO events. They reproduced the salient features of the eastern ocean upper layer depth variability.

Figure 23 shows the vertical structure of the two layer

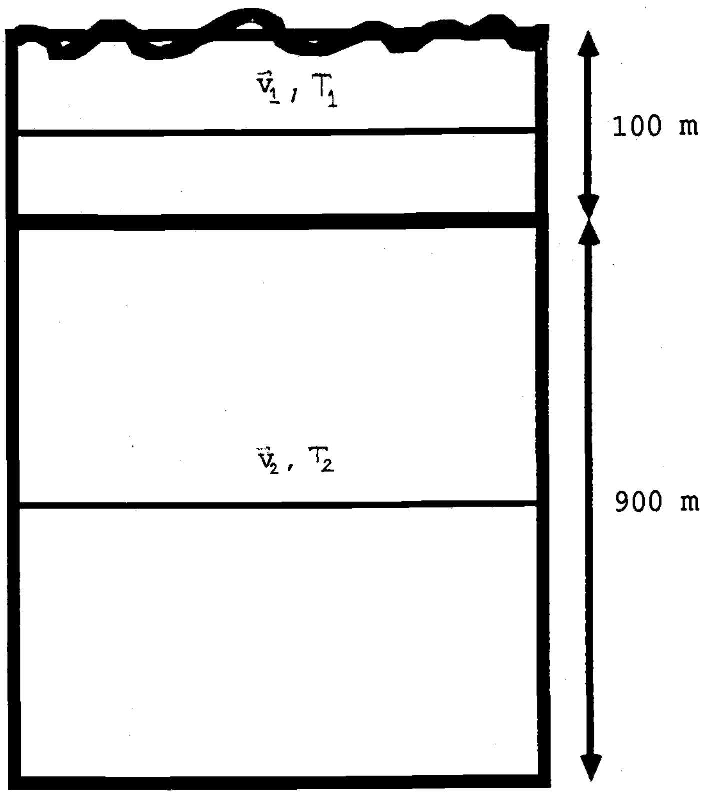

Fig.23. Two layer ocean model. The velocity vectors $\vec{v}$ and the temperatures T are carried at the middle of each layer.

model. Observations indicate that wind stress acts as a body force only over a shallow surface layer, making it dynamically most active. Therefore, to resolve this an upper layer depth of only 100 m is necessary. The lower layer depth of 900 m gives the total depth of 1000 m. This is not a serious deficiency since the barotropic mode is not relevant to the dynamics of the solution.

The velocities and temperature are evaluated at the center of each layer, i.e., at 50 m and 550 m depth, respectively. The momentum and thermodynamic equations for the two layers are given as

$$\frac{\partial \vec{v}_1}{\partial t} + f\hat{k}x\vec{v}_1 + \rho_0^{-1}\nabla p_1 = \gamma \vec{V}_s - k(\vec{v}_1 - \vec{v}_2) \quad (17)$$

$$\frac{\partial T_1}{\partial t} + w\frac{\partial \bar{T}}{\partial z} = \frac{Q_1}{\rho_1 c} - k(T_1 - T_2) \quad (18)$$

$$\frac{\partial \vec{v}_2}{\partial t} + f\hat{k}x\vec{v}_2 + \frac{\nabla p_2}{\rho_0} = k(\vec{v}_1 - \vec{v}_2) \quad (19)$$

$$\frac{\partial T_2}{\partial t} + w\frac{\partial \bar{T}}{\partial z} = k(T_1 - T_2) \quad (20)$$

where

$\vec{v}_1, \vec{v}_2$ are the horizontal velocity vector of each layer

T_1, T_2 is the temperature of each layer

$\vec{V}_s$ is the atmospheric wind acting as a stress on the upper layer

p_1, p_2 are the hydrostatic pressures at the mean depth of each layer

w is the vertical velocity at the interface layer

γ, k are transfer coefficients of stress and momentum respectively

$\bar{T}$ is the mean temperature of the model

c is the specific heat of sea water

ρ_1 is the density in the upper layer

ρ_0 is the mean density.

Assuming that ρ is linearly related to T by

$$\rho = \rho_0 (1 - \alpha T) \tag{21}$$

where α is the thermal expansion coefficient of sea water, and that the temperature difference ΔT of the two layers is constant, the total heat content in the model can be derived to be

$$h = \alpha (T_1 + T_2)(h_1 + h_2)/4 \tag{22}$$

As only the baroclinic mode is to be studied, subtracting equation (19) from equation (17) and using the definition of (22), the baroclinic equation is given by

$$\frac{\partial \vec{v}_d}{\partial t} + f\hat{k}x\vec{v}_d = -\ g\nabla h\ -\ 2k\vec{v}_d\ +\ \gamma\vec{V}_s \tag{23}$$

where $\vec{v}_d = \vec{v}_1 - \vec{v}_2$ is the shear velocity. Similarly adding equation (18) and (20), and using equation (22), the prognostic equation for the total heat content is given as

$$\frac{\partial h}{\partial t} + h_e\nabla.\vec{v}_d = \frac{Q}{4\rho c}\alpha H \tag{24}$$

where $h_e = \alpha\ H\ \Delta T/8$ is the equivalent depth. (25)

The values of α, ΔT and c were 0.0003 K^{-1}, 10 C and 4189.9 J kg^{-1} K^{-1}, respectively. This gives the equivalent depth as 37.5 cm. The values of k and γ are 1.1574 x 10^{-6} s^{-1} and 5.0 x 10^{-5} s^{-1}, respectively. The surface velocity is determined by dividing the wind stress by 1.04. This corresponds to a wind stress of 1 dyne cm^{-2} at a surface wind speed of 5 m s^{-1}.

The relevance of such a model to ENSO has already been explored by several authors. Hurlburt et al.(1976) and McCreary (1976) tested such a model with prescribed wind stress anomalies and showed that it captures the thermocline depth anomalies during a typical ENSO. Another point of interest in the present model is the simplicity of the projected coupling between the ocean and atmosphere models. The atmosphere model is driven by the changing thermal boundary at the sea surface while the ocean is driven by the effects of wind stress. This will greatly simplify the computations when the two models are coupled.

3.3 Numerical Procedure

Similar to the atmosphere model, finite difference analogs of equations (23) and (24) are solved numerically on a horizontal grid spanning the Pacific Ocean. The north-south and east-west extent of the model domain is similar to that of the atmospheric model. However, unlike the atmosphere model, closed boundary conditions are used around the model basin. Batteen and Han (1981) have shown that for ocean modeling the Arakawa B-grid (given in Fig.2) is stable for grid spacing greater than or equal to the Rossby radius. With a typical radius of deformation for the ocean of 100 km, the B-grid scheme is therefore adopted for the present study.

To speed up the computations, the leap-frog scheme is used as in the atmosphere case. The first time step is evaluated with the Euler-forward scheme, while every 10 time steps an Euler-backward scheme is adopted to prevent time splitting. After extensive experimentation with various grid spacings and time steps, it was found that a time step of 60 min satisfied the CFL condition for the grid spacing used in the present model. The grid spacing used was 1° latitude x 4° longitude giving Δx= 450 km and Δy= 112 km on a spherical Earth.

The finite difference form of equations (23) and (24) are given below in component form with the subscript d removed.

$$u^{n+1}_{i+\frac{1}{2},\, j+\frac{1}{2}} = u^{n-1}_{i+\frac{1}{2},\, j+\frac{1}{2}} + 2\Delta t\,[f_{j+\frac{1}{2}} v^{n}_{i+\frac{1}{2},\, j+\frac{1}{2}} - g\,\frac{h^{n}_{i+\frac{1}{2},\, j+\frac{1}{2}} - h^{n}_{i-\frac{1}{2},\, j+\frac{1}{2}}}{\Delta x}$$

$$- 2ku^{n-1}_{i+\frac{1}{2},\, j+\frac{1}{2}} + \gamma U_s] \tag{25}$$

$$v^{n+1}_{i+\frac{1}{2},\, j+\frac{1}{2}} = v^{n-1}_{i+\frac{1}{2},\, j+\frac{1}{2}} - 2\Delta t\,[f_{j+\frac{1}{2}} u^{n}_{i+\frac{1}{2},\, j+\frac{1}{2}} + g\,\frac{h^{n}_{i+\frac{1}{2},\, j+\frac{1}{2}} - h^{n}_{i+\frac{1}{2},\, j-\frac{1}{2}}}{\Delta y}$$

$$+ 2kv^{n-1}_{i+\frac{1}{2},\, j+\frac{1}{2}} - \gamma V_s] \tag{26}$$

$$h^{n+1}_{i,j} = h^{n-1}_{i,j} - 2\Delta t\ h_e\left[\frac{u^n_{i+\frac{1}{2},j} - u^n_{i-\frac{1}{2},j}}{\Delta x} + \frac{v^n_{i,j+\frac{1}{2}} - v^n_{i,j-\frac{1}{2}}}{\Delta y}\right]$$

$$+ \frac{\alpha H}{4\rho c} Q_{i,j} \tag{27}$$

$$u^{n+1}_{*i+\frac{1}{2},j+\frac{1}{2}} = u^n_{i+\frac{1}{2},j+\frac{1}{2}} + \Delta t\left[f_{j+\frac{1}{2}} v^n_{i+\frac{1}{2},j+\frac{1}{2}} - g\frac{h^n_{i+\frac{1}{2},j+\frac{1}{2}} - h^n_{i-\frac{1}{2},j+\frac{1}{2}}}{\Delta x}\right.$$

$$\left. - 2ku^n_{i+\frac{1}{2},j+\frac{1}{2}} + \gamma U_s\right] \tag{28}$$

$$v^{n+1}_{*i+\frac{1}{2},j+\frac{1}{2}} = v^n_{i+\frac{1}{2},j+\frac{1}{2}} - \Delta t\left[f_{j+\frac{1}{2}} u^n_{i+\frac{1}{2},j+\frac{1}{2}} + g\frac{h^n_{i+\frac{1}{2},j+\frac{1}{2}} - h^n_{i+\frac{1}{2},j-\frac{1}{2}}}{\Delta y}\right.$$

$$\left. + 2kv^n_{i+\frac{1}{2},j+\frac{1}{2}} - \gamma V_s\right] \tag{29}$$

$$u^{n+1}_{i+\frac{1}{2},j+\frac{1}{2}} = u^n_{i+\frac{1}{2},j+\frac{1}{2}} + \Delta t\left[f_{j+\frac{1}{2}} v^{n+1}_{*i+\frac{1}{2},j+\frac{1}{2}} - g\frac{h^n_{i+\frac{1}{2},j+\frac{1}{2}} - h^n_{i-\frac{1}{2},j+\frac{1}{2}}}{\Delta x}\right.$$

$$\left. - 2ku^{n+1}_{*i+\frac{1}{2},j+\frac{1}{2}} + \gamma U_s\right] \tag{30}$$

$$v^{n+1}_{i+\frac{1}{2}, j+\frac{1}{2}} = v^{n}_{i+\frac{1}{2}, j+\frac{1}{2}} - \Delta t [f_{j+\frac{1}{2}} u^{n+1}_{*i+\frac{1}{2}, j+\frac{1}{2}} + g \frac{h^{n}_{i+\frac{1}{2}, j+\frac{1}{2}} - h^{n}_{i+\frac{1}{2}, j-\frac{1}{2}}}{\Delta y}$$

$$+ 2kv^{n+1}_{*i+\frac{1}{2}, j+\frac{1}{2}} - \gamma V_s] \tag{31}$$

The subscripts refer to the grid points while the superscripts refer to the time steps. Note from Fig.2 that the velocity grid points are displaced half a grid length in both directions from the height grid points. Equations (25), (26) and (27) correspond to the leap frog scheme, while equations (28), (29), (30) and (31) correspond to the Euler-backward scheme. As before the starred equations are the predictor steps in the Euler-backward scheme. A zero velocity field and a uniform heat content of 43.2 m were used as initial conditions. The model simulations are discussed in the next section.

3.4 Model Simulations

(1) Spin-up Experiment

Wind-driven circulation is a major component of the oceanic general circulation. There are many observational as

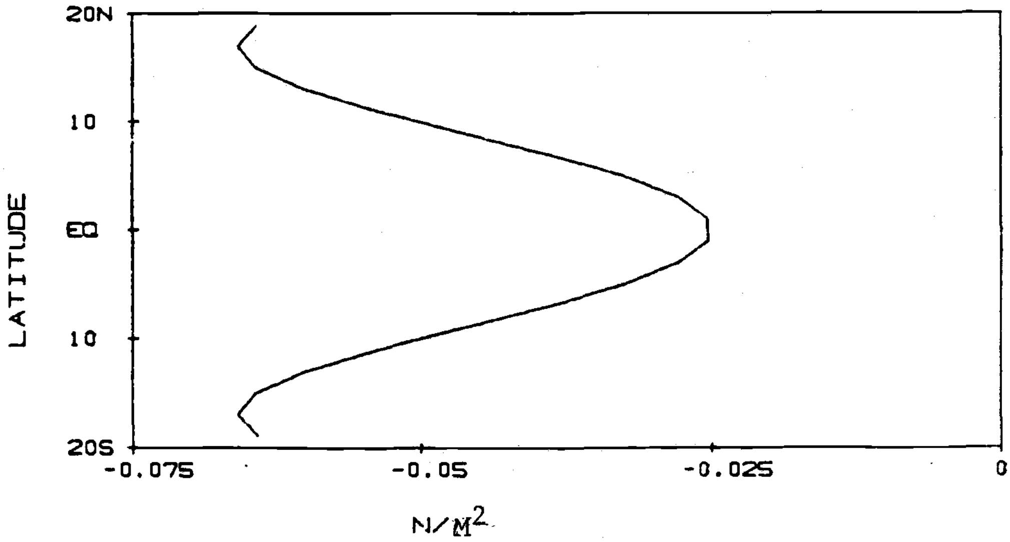

Fig.24. Mean wind stress prescribed over the ocean for run 1 as analysed by Han and Lee (1984).

(a)

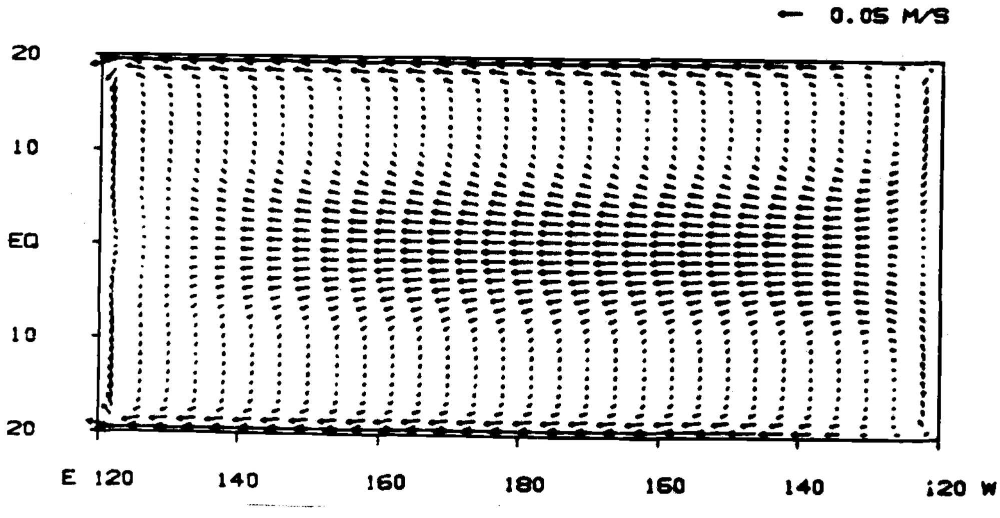

(b)

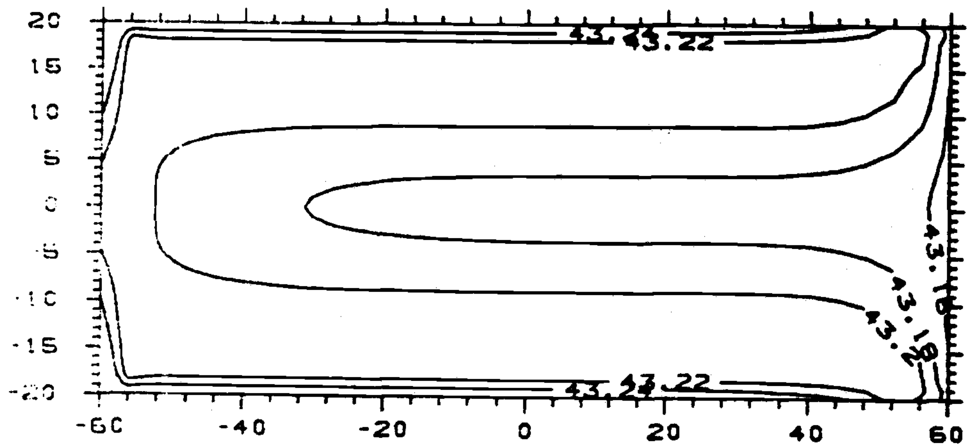

Fig.25. Ocean model simulations for steady wind stress forcing after 50 days. (a) Model upper layer currents. (b) Heat content field. Contour interval is 0.02 m. Initial heat content was 43.2 m everywhere.

well as model studies showing the effect of anomalous surface winds on the ocean during ENSO. Rasmusson and Carpenter (1982) show that the easterlies are stronger in the eastern ocean before the occurrence of El Nino. There is strong correlation between the weakening of the easterlies in the western ocean and the appearance of warm SST anomalies in the eastern ocean during the onset El Nino phase, indicating that the weakening of the trades is a precursor to the occurrence of El Nino.

To test this hypothesis and to check the model behavior, a mean stress field as analysed by Han and Lee (1983) and reproduced in Fig.24 was prescribed throughout the model domain. The model was allowed to spin up for 50 days to attain equilibrium. The simulated upper layer current anomaly is given in Fig.25 (a) while the corresponding heat content is given in Fig.25 (b). In this run the model extended only 20° on either side of the equator to give better resolution This is reasonable because observations indicate that wind stress anomalies beyond 5° latitude are not important for ENSO.

The strong equatorial current is to be expected from theory. The wind stress pushes the surface water from the eastern ocean to the western boundary where it sinks, giving a deep counter current rising at the eastern boundary. Beyond

5° on either side of the equator, the Coriolis term turns the flow which then appears as a meridional current. This meridional current, along with the closed boundary condition at the northern and southern walls, accumulates mass at the walls and creates a strong meridional pressure gradient. The zonal current along the walls is necessary to geostrophically adjust to the pressure gradient. The same is observed in the heat content.

Due to the downwelling along the western boundary and upwelling along the equator and in the eastern Pacific, the thermocline is deeper in the western ocean and shallower along the equator. This is similar to observations in the Pacific before the occurrence of ENSO. The estimated upwelling at the eastern boundary in the model is approximately 0.172 m per day and the downwelling is estimated at 0.3 m per day. This corresponds well with the results of Hurlburt et al. (1983) except for the presence of the strong current along the boundary. This difference is due to the type of boundary conditions used in these two studies. Hurlburt et al. used an open boundary while the present study has adopted a closed boundary. Introducing an open boundary would complicate the computations, as an implicit method is necessary to solve for the boundary condition. Therefore, to maintain simplicity only a closed boundary was used; it is believed this will not impair the model in any case.

(2) Spin-down Experiment (a)

To see how the model behaves for spin down, the wind stress was suddenly relaxed at day 50 throughout the domain. The model was run in this manner for an additional 50 days. Figs.26(a) and 26(b) give the current field and the heat content at day 100. The reversal of the current from the western boundary along the equator and the westward flowing current 8° on either side of the equator correspond to the Kelvin waves and to the detached Rossby wave, respectively. From the western boundary, Kelvin waves propagate eastward, depressing the thermocline along its path. Due to the characteristics of the Kelvin wave, it propagates poleward along the eastern coast and thereby excites Rossby wave which propagate westward. The wave speed can be verified by taking a time series of the flow; such an analysis has confirmed the model's ability to simulate Kelvin and Rossby waves successfully. Another way to verify the Kelvin wave is to look at the meridional structure of the flow. However, the resolution is not fine enough along the eastern boundary to resolve the coastally trapped Kelvin wave.

Physically the presence of these waves can be explained as follows. Due to the wind stress forcing, mass is

(a)

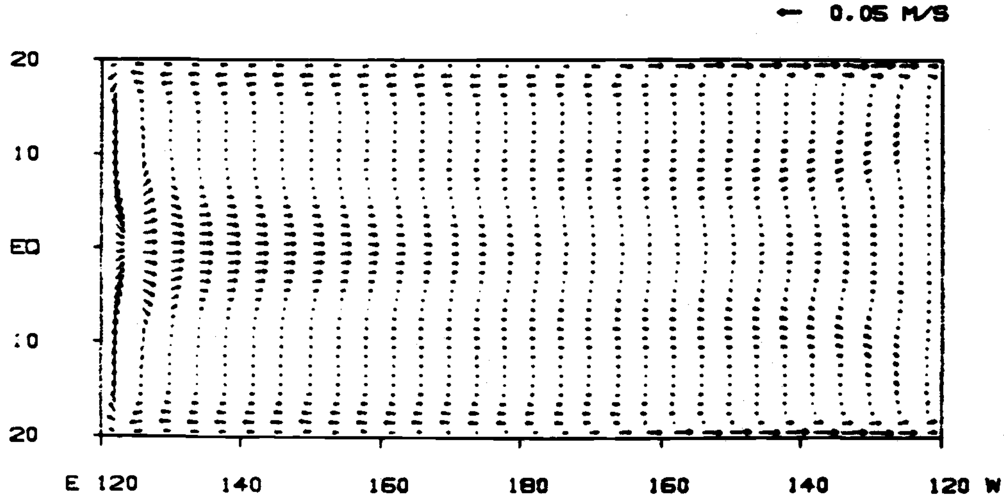

(b)

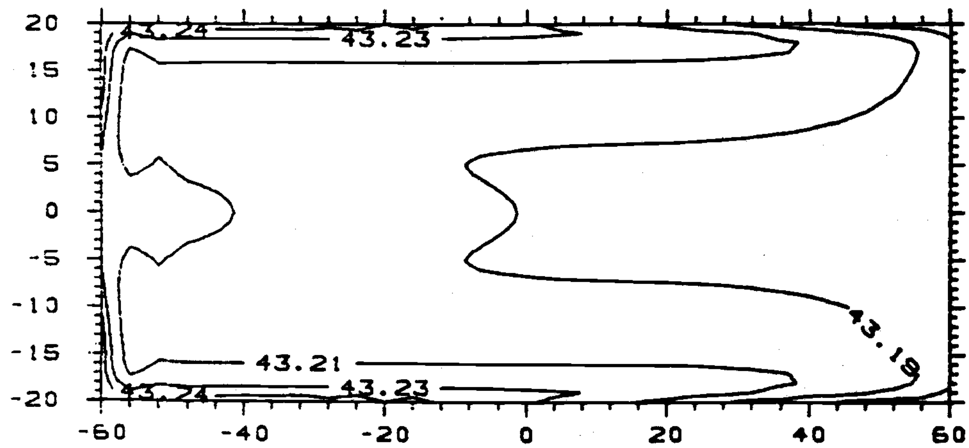

Fig.26. Ocean model simulations at day 100 following a relaxation of the wind stress at day 50 over the whole ocean. (a) Model upper layer currents. (b) Heat content field. Contour interval is 0.02 m.

accumulated along the western boundary creating a horizontal pressure gradient. When the wind is relaxed, this pressure gradient drives an eastward flowing current in the form of a Kelvin wave. Since the Kelvin wave exhibits a non-linear character, it propagates poleward to adjust to the pressure gradient, thereby exciting westward propogating Rossby waves. Similar propagation of the thermocline depth is seen from Fig.26(b). This demonstrates the importance of the relaxation of the wind during ENSO to the presence of SST anomalies. The warm waters from the western ocean propagate eastward while depressing the thermocline there, and the resulting reduction in upwelling is manifested as positive sea surface temperature anomalies in the eastern ocean. This demonstrates the model's ability to capture the essential features of Kelvin waves and Rossby waves during ENSO.

(3) Spin-down Experiment (b)

Observations indicate that the easterly trades are weaker only in the western Pacific and not over the whole domain as was assumed in the previous run. Figures 27 (a) and 27 (b) give the velocity field and the heat content, respectively, at day 100 after relaxing the wind stress suddenly at day 50 but only over the western ocean. Similar eastward propagating Kelvin waves are visible, depressing the

(a)

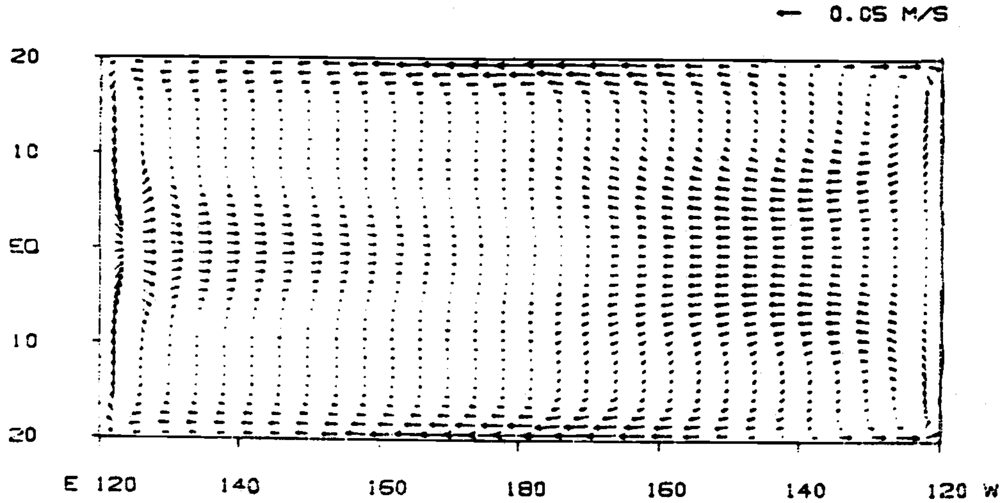

(b)

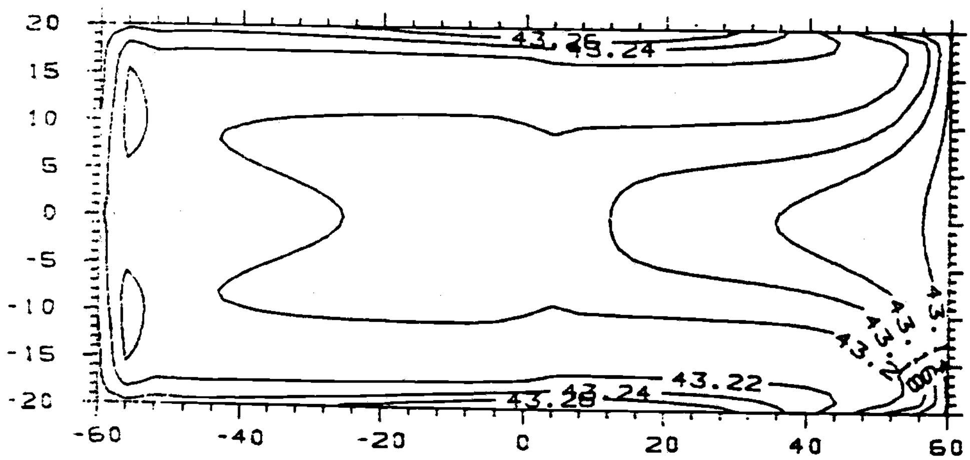

Fig.27. Same as in Fig.26 except for wind stress relaxed at day 50 over only the western half of the ocean.

thermocline along its way. Westward propagating Rossby waves are visible about 10° on either side of equator. However, the poleward propagating Kelvin waves are not present due to the strong wind stress in the eastern ocean. In the heat content, the depression of the thermocline is seen as the Kelvin wave propagates.

(4) Anomalous Wind Stress Forcing

It has been suggested by many studies that wind stress is one of the major forcings on the ocean in producing the large-scale current systems on the globe. Therefore, it is reasonable to assume that the anomalous winds would be important in the occurrence of El Nino. In this run the anomalous wind field from the COADS data is prescribed as a body force acting on the top layer of the ocean model. The perturbation field is found by subtracting the long term mean wind vector field from the monthly mean field, after using a nine point filter on each component. The wind stress factor γ is $5.0 \times 10^{-6}\ s^{-1}$ which corresponds to a stress of 1 dyne cm^{-2} at a wind speed of 5 m s^{-1}. As before, the four phases of ENSO are discussed.

(i) Onset Phase

Figure 28 (a,b) shows the model simulated anomalous currents and heat content for January 1957 corresponding to

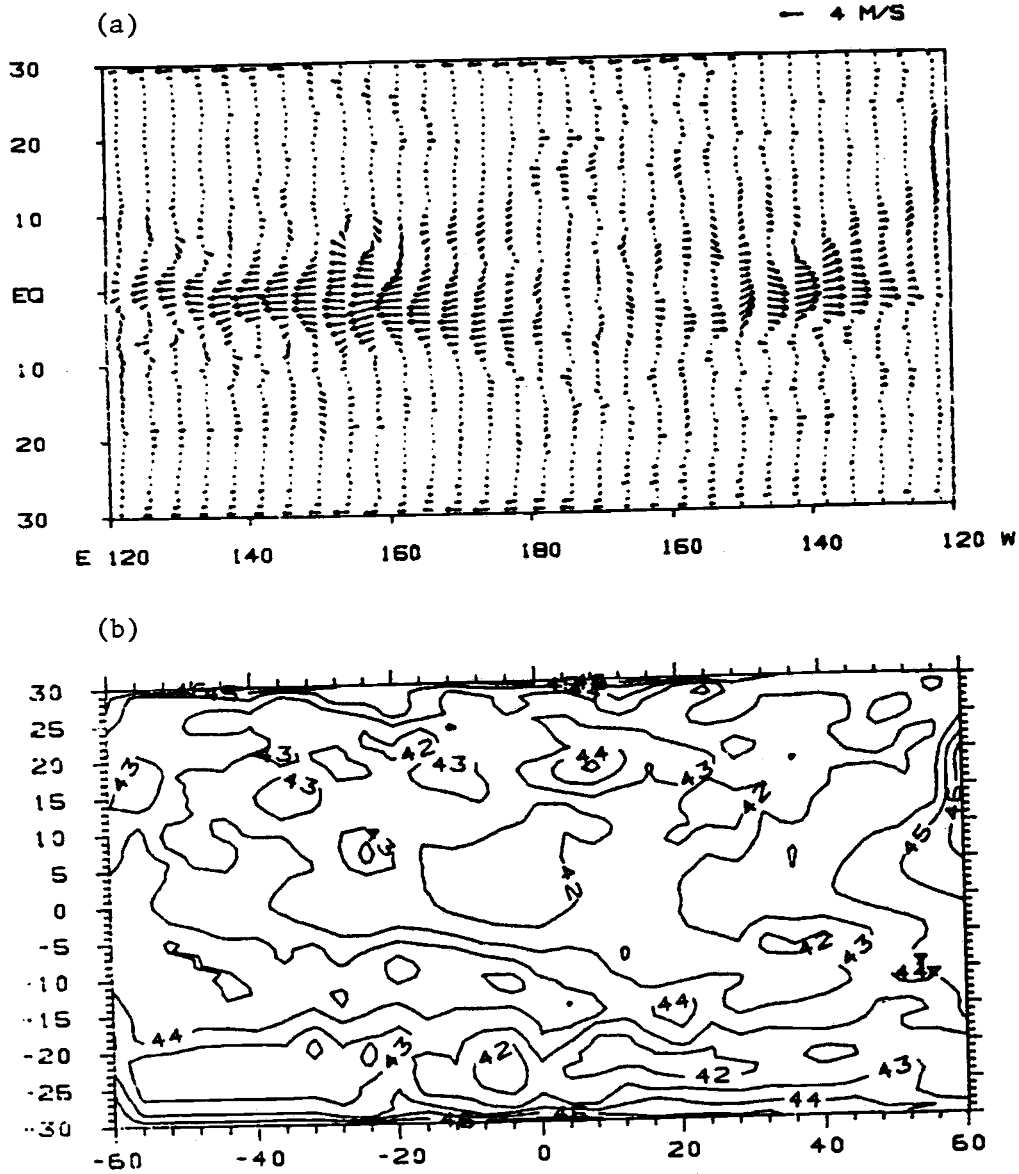

Fig. 28 . Anomalous wind stress effects for January 1957. (a) model simulated currents (b) model simulated heat content field. Contour interval is 1 m.

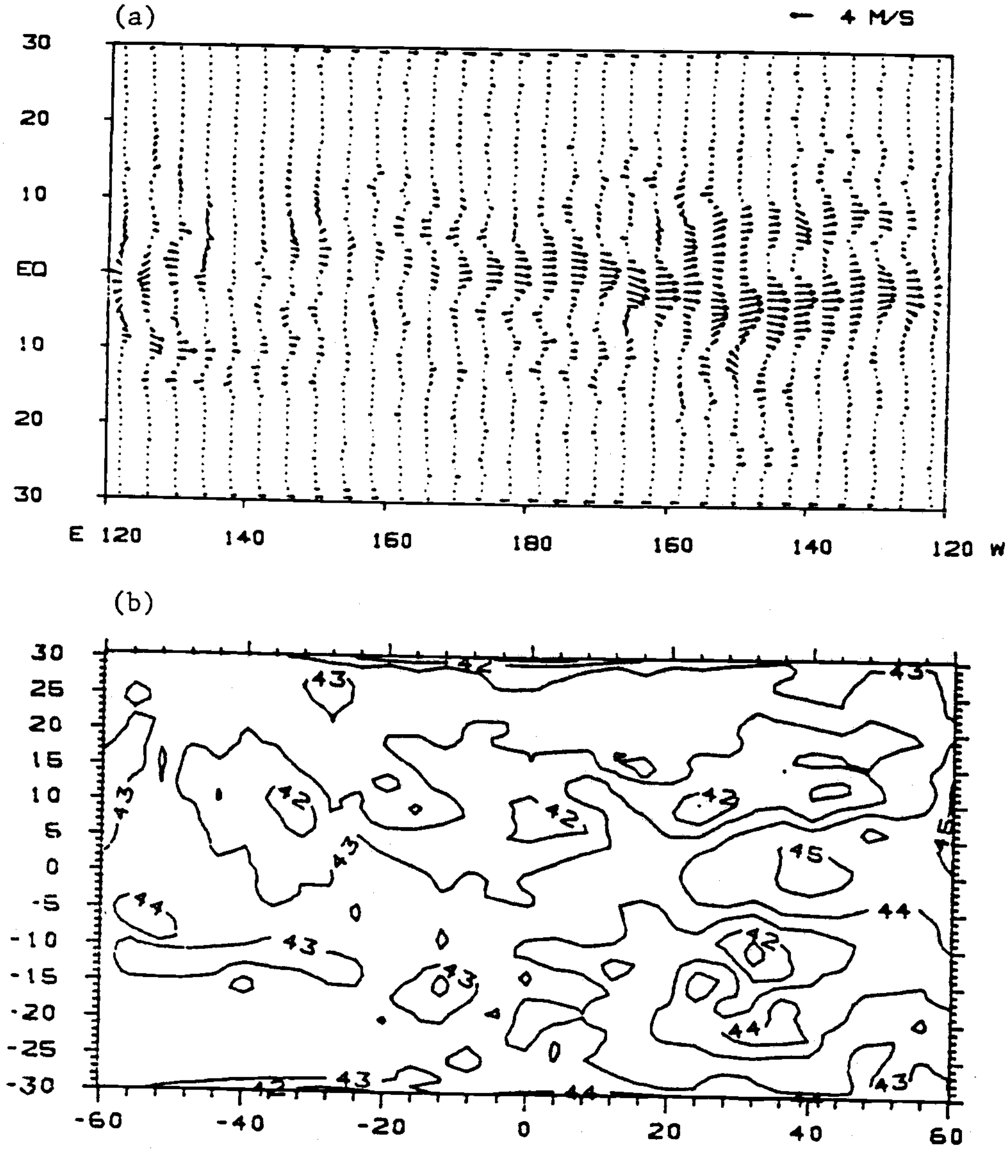

Fig.29. Same as in Fig. 28 except for January 1965.

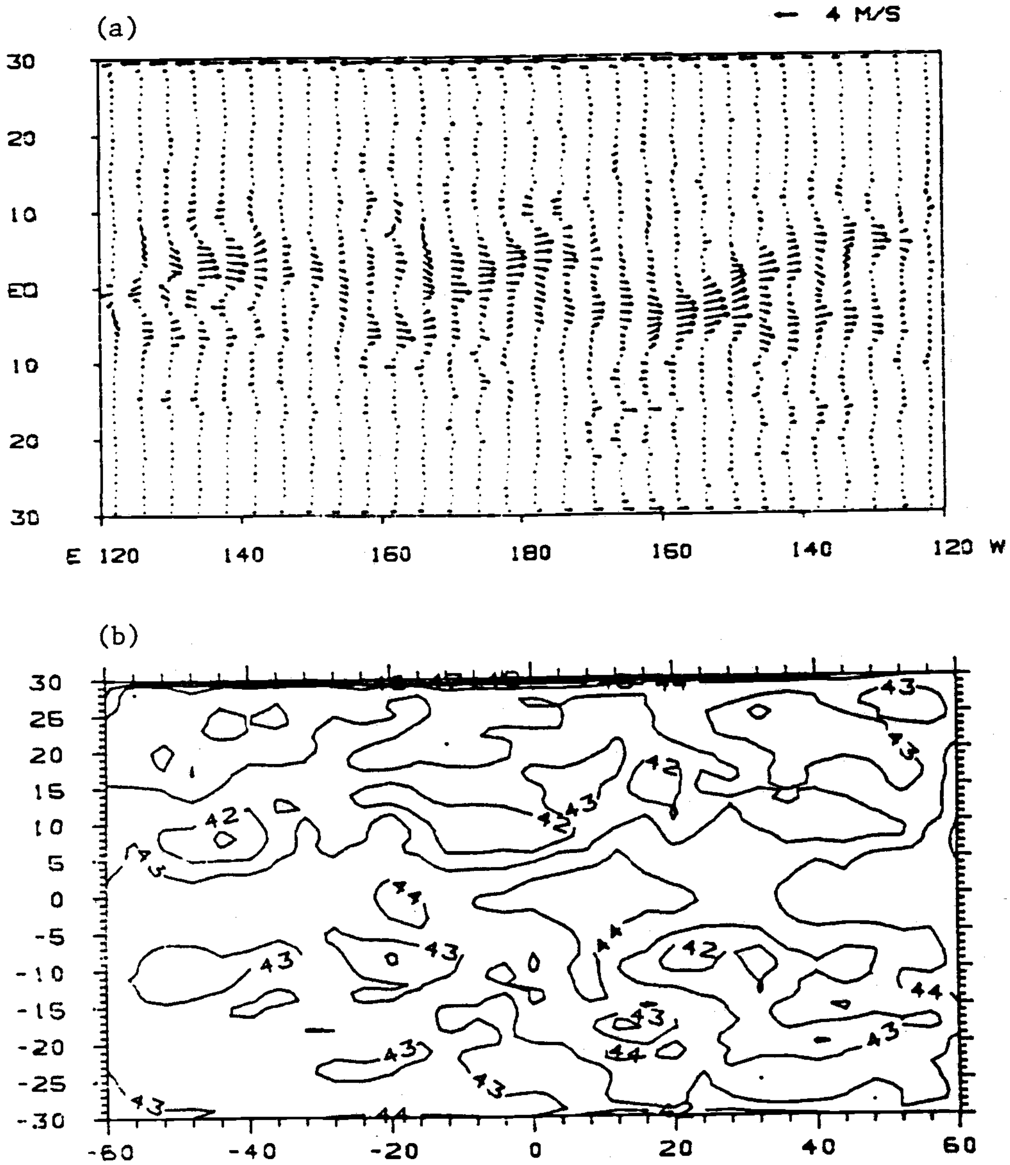

Fig.30. Same as in Fig.28 except for January 1972.

the onset phase of ENSO. Figures 29 and 30 follow similarly for January 1965 and 1972, respectively. The onset phase is characterized by westerlies over the eastern ocean and easterlies over the central and western ocean. The currents follow closely the wind stress forcing in a narrow equatorial band of about 10° width. This is seen in all the runs in the present model. This result corresponds to that of Busalacchi and O'Brien (1981) and Cane (1984) who found that anomalous wind stress poleward of 5° are not important. The eastward current in the east produces anomalous downwelling, causing deepening of the thermocline there and suppressing upwelling. In the case of 1965 and 1972, the eastward current is widespread, and could transport normally warm waters from the west to the eastern ocean. As mentioned earlier, the deeper thermocline is present in the east in the model simulated heat content. Recall that the model was initialized with 43.2 m depth. Relating directly the difference in the heat content from the initial value to the SST anomaly; the model simulates anomalies greater than 1 C in the eastern ocean. In the central and western Pacific, cooler waters are simulated.

(ii) Peak Phase

Figure 31 shows results similar to those of Fig.28 except for July 1957 corresponding to the peak phase. Figures 32, 33 are for July of 1965 and 1972, respectively. The

(a)

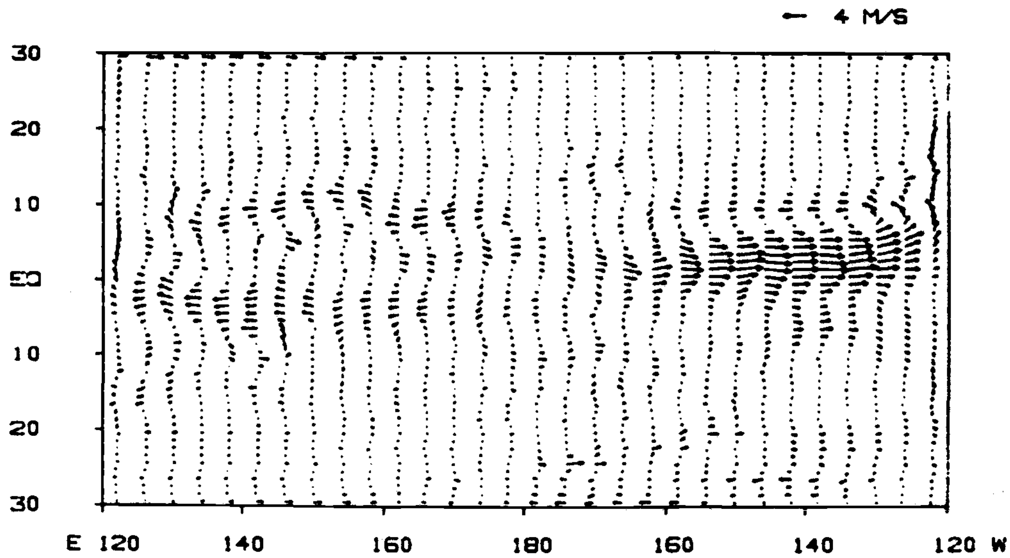

(b)

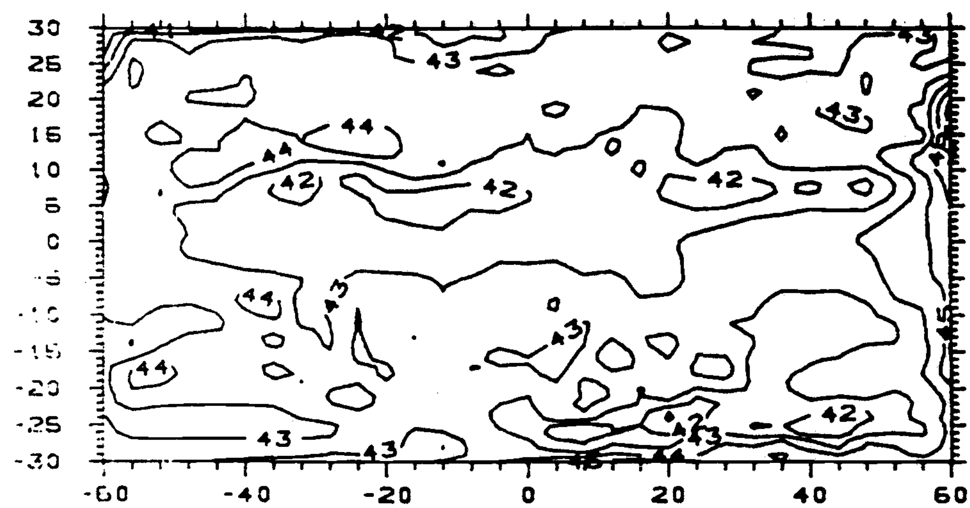

Fig.31. Anomalous wind stress effects for July 1957. (a) model simulated currents (b) model simulated heat content field. Contour interval is 1 m.

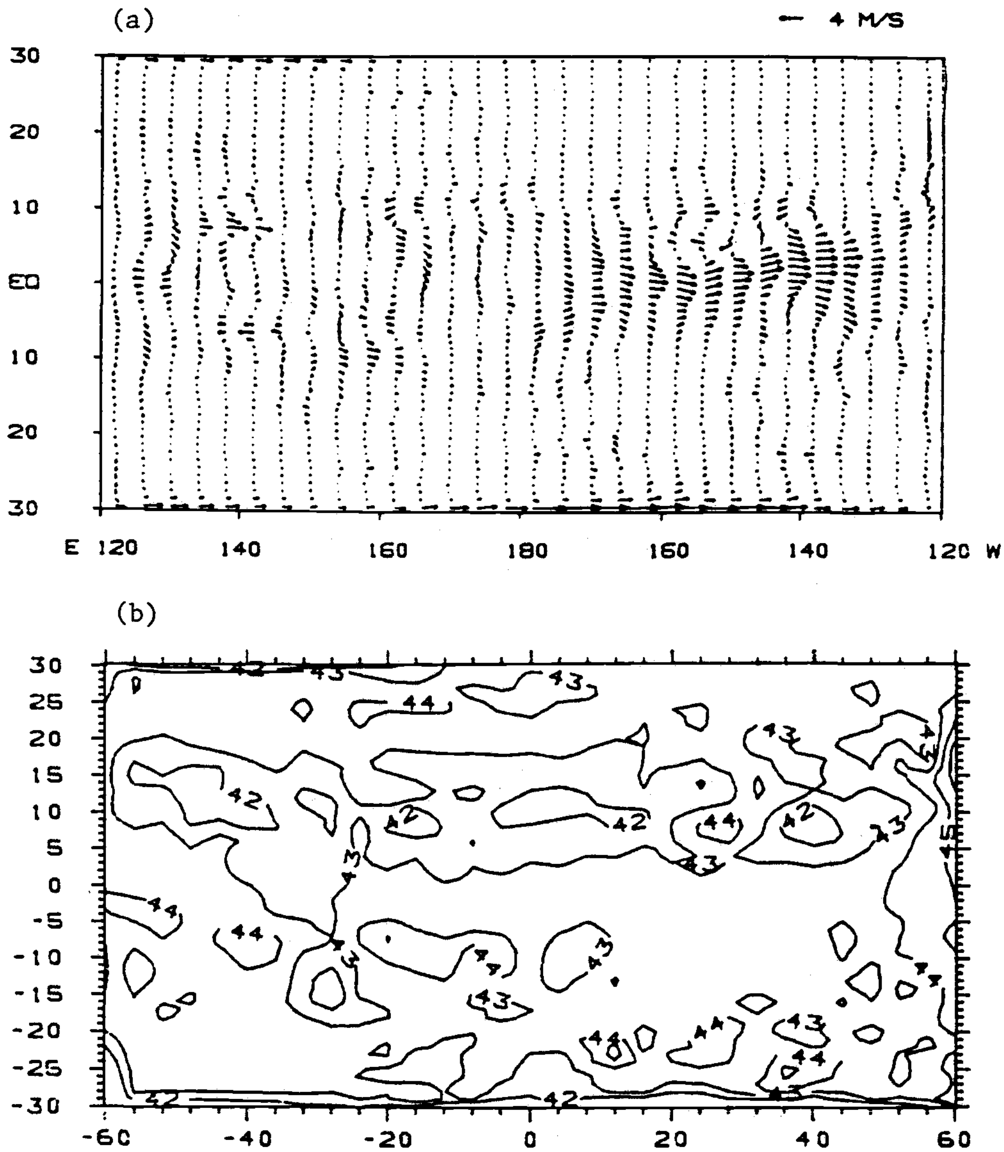

Fig.32. Same as in Fig.31 except for July 1965.

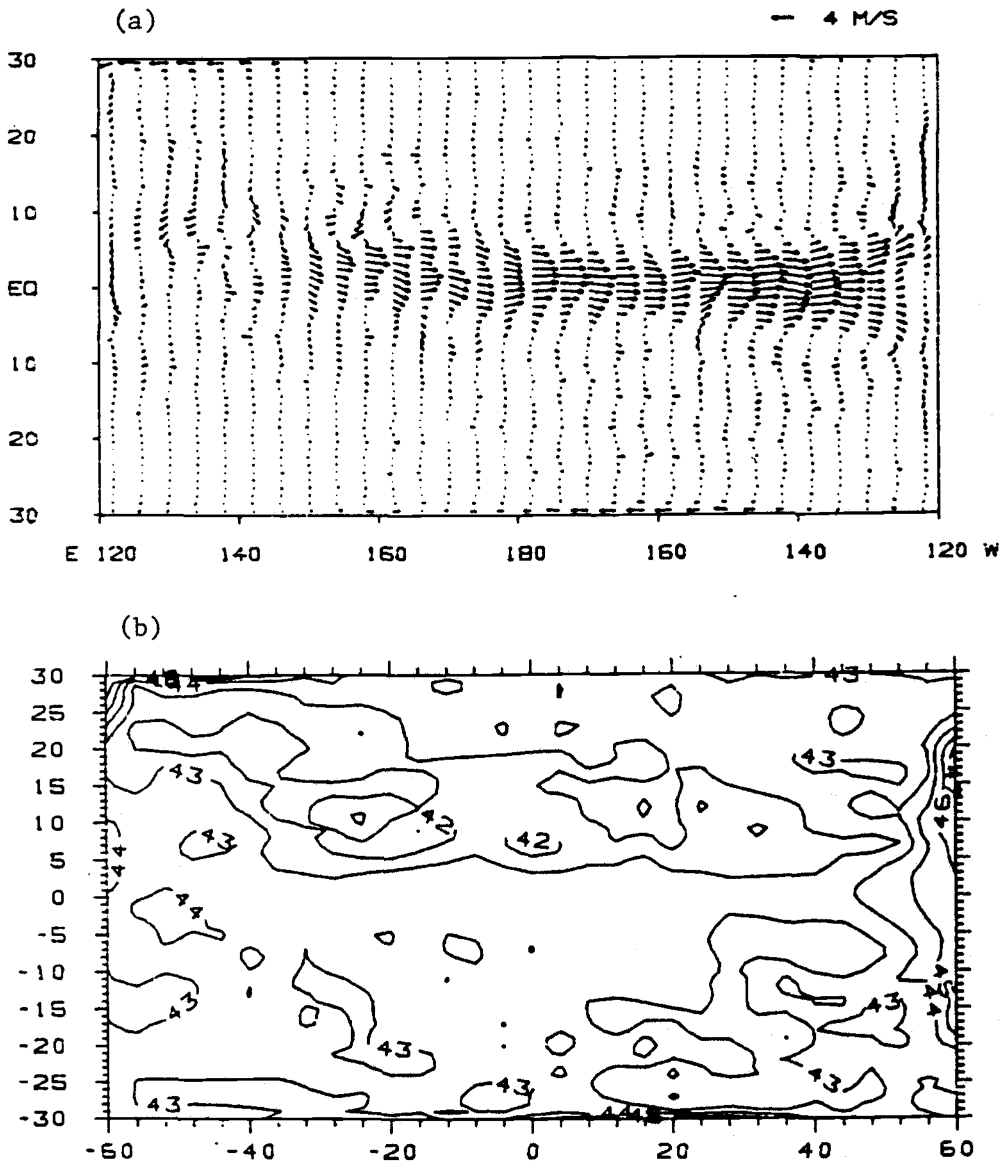

Fig.33. Same as in Fig.31 except for July 1972.

strength of the eastward current has increased in all cases, and in July 1957 the current has become widespread. However, there are still some westward simulated currents corresponding to the presence of easterlies there at this time. Another important feature at this phase is the presence of a coastally trapped poleward current along the eastern boundary. This indicates the beginning of poleward spreading of the warm water which is characteristic at this phase. This is seen in the heat content also. The 44 m contour covers the whole north-south extent in the eastern ocean. However, the heat content is cooler in the central and the western ocean.

(iii) Mature Phase

Figure 34 (a,b) shows the current and the heat content for January 1958. Figs. 35 and 36 are for January 1966 and 1973, respectively. By this time the SST anomaly is off the coast and appears to peak in the central Pacific. Easterly winds also appear over the western ocean at this time. The extent and strength of the eastward currents appear to be reducing, following the wind stress; only in 1958 is it stronger and wider because the 1957 event was particularly strong. As in the previous case the heat content follows closely the current field. The 44 m isoline spreads longitudinally into the central ocean as does the SST

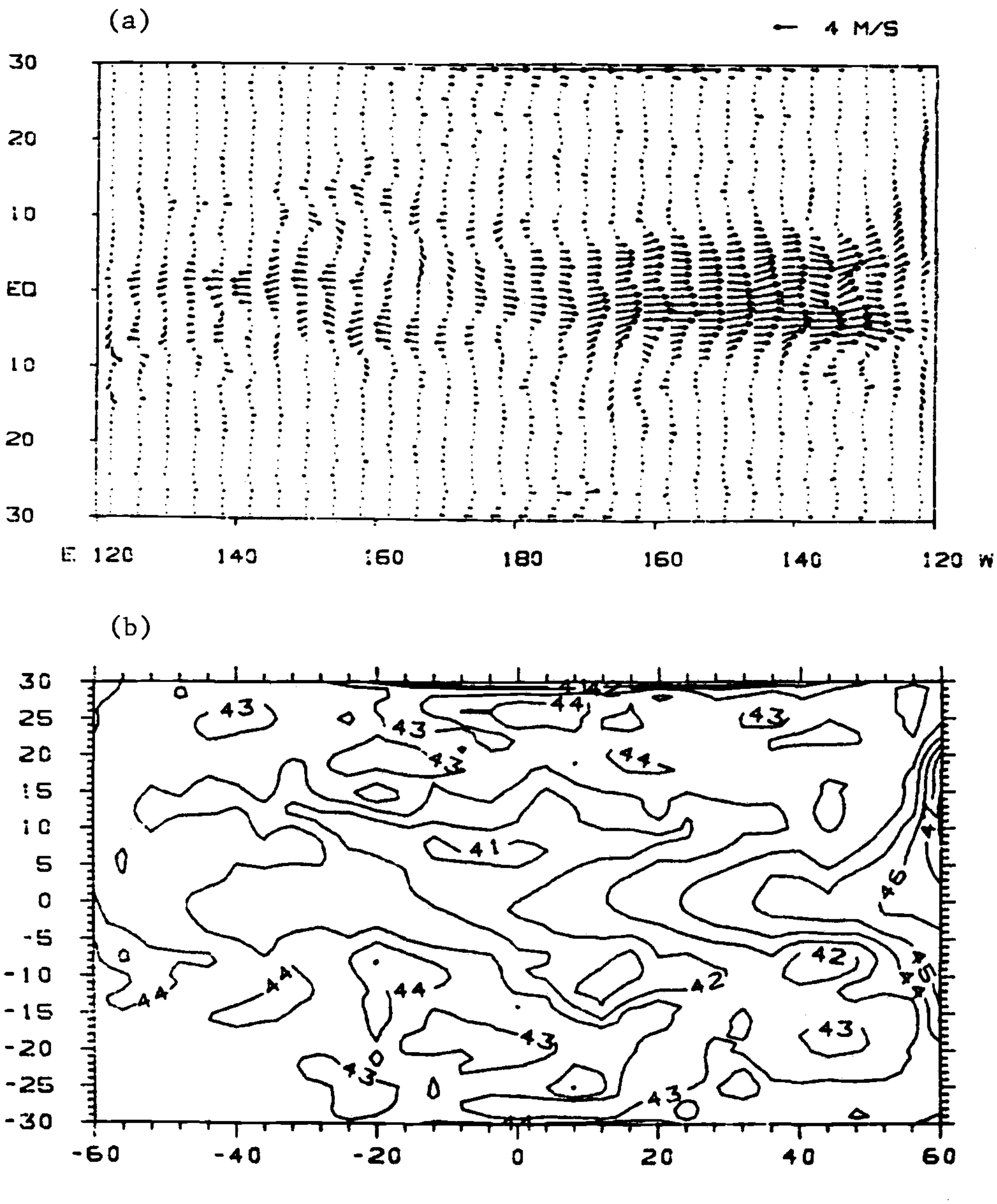

Fig.34. Anomalous wind stress effects for January 1958. (a) model simulated currents (b) model simulated heat content field. Contour interval is 1 m.

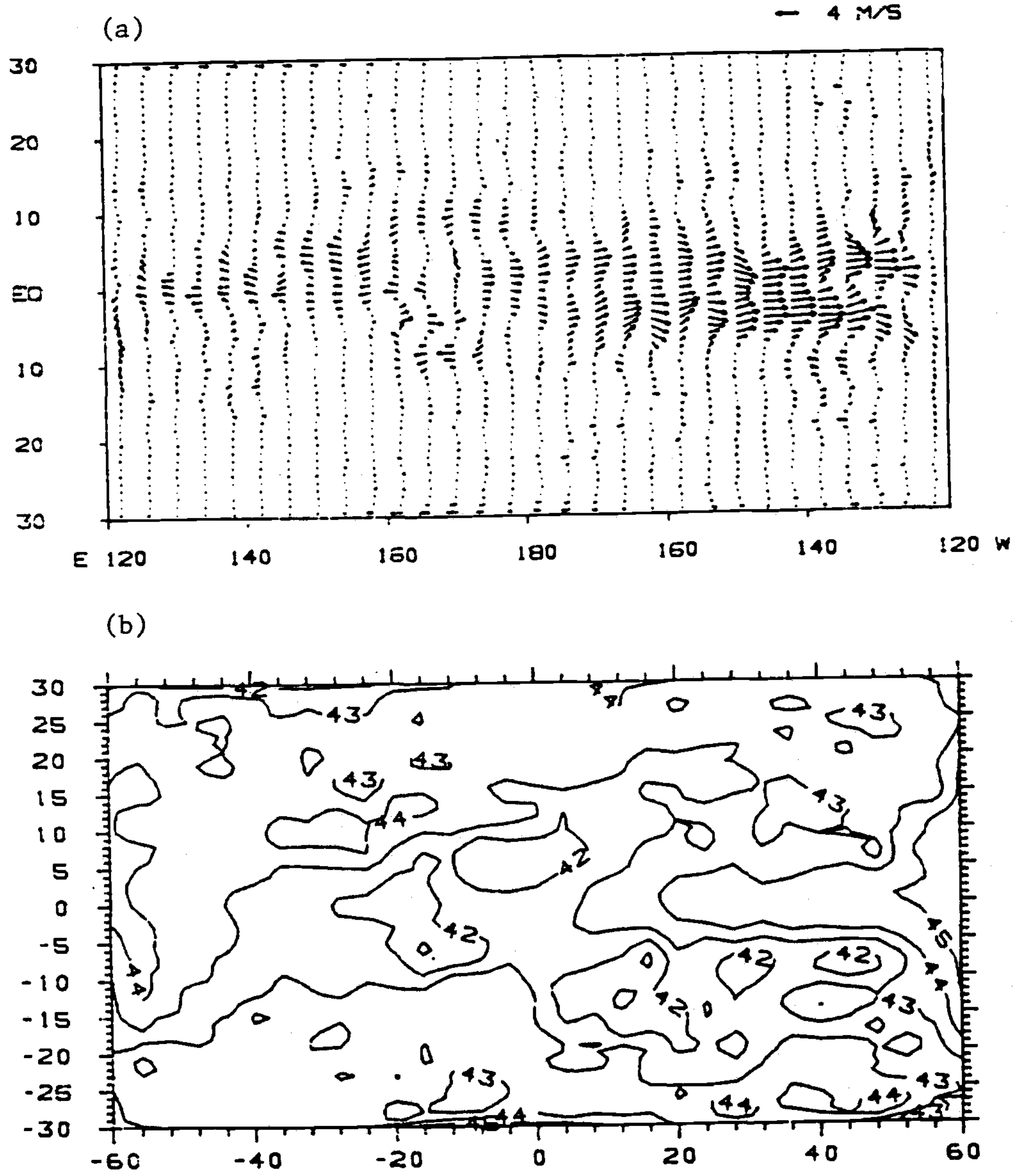

Fig.35. Same as in Fig.34 except for January 1966.

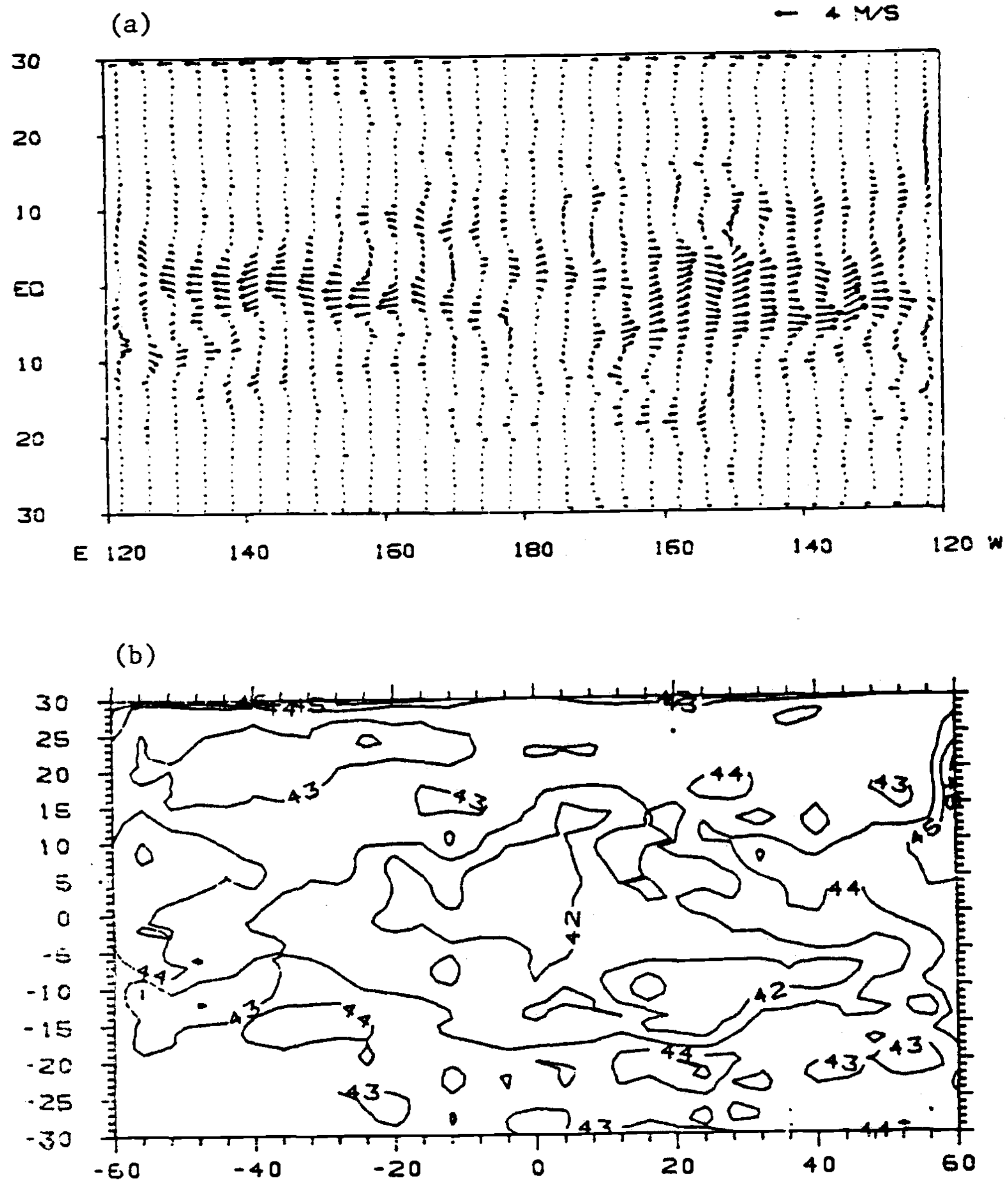

Fig.36.. Same as in Fig.34 except for January 1973.

anomaly. This result is closely related to the observation that in the eastern ocean the thermocline depth is proportional to the SST anomaly. In the present case, from this assumption the predicted SST anomaly maximum would be approximately 3 C. This is about the same as that observed. However, observations indicate that this relationship is not true in the central and western ocean.

(iv) Retrieval Phase

Figures 37, 38 and 39 show the model currents and height for July of 1958, 1966 and 1973, respectively, corresponding to the retrieval phase of El Nino. At this time the SST and wind anomaly is returning to normal. The SST anomaly in the east is gone and the winds are easterly over most of the ocean. Following this the westward currents appear all along the equatorial portion of the ocean. The coastally trapped poleward current is not present and therefore the small SST anomaly that is present is limited in both east-west and north-south extent. This demonstrates the importance of wind stress effects during the El Nino event and justifies coupling with the atmosphere through the wind stress.

3.5 Conclusions

The linear two layer oceanic model presented here

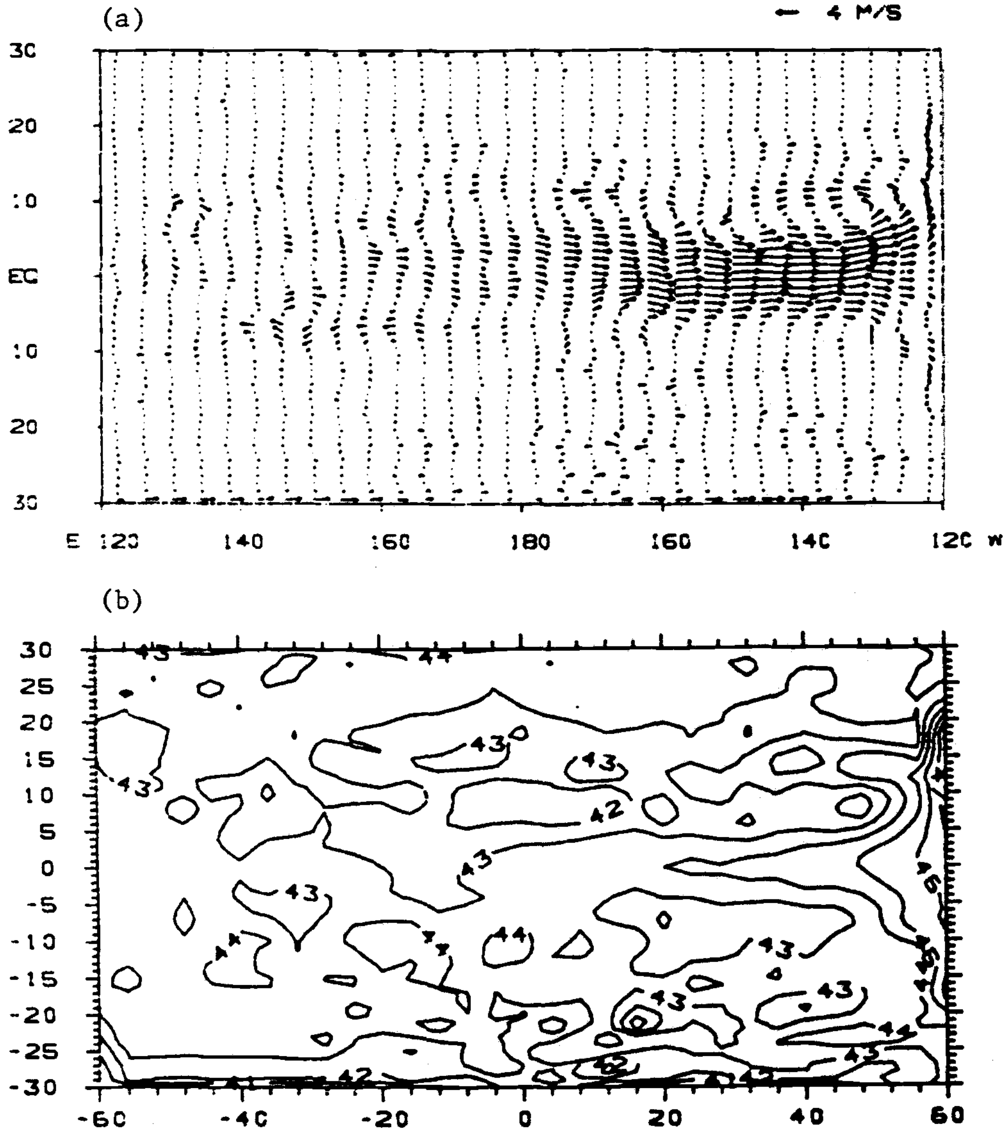

Fig.37 . Anomalous wind stress effects for July 1958. (a) model simulated currents (b) model simulated heat content field. Contour interval is 1 m.

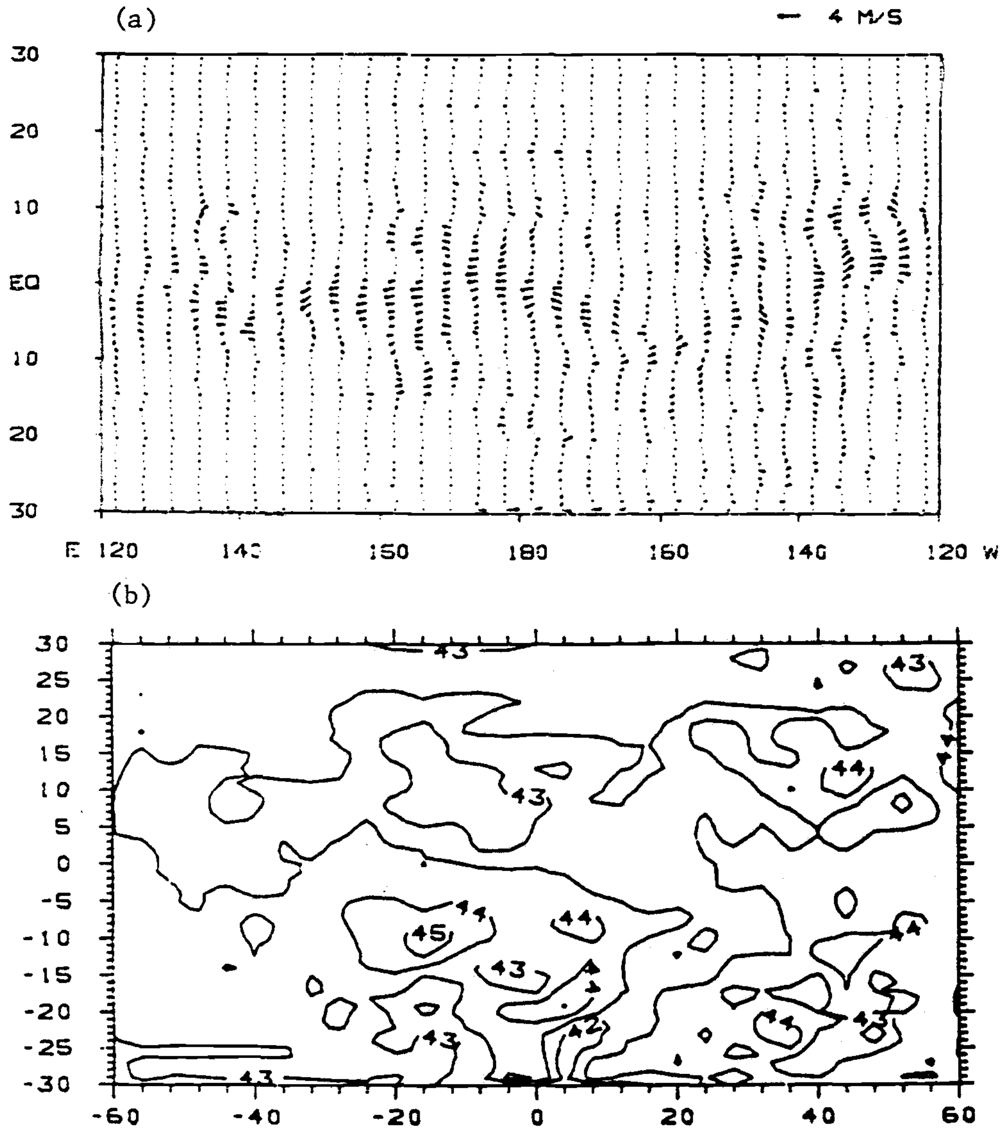

Fig.38. Same as in Fig.37 except for July 1966.

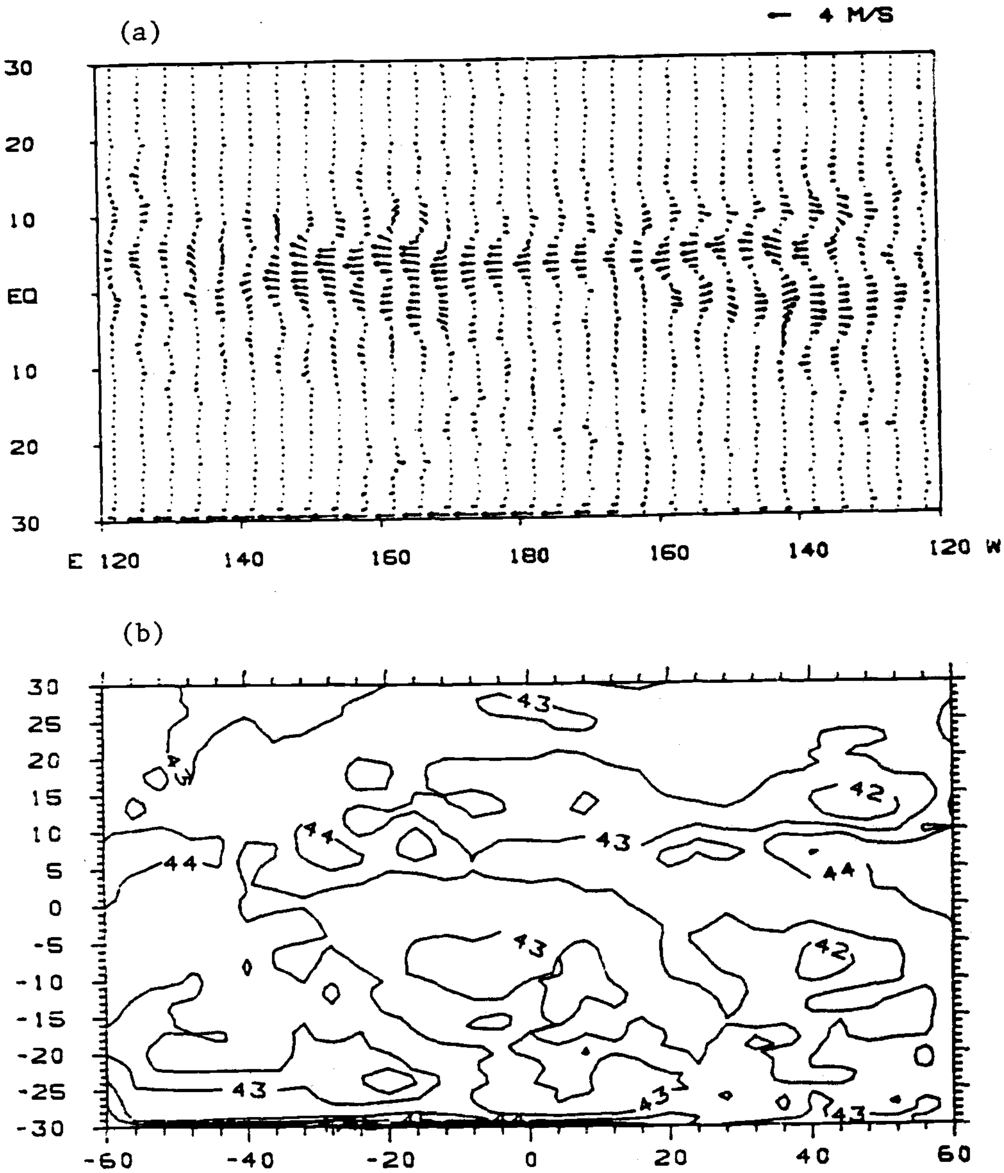

Fig.39. Same as in Fig.37 except for July 1973.

simulated the currents associated with wind stress forcing with reasonable accuracy. When the model was forced by a sudden relaxation of the wind stress in the tropics, strong eastward flowing currents along the equator were realistically simulated. A strong boundary current along the northern and southern walls was determined to be due to mass accumulation along the walls by the closed boundary condition. This contrasted with the result of Hurlburt et al.(1981) who used an open boundary along the north-south walls.

After the model achieved equilibrium with the wind stress forcing, spin-down calculations were carried out by first relaxing the wind in the whole domain and then by relaxing the wind only in the western half. Equatorially trapped Kelvin waves excited along the eastern and western boundaries could be tracked in the model. However, the model resolution was not fine enough to resolve the coastal Kelvin waves. In the second case, poleward propagating Kelvin waves were not detected. Westward propagating Rossby waves were visible from the eastern boundary in the first case and from the longitude of the wind stress in the second case. The model's ability to simulate these two important wave characteristics was determined to be reasonable.

Anomalous wind stress was calculated from the COADS data for the years 1957, 1965 and 1972. As in the atmosphere model the four phases of El Nino were examined. Only wind stress effects were studied in the model. When the model was forced by the anomalous wind stress for these warm events from the COADS data, the current and the heat content exhibited many characteristics of El Nino. The currents followed the wind stress very closely, but only in the equatorial band of 10°. Beyond this latitude the anomalous wind stress did not play an important role. The heat content is closely related to the current. Relating directly the deviation in the simulated heat content from the initial condition in the eastern ocean gave a reasonable estimate of observed SST anomaly. This suggests that anomalous wind stress is critical in the simulation of ENSO.

4.0 Summary and Suggestions for Further Research

The atmosphere model presented here is seen to simulate the observed anomalies over the western and the central Pacific Ocean quite well, especially for the mature phase of El Nino. It is seen that the model could be improved by including the mean field effects in the atmospheric latent heat release and extending the east-west domain of the model to reduce the effects of cyclic boundary conditions. The atmospheric latent heat release parameterization in terms of the CISK process was found to be realistic, and the model divergence follows the parameterized heating closely. It was demonstrated that linear models cannot simulate the anomalies in the higher latitudes where advection of heat is critical.

The ocean model demonstrated the importance of wind stress in the occurrence of an oceanic El Nino event. It is seen that wind stress anomalies poleward of about 10° are not important in the simulation of ENSO events. This suggests the use of a narrower ocean in the coupled ocean-atmosphere model to save computational time. The present study has demonstrated that for ocean models, the effect of surface heating is negligible. This justifies coupling with the atmosphere through only the wind stress.

Before coupling the two models, some important aspects have to be looked in to. The atmosphere model has to be closely studied to determine the cause of the easterlies east of the heating. One of the areas to explore in the model is the feedback processes in the estimation of latent heat release. The atmosphere model also has to be tuned with regard to the friction coefficients by exploring other numerical schemes that give stable methods for lower order friction coefficients. It is critical to simulate correct velocities in the coupled model because the simulated SST in the ocean follows closely the velocity field.

In the ocean model, parameterization of the SST in terms of other variables has to be introduced and tested. It is clear from the present study and that of others, that advection effects are important in the simulation of SST. In the eastern ocean the relation between height anomaly and SST anomaly seems to be close. Zebiak has suggested that in the ocean model boundary layer effects are important to successfully simulate an El Nino phenomenon. The present study cannot determine this to be true but it would be worthwhile to explore this possibility.

Finally, due to the inherent grid mismatch present in atmosphere-ocean models, the effects of averaging methods should be determined. It is hoped that the successful latent heat parameterization in the present model will permit an ENSO-like disturbance to be simulated in a coupled model.

The conceptual method to introduce interactions between the atmosphere and ocean models is as follows. The atmosphere drives the ocean through the wind stress thereby changing the SST distribution by the horizontal and vertical currents. The changing thermal boundary drives the atmospheric model through the sensible heat flux and the latent heat thus completing the feedback cycle. At present, the relationship of SST to the ocean currents is not specified in the model.

5.0 References

Anderson,D.L.T., and J.P.McCreary,1985. Slowly propogating disturbances in a coupled ocean-atmosphere model. J. Atmos. Sci., 42:615-628.

Anonymous,1985. COADS (Comprehensive Ocean-Atmosphere Data Set), Release 1. NOAA/ERL, Boulder, CO, pp.225.

Arakawa,A., and V.R.Lamb,1977. Computational design of the basic dynamical processes of the UCLA general circulation model. In Methods of Computational Physics, Vol.17, Academic Press, New York, 173-265.

Barnett,T.P.,1983. Interaction of the monsoon and Pacific trade wind system at interannual time scales: Part I, the equatorial band. Mon. Wea. Rev., 111:756-773.

Batteen,M.L., and Y.J.Han,1981. On the computational noise of finite difference schemes used in ocean models. Tellus, 33:387-396.

Berliand,T.C.,1960. Method of climatological estimation of global radiation. Meteor. Gidrol., 6:9-12.

Busalacchi,A., and J.J.O'Brien,1980. The seasonal variability in a model of the tropical Pacific. J. Phys. Oceanogr., 10:1929-1951.

____________, and ___________,1981. Interannual variability of the equatorial Pacific in the 1960's. J.

Geophys. Res., 86:10901-10907.

Cane,M.A.,1984. Modeling sea level during El Nino. J. Phys. Oceanogr.,14:1864-1874.

Caviedes,C.,1975. El Nino 1972: Its climate, ecological, human and economic implications. Geograph. Rev., 65:493-509.

Gates,W.L., Y.J.Han, and M.E.Schlesinger,1985. The global climate simulated by a coupled atmosphere-ocean general circulation model. Preliminary results. In Coupled Ocean-Atmosphere Models, J.C.J.Nihoul(Ed.), Elsevier, Amsterdam, pp.131-151.

Gill,A.E.,1980. Some simple solutions for heat induced tropical circulation. Quart. J. Roy. Meteor. Soc., 106:447-462.

Han,Y.J.,1984. A numerical world ocean general circulation model. Part I. Basic design and barotropic experiment. Dyn. Atmos. Oceans.,8:107-140.

________, and S.W.Lee,1983. An analysis of monthly mean wind stress over the global ocean. Mon. Wea.Rev.,111:1554-1566.

Heddinghaus,T.R., and A.F.Krueger,1981. Annual and interannual variations in outgoing longwave radiation over the tropics. Mon. Wea. Rev.,109:1208-1218.

Hirst,A.C.,1985. Free equatorial instabilities in simple coupled atmosphere-ocean models. In Coupled Ocean-Atmosphere Models, J.C.J. Nihoul (Ed.), Elsevier, Amsterdam, pp.153-165.

Horel,J.D., and J.M.Wallace,1981. Planetary scale atmospheric phenomena associated with Southern Oscillation. Mon. Wea. Rev.,109:813-829.

Hoskins,B.J., and D.J.Karoly,1981. The steady linear response of a spherical atmosphere to thermal and orographic forcing. J. Atmos. Sci.,38:1179-1196.

Hughes,R.L.,1979. A highly simplified El Nino model. Ocean Modeling, 22. (unpublished manuscript).

__________,1984. Development of a highly simplified El Nino model. Ocean Modeling,54. (unpublished manuscript).

Hurlburt,H.E., J.C.Kindle, and J.J.O'Brien,1976. A numerical simulation of the onset of El Nino. J. Phys. Oceanogr., 6:621-631.

Keshavamurthy,R.N.,1983. Southern Oscillation: further studies with a GFDL general circulation model. Mon. Wea. Rev., 111:1988-1997.

Lau,K.M.,1982. A simple model of atmosphere-ocean interaction during ENSO. Trop. Ocean-Atmos. Newsl.,13:1-2.

________,1985. Subseasonal scale oscillation, bimodal climatic state and the El Nino/Southern Oscillation. In Coupled Ocean-Atmosphere Models, J.C.J. Nihoul(Ed.), Elsevier, Amsterdam, pp.29-40.

Leetmaa,A.,1983. The role of local heating in producing temperature variations in the offshore waters of the eastern tropical Pacific. J. Phys. Oceanogr., 13:467-473.

Matsuno,T.,1966. Quasi-geostrophic motions in the equatorial area. J. Meteor. Soc., Japan, II, 44:25-43.

McCreary,J.P.,1976. Eastern tropical ocean response to changing wind systems: with application to El Nino. J. Phys. Oceanogr., 6:632-645.

___________,1983. A model of tropical ocean-atmosphere interaction. Mon. Wea. Rev., 111:370-389.

___________, and D.L.T. Anderson,1984. A simple model of El Nino and the Southern Oscillation. Mon. Wea. Rev., 112:934-946.

Myers,G.,1979. Annual variation in the slope of the 14°C isotherm along the equator in the Pacific Ocean. J. Phys. Oceanogr., 9:885-891.

Philander,S.G.H., T.Yamagata, and R.C.Pacanowski,1984. Unstable air-sea interactions in the tropics. J. Atmos. Sci., 41:604-613.

Ramage,C.S.,1975. Preliminary discussion of the meteorology of the 1972-73 El Nino. Bull. Amer. Meteor. Soc., 56:234-242.

Rasmusson,E.M., and T.H.Carpenter,1982. Variations in tropical sea-surface temperature and surface wind fields associated with the Southern Oscillation/El Nino. Mon. Wea. Rev., 110:354-384.

Schoenstadt,A.L.,1978. A transfer function analysis of numerical schemes used to simulate geostrophic adjustment. Report NPS-53-79-001, Naval Postgraduate School, Monterey, Calif., pp.44.

Shukla,J., and J.M.Wallace,1983. Numerical simulation of the atmospheric response to equatorial Pacific sea surface temperature anomalies, J. Atmos. Sci., 40:1613-1630.

Trenberth,K.E.,1976. Spatial and temporal variations in the Southern Oscillation. Quart. J. Roy. Meteor. Soc., 102:639-653.

Weare,B.C., A.R.Navato, and R.E.Newell,1976. Empirical orthogonal analysis of Pacific sea surface temperatures. J. Phys. Oceanogr., 6:671-678.

Webster,P.J.,1972. Response of the tropical atmosphere to local steady forcing. Mon. Wea. Rev., 100:518-541.

____________,1983. The large scale structure of the tropical atmosphere. In Large Scale Dynamical Processes in the Atmosphere, B.J.Hoskins and R.P.Pearce(Eds.), Academic Press, New York, pp.397.

Winninghoff,F.,1968. On the adjustment toward a geostrophic balance in a simple primitive equation model with application to the problem of initialization and objective analysis. Ph.D dissertation, Univ. of Calif., Los Angeles, pp.161.

Wyrtki,K.,1975. El Nino-the dynamic response of the equatorial Pacific Ocean to atmospheric forcing. J. Phys. Oceanogr., 5:572-584.

Yamagata,T.,1985. Stability of a simple air-sea coupled model in the tropics. In Coupled Ocean-Atmosphere Models, J.C.J.Nihoul(Ed.), Elsevier, Amsterdam, pp.637-657.

Yanai,M., S.K.Esbensen, and J.Chu, 1973. Determination of bulk properties of tropical cloud clusters from large-scale heat and moisture budgets. J. Atmos. Sci., 30:611-627.

Zebiak,S.E.,1982. A simple atmospheric model of relevance to El Nino. J. Atmos. Sci., 39:2017-2027.

___________,1986. Atmospheric convergence feedback in a simple model for El Nino. Mon. Wea. Rev., 114:1263-1271.